



Norwegian University of  
Science and Technology

# Real-Time Harmonics Tracking for Stability Assessment of a Microgrid

**Anders Kjeka Broen**

Master of Science in Cybernetics and Robotics

Submission date: June 2016

Supervisor: Marta Maria Cabrera Molinas, ITK

Norwegian University of Science and Technology  
Department of Engineering Cybernetics



---

# Project Description

**Name:** Anders Kjeka Broen  
**Department:** Department of Engineering Cybernetics  
**Title:** Real-Time Harmonics Tracking for Stability Assessment of a Microgrid  
**Tittel:** Følging av Harmoniske Komponenter i Sanntid for Stabilitetsanalyse av et Microgrid  
**Start date:** 2016-01-11  
**Due date:** 2016-06-06  
**Supervisor:** Professor Marta Molinas

**The purpose of this thesis** is to, in real-time, measure the magnitude and phase of harmonics from the measured voltages and currents in a microgrid by using Kalman filter technique, and based on this, estimate parameters in the system. From the estimated parameters, system stability is assessed.

**The work description of this thesis is:**

1. Develop a method for tracking harmonics in a three-phase signal based on Kalman filter and write a digest and a paper for the COMPEL workshop in Trondheim, Norway, 27 – 30 June 2016.
2. Develop an analytical impedance model for separation of a microgrid into a source and a load impedance system.
3. Develop an impedance estimation model for a microgrid based on Kalman filter with an adaptive update law for the model error.
4. Develop a simulation model for the microgrid in Matlab Simulink to verify the estimate in the previous two points.
5. Conclude the findings of this work.



---

# Abstract

The advancement in power electronics technology and in particular the use of nonlinear loads in microgrids where such devices are connected into distributional power grid can cause instabilities. Stability assessment of such grids is done by modeling the grid as two subsystems namely the source and load and use Nyquist stability criterion for the said source and load impedance. Stability analysis of such a grid is a difficult task where the state of the art consists of injecting a perturbation current or voltage to each subsystem of the microgrid structure which is time-consuming or may not be practically feasible.

In a microgrid, there are components which are time-varying where the properties may change with time due to temperature rise because of high power consumption, faults or aging of equipment. These effects call for a method where the system parameters are detected in real-time and from the parameters of the grid the system stability can be calculated without the need of signal injection of a perturbation current or voltage into the microgrid.

In this master's thesis, the problem is dealt with by measuring current and voltage harmonics distortions on the bus lines in an AC system caused by nonlinear loads by using a Kalman filter. An online recursive least squares estimator is used to estimate the impedance parameters based on the harmonic components at different frequencies in the frequency domain. The method for measuring harmonic components has a fast response and can be used for time-varying signals. The method is also verified in systems with dynamics and concluded that this is a steady state method. The impedance of the subsystems of the microgrid is found in real-time which leads to straightforward stability analysis based on the grid impedance, also in real-time.

The methods were verified by simulations with the use of Matlab Simulink with the aid of the SimPowerSystems library for modeling the grid. The impedance estimated from the estimated parameters of the grid were verified by numerical simulations by injecting a small-signal perturbation into relevant subsystems of the grid. A good accordance between the measured impedance by signal injection and the parameterized model was found.



---

# Sammendrag på Norsk

Teknologiske fremskritt innenfor kraftelektronikk har ført til at flere ulike typer ulineære laster blir koblet sammen i distribuerte kraftnettverk. Samspillet mellom slike laster kan føre til at nettverket blir ustabil. Stabilitetsanalyse av slike kraftnett gjøres ved å dele systemet inn i kilde- og lastsystemer, og så bruke Nyquists stabilitetskriterium basert på kilde og lastsystemet. Dette er en vanskelig oppgave, hvor det som oftest gjøres ved å injisere et lite forstyrrelsessignal og så måle responsen. Dette gjøres for mange frekvenser, og kan derfor være en tidkrevende prosess.

I distribuerte kraftnettverk kan det være komponenter som endrer egenskaper over tid. Det være seg om komponentene blir påvirket av temperatur, aldring, eller feilmoduser i nettverket. Disse effektene gjør at man ønsker en metode for å identifisere parametere for slikt utstyr, og å gjøre stabilitetsanalyse i sanntid uten injeksjon av forstyrrelsessignaler.

I denne masteroppgaven er problemet med å måle harmoniske komponenter i et elektrisk AC distribusjonsnettverk gjort ved bruk av Kalmanfilter. Fra de målte harmoniske komponentene for strøm og spenning, blir parametere relatert til impedans i nettverket estimert ved bruk av en rekursiv minste kvadraters metode. Metoden for å måle de harmoniske komponentene i inngangssignal, har en rask respons for tidsinvariante signaler. Denne metoden er også verifisert ved å bruke den på systemer med dynamikk, og det ble konkludert med at metoden fungerer best når systemet er i likevekt (steady state). Impedansen for de ulike undersystemene i nettverket ble funnet i sanntid, og basert på dette ble stabilitetsanalyse gjort.

Metoden ble verifisert ved hjelp av simuleringer ved bruk av Matlab Simulink, og spesielt ved hjelp av biblioteket SimPowerSystems for modellering av kraftnettverket. Impedansen i relevante komponenter ble målt ved bruk av en metode hvor et lite forstyrrelsessignal ble injisert for systemet og responsen ble målt. Denne ble så sammenlignet med den estimerte impedansen, og det ble funnet at den parametriserte impedansmodellen stemte godt med den målte impedansen.



---

# Preface

This is the master's thesis to conclude the Master of Science degree in Cybernetics and Robotics at the Norwegian University of Science and Technology. The work was carried out during the spring semester of 2016 at the Department of Engineering Cybernetics with useful inputs from people in association with this department.

I would like to thank Professor Marta Molinas for the guidance with this work. Ph.D. candidate Espen Skjong has been very helpful to provide help with setting up a microgrid simulation platform for simulation verification. I would like to thank Ph.D. candidate Mohammad Amin for input regarding stability analysis for power systems. I would like to thank my fellow Master of Science students in the room B117 for a work-friendly environment.

*Anders Kjeka Broen  
Trondheim, June 2016*



# Table of Contents

<b>Project Description</b>	<b>i</b>
<b>Abstract</b>	<b>iii</b>
<b>Sammendrag på Norsk</b>	<b>v</b>
<b>Preface</b>	<b>vii</b>
<b>Table of Contents</b>	<b>xii</b>
<b>List of Tables</b>	<b>xiii</b>
<b>List of Figures</b>	<b>xvi</b>
<b>Abbreviations</b>	<b>xvii</b>
<b>1 Introduction</b>	<b>1</b>
1.1 Background . . . . .	1
1.2 Related Works . . . . .	2
1.2.1 Measuring Harmonic Components . . . . .	2
1.2.2 Measuring Impedance by Signal Injection . . . . .	2
1.2.3 Impedance Estimation by System Identification . . . . .	3
1.2.4 Stability Analysis . . . . .	3
1.3 Structure of the Report . . . . .	4
<b>2 Theory</b>	<b>5</b>
2.1 Electrical Power Systems . . . . .	5
2.1.1 Symmetrical Components . . . . .	6
2.1.2 Fault . . . . .	6
2.1.3 AC Generator . . . . .	6
2.1.4 Line-Commutated Rectifiers . . . . .	7
2.2 Clarke Transform . . . . .	9

---

2.3	Small-Signal Methods . . . . .	10
2.4	Generalized Nyquist Stability Criterion . . . . .	10
2.5	Total Harmonics Distortion . . . . .	11
2.6	Kalman Filter . . . . .	12
2.6.1	Discrete Kalman Filter . . . . .	12
2.7	Recursive Online Parameter Estimation . . . . .	12
2.8	Grid Synchronization Method . . . . .	13
2.9	Network Analysis . . . . .	13
2.10	Phasor Theory . . . . .	14
2.11	Real-Time Systems . . . . .	15
<b>3</b>	<b>Summary of Previous Work</b>	<b>17</b>
3.1	Mathematical Model . . . . .	17
3.2	Estimating the Grid Equivalent Parameters with Augmented Kalman Filter	18
<b>4</b>	<b>Harmonics Tracking Based on Kalman Filter</b>	<b>21</b>
4.1	Single-Phase Harmonics Tracking Based on Kalman Filter . . . . .	22
4.1.1	Single-Phase Harmonics Tracker Implementation . . . . .	24
4.2	Three-Phase Harmonics Tracking Based on Kalman Filter . . . . .	24
4.2.1	Three-Phase Harmonics Tracker Implementation . . . . .	27
4.3	Performance Testing of the Three-Phase Tracking Method . . . . .	28
4.3.1	Experiment 1: Tracking Without Noise . . . . .	28
4.3.2	Experiment 2: Noise and Non-Modeled Harmonics . . . . .	29
4.3.3	Experiment 3: Tracking with Angular Frequency Deviation . . . . .	31
4.4	Discussion . . . . .	32
<b>5</b>	<b>Proposed Method</b>	<b>35</b>
5.1	AC Side Real-Time Parameter Estimator . . . . .	36
5.1.1	Pre-Processing . . . . .	36
5.1.2	Three-Phase Harmonics Analyzer . . . . .	37
5.1.3	Phase Correction . . . . .	37
5.1.4	Complex Division per Harmonic Component . . . . .	37
5.1.5	ParameterEstimation . . . . .	37
5.2	DC Side Real-Time Parameter Estimator . . . . .	38
5.2.1	Pre-Processing . . . . .	38
5.2.2	Single-Phase Harmonics Analyzer . . . . .	39
5.2.3	Phase Correction . . . . .	39
5.2.4	Parameter Estimation . . . . .	39
<b>6</b>	<b>Impedance Model of a Harmonic Source</b>	<b>41</b>
6.1	AC input impedance model . . . . .	42
6.2	DC Side Impedance . . . . .	44
6.2.1	DC Side Impedance Estimation Method . . . . .	44
6.3	Small-Signal Measurement by Voltage Perturbation . . . . .	46
6.4	Simulation Results . . . . .	46
6.5	Discussion . . . . .	47

---

---

<b>7</b>	<b>Case Study: Real-Time Stability Analysis of a Shipboard Microgrid</b>	<b>49</b>
7.1	Mathematical Model . . . . .	50
7.2	Microgrid Implementation . . . . .	50
7.3	Bus Line Voltage . . . . .	50
7.4	DC Side Voltage and Current of the Three-Phase Rectifier Load . . . . .	52
7.5	Limitation to the Steady State . . . . .	53
7.6	Building the Impedance Model . . . . .	54
7.7	Parameter Estimation Model . . . . .	56
7.7.1	DC Side Parameters . . . . .	56
7.7.2	AC Side Parameters . . . . .	56
7.8	Initialization of the Estimation Method . . . . .	56
7.9	Results . . . . .	57
7.9.1	Parameter Estimation . . . . .	57
7.9.2	AC Side Impedance Estimation . . . . .	58
7.9.3	Harmonic Load Impedance Estimation . . . . .	58
7.9.4	System Transfer Function Estimation Result . . . . .	60
7.9.5	Stability Analysis . . . . .	60
7.10	Discussion . . . . .	61
<b>8</b>	<b>Discussion</b>	<b>63</b>
<b>9</b>	<b>Conclusion</b>	<b>65</b>
<b>10</b>	<b>Future Work</b>	<b>67</b>
	<b>Bibliography</b>	<b>69</b>
	<b>Appendices</b>	<b>73</b>
<b>A</b>	<b>Submitted digest for COMPEL</b>	<b>75</b>
<b>B</b>	<b>Submitted paper for COMPEL</b>	<b>81</b>
<b>C</b>	<b>Matlab Simulink Models</b>	<b>89</b>
C.1	AKF Simulink Model for Single-Phase Signal . . . . .	89
C.2	AKF Simulink Model for Three-Phase Signal . . . . .	90
C.3	Distributional Power Grid Model . . . . .	90
C.4	Ideal Three-Phase Sequence Generator . . . . .	90
C.5	Phase correction Simulink model . . . . .	91
C.6	AC side parameter estimation Simulink model . . . . .	91
C.7	Small-signal measurement of input impedance of rectifier load . . . . .	91
C.8	DC Side Impedance Parameter Estimator Simulink Model . . . . .	92
C.9	AC side to DC side voltage and current Simulink model . . . . .	92
C.10	Harmonic Content and Parameter Estimator Simulink Model . . . . .	93

---

---

<b>D</b>	<b>Matlab Code</b>	<b>95</b>
D.1	Matlab Adaptive Kalman Filter Matlab Function Implementation . . . . .	95
D.2	Matlab Function Single-Phase Measurement Matrix Calculation . . . . .	96
D.3	Matlab Function Three-Phase Measurement Matrix Calculation . . . . .	96
D.4	Matlab Function for Calculating Harmonic Phasor . . . . .	97
D.5	Matlab Function for Initializing the Adaptive Kalman Filter for Single-Phase Signal . . . . .	97
D.6	Matlab Function for Initializing the Adaptive Kalman Filter for Three-Phase Signal . . . . .	97
<b>E</b>	<b>Linear KF Implementation for Three-Phase Harmonics Tracking</b>	<b>99</b>
E.1	Implementation . . . . .	99
E.2	Experiment 1 . . . . .	100
E.3	Experiment 2 . . . . .	101
E.4	Experiment 3 . . . . .	102
<b>F</b>	<b>Algorithms</b>	<b>105</b>
F.1	Adaptive Kalman Filter . . . . .	105
<b>G</b>	<b>Additional Plots</b>	<b>107</b>
G.1	Harmonic Loads . . . . .	107
G.2	Low-pass Filter . . . . .	108
G.3	FFT Analysis . . . . .	109
G.4	Transient Analysis . . . . .	110

# List of Tables

4.1	Description of AKF parameters . . . . .	24
4.2	Description of AKF parameters . . . . .	27
4.3	Initialization of the AKF parameters for Experiment 1 . . . . .	29
4.4	Reference harmonics signal . . . . .	29
4.5	Test 2 setup . . . . .	29
4.6	Optimal $q$ for experiment 2 . . . . .	30
6.1	Description of parameters for the impedance model in Lei et al. (2013) . .	43
6.2	DC side impedance parameters . . . . .	44
7.1	Description of grid parameters . . . . .	51
7.2	THD content for some measured values given in % of the fundamental . .	52
7.3	Grid impedance subsystems . . . . .	54
7.4	Description grid parameters . . . . .	57



# List of Figures

2.1	Balanced three-phase AC signals . . . . .	6
2.2	AC generator electrical model . . . . .	7
2.3	Three-phase line-commuted rectifier . . . . .	7
2.4	Typical balanced three-phase signal, mapping function for each phase and Dc side voltage . . . . .	8
2.5	Impedance as source load system . . . . .	11
3.1	Estimated grid parameters . . . . .	19
4.1	Experiment 1: Magnitude, phase angle and error for the AKF . . . . .	30
4.2	Experiment 2: Magnitude, phase angle, and error for the AKF . . . . .	31
4.3	Evolution of $q_a$ per sample and the median filtered $q_a$ for 10 samples . . . . .	32
4.4	Experiment 3: Magnitude, phase angle and error for the AKF . . . . .	33
4.5	Evolution of $q_a$ per sample and the median filtered $q_a$ for 10 samples and the frequency deviation for each sample . . . . .	34
4.6	Linear error with increased frequency deviation . . . . .	34
5.1	AC side real-time parameter estimator . . . . .	36
5.2	DC side real-time parameter estimator . . . . .	38
6.1	Diode bridge with RLC load . . . . .	41
6.2	Real and imaginary part of impedance for the three test systems . . . . .	45
6.3	Measured impedance using Figure C.7 and compared to the model Bing in Bing et al. (2007) and Lei in Lei et al. (2013) for System 3 . . . . .	47
7.1	Power grid model for case study . . . . .	49
7.2	Input source voltages and voltages at bus 1 and bus 2 . . . . .	51
7.3	Measured DC side voltages and currents . . . . .	52
7.4	Equivalent impedance model represented as a source load system . . . . .	54
7.5	Estimated power grid parameters with the use of AKF and RLSE . . . . .	58

---

7.6	Estimated linear impedance model using AKF and RLSE compared to the reference impedance for $Z_{mb}$ , $Z_{s1}$ and $Z_{s2}$ . . . . .	59
7.7	Estimated impedance model of Load 1 and Load 2 with use of AKF, RLSE and the Bing small-signal impedance model, compared to the measured impedance using small-signal injection. . . . .	59
7.8	Estimated $H_{sys1}$ and $H_{sys2}$ with use of AKF, RLSE and the Bing small-signal impedance model, compared to the measured impedance using small-signal injection. . . . .	60
7.9	Estimated $H_{01}$ and $H_{02}$ with use of AKF, RLSE and the Bing small-signal impedance model, compared to the measured transfer function using small-signal injection. . . . .	61
C.1	AKF Simulink Model for Single-Phase Signal . . . . .	89
C.2	AKF Simulink Model for Three-Phase Signal . . . . .	90
C.3	Power Distributional Grid Model . . . . .	90
C.4	Ideal Three-Phase Sequence Generator . . . . .	90
C.5	Phase correction . . . . .	91
C.6	AC side parameter estimation Simulink model . . . . .	91
C.7	Model in order to measure small-signal impedance of a three phase rectifier load . . . . .	91
C.8	Proposed method in order to extract DC side parameters . . . . .	92
C.9	DC side current and voltage estimate from AC side . . . . .	92
C.10	Implemented block model for estimating all the harmonics and parameters of the grid . . . . .	93
E.1	Description of Kalman parameters . . . . .	99
E.2	initialization of parameters for experiment 1 . . . . .	100
E.3	Experiment 1 using linear KF . . . . .	100
E.4	Experiment 2 using linear KF with $\mathbf{Q} = \mathbf{I}$ . . . . .	101
E.5	Experiment 2 using linear KF with $\mathbf{Q} = 1 \times 10^{-3}\mathbf{I}$ . . . . .	102
E.6	Experiment 2 using linear KF with; magnitude, phase and deviation from the reference . . . . .	103
G.1	Measured impedance using Figure C.7 and compared to the model Bing in Bing et al. (2007) and Lei in Lei et al. (2013) for system 1 . . . . .	107
G.2	Measured impedance using Figure C.7 and compared to the model Bing in Bing et al. (2007) and Lei in Lei et al. (2013) for system 2 . . . . .	108
G.3	Low-pass filter magnitude and phase response with configuration in Table 7.4 . . . . .	108
G.4	FFT analysis of $V_{bus1}$ and $i_{s1}$ using FFT analysis tool . . . . .	109
G.5	The three-phase harmonics tracking used on $i_{s1}$ dynamic system's transient response and the three-phase signal in $abc$ frame . . . . .	110

---

# Abbreviations

**AC** Alternating Current

**AKF** Adaptive Kalman Filter

**DC** Direct Current

**EKF** Extended Kalman Filter

**FFT** Fast Fourier Transform

**FIR** Finite Impulse Response

**KF** Kalman Filter

**PCC** Point of Common Coupling

**PLL** Phase Locker Loop

**PWM** Pulse Width Modulated

**RLSE** Recursive Least Squares Estimator

**RMS** Root Mean Square



# Introduction

## 1.1 Background

In the later years, the preferred propulsion system for marine vessels has been electric drive. With the many oil and gas resources available in deeper seas efficient marine vessels are needed to keep the cost down, where the typical range for such offshore vessels are in the power range 10-40MW (Ådnanes et al., 1997). Many marine vessels operate with the use of a diesel-electric propulsion system (Sørfonn, 2007). The main diesel generators will produce the necessary electric power for the propulsion systems and other loads in the vessel where typically this will be two or more generators to meet the required redundancy needed for operations far from land.

Knowledge of the source and load impedances in an electrical power distributional grid is essential to calculate the stability of the grid using the impedance-based method with the generalized Nyquist stability criterion first described in Desoer and Wang (1980) with an application for AC systems in Sun (2011). The impedance-based method requires, however, the injection of small signals in a wide range of frequency to obtain a good estimate of the stability of the grid. This frequency scanning technique does not allow for a real-time estimation of the impedances and stability.

The real-time identification of the impedances of the grid can be relevant considering the non-stationary environment where the impedance may vary with the operating conditions and with parameter variations over time Cespedes and Sun (2014).

Electrical grids that are already affected by distorted voltages and currents can readily benefit from a non-invasive approach of impedance identification that makes use of the information provided by such distortions and can lead to a straightforward grid stability assessment in time-domain. The tracking, at a given node, of each of the harmonic components present in the voltage and current, can enable the identification of the grid impedances in a non-invasive way, by simply calculating the ratio  $V(\omega)/I(\omega) = Z(\omega)$  at each harmonic distortion when the grid is operating in the steady state with sinusoidal input.

Harmonics estimation in the time-domain using Kalman theory will track the phase

and amplitude of the harmonics of a distorted signal (voltage and current) using state-space form and has a potential for real-time processing due to the low computational load. The use of Kalman filter for this problem is proposed in Girgis et al. (1991) using a linear Kalman filter as first described in Kalman (1960). These methods conclude that Kalman theory can estimate accurately harmonic components even during high power system disturbance conditions.

In the paper attached in Appendix B proposes a non-invasive method to identify the impedances of the grid based on the use of the information of the distortions already present in the current and voltage waveforms, without resorting to any small-signal injection.

This master's thesis will use the methods presented in the paper to calculate the stability of a grid in real-time by transformation of the grid into a source and load connected system where output and input impedance is calculated. The methods are tested on a microgrid typically found in a marine vessel where the small-signal impedance calculations are carried out.

## 1.2 Related Works

In this section, some related papers are investigated. Some notable works related to estimating harmonic components, small-signal impedance measurement and use of Nyquist stability criterion for stability analysis for source and load.

### 1.2.1 Measuring Harmonic Components

Several works have successfully implemented methods to track harmonics in a power electronic system with the main motivation of tracking voltage and current harmonics created by nonlinear equipment. In Girgis et al. (1991), the problem of tracking harmonics using a time domain method based on the Kalman filter is proposed with the main advantages of using a time domain method in contrast to methods in the frequency domain.

### 1.2.2 Measuring Impedance by Signal Injection

Measuring impedance is done by measuring the input voltage and input current for the same frequency and in the frequency domain the impedance is  $Z(\omega) = V(\omega)/I(\omega)$ . In normal grid operation, the system may not have a frequency component at each relevant frequency, which can be solved by injecting a current or voltage and measuring the output. In Rhode et al. (1995) the line impedance of an energized power system is measured as a function of frequency by injecting a small sinusoidal current signal with a given frequency. Measured impedance is of high accuracy, and the method is implemented using inexpensive equipment.

In Familiant et al. (2009) three methods on how to inject current signal is discussed. The methods are by using a three-phase bridge for low power systems, a novel chopper circuit and a third with the use of wound rotor induction motor. The main motivation for this is the increasing use of power electronic devices in naval ships and aerospace which such systems may be prone to negative impedance instability.

In Huang et al. (2009), the current is injected between two of the three lines in the three-phase system and all the impedance information can be obtained. The proposed method has some advantages such that it is simpler and more cost effective in medium-voltage systems, simple implementation and can be used to measure both AC and DC systems.

In Sumner et al. (2004), the system is injected a short duration spike into the system, and the impedance is measured from the input voltage and current response.

### 1.2.3 Impedance Estimation by System Identification

Some cases where the impedance is known to have a predetermined model one can extract parameters from voltage and current measurement and fit those to the model. The methods here are based on recursive least squares method, Kalman filter or neural networks.

One example of such work based on least squares can be found in Cobreces et al. (2009) where a method of estimating the equivalent grid impedance and voltage source online is investigated and implemented. The motivation for the estimation is to monitor the grid from the point of common coupling (PCC) to detect islanding situations and optimizing the converter control. This setup, however, requires the grid model to be linear on the parameters to use a recursive least square method for best fit of the parameters. It is assumed that the grid can be modeled as an ideal voltage source in series with an inductor and a resistor and that the grid is operating in different set-points for the least squares method to work.

An Extended Kalman filter approach is implemented in Hoffmann and Fuchs (2014) with the objective of estimating the equivalent grid impedance parameters. The system at hand is a distributional grid with a non-negligible grid impedance and this impedance seen from the power converter at the PCC are to be identified. The three-phase current and voltage measurement at the PCC are converted into  $\alpha$  and  $\beta$  components with the use of the Clarke transform for measurement input to the Extended Kalman filter. The Extended Kalman filter state vector is then augmented to include the equivalent grid parameters  $R_{grid}$  and  $L_{grid}$ . This method also needs a predetermined model to fit the parameters.

A neural network approach to the problem is proposed in Xiao et al. (2007) where the impedance is identified by shunt injecting a random Pulse Width Modulated signal produced by a chopper circuit. The neural network learns from the current and voltage relationship and estimates the impedance based on this. This method has the potential of significantly reduce the time for which the time which is needed for the estimation process because of only one perturbation signal is necessary.

### 1.2.4 Stability Analysis

In Feng et al. (2002) the problem of joining multiple load and source subsystems such that one can use the theory of Nyquist stability criterion for source and load connected systems with multiple subsystems as well.

The problem with defining specifications for stability for such systems is dealt with in Wildrick et al. (1995) where a concept of forbidden region is introduced as a requirement for stability margin.

## 1.3 Structure of the Report

**Chapter 1: Introduction:** This chapter presents the background for the thesis and some important related works, before an outline of this thesis.

**Chapter 2: Theory:** This chapter starts the main part of the thesis by introducing some useful theory necessary for the following chapters.

**Chapter 3: Summary of Previous Work:** This chapter is a summary of the work done in the specialization project done Autumn 2015.

**Chapter 4: Harmonics Tracking Based on Kalman Filter:** This chapter presents a Kalman filter for tracking positive and negative sequence harmonics in a three-phase signal and harmonics in a single-phase signal.

**Chapter 5: Proposed Method:** This chapter explains how to estimate impedance of a linear load based on the present harmonics and estimate the DC side impedance of a rectifier load.

**Chapter 6: Impedance Model of a Harmonic Source:** The small-signal impedance model of a diode bridge rectifier is presented in this chapter.

**Chapter 7: Case Study: Real-Time Stability Analysis of a Shipboard Microgrid:** A case study is presented to unify all the other work done in this thesis by doing stability analysis on a microgrid in real-time based on the measured harmonics.

**Chapter 8: Discussion:** Discussion of the results obtained in this thesis.

**Chapter 9: Conclusion:** Conclusion of this thesis.

**Chapter 10: Future Work:** Ending the thesis by stating some recommendations for future work.

**Appendix A:** Submitted digest for COMPEL workshop in Trondheim 2016.

**Appendix B:** Submitted paper for COMPEL workshop in Trondheim 2016.

**Appendix C:** Matlab Simulink models used to implement the microgrid and the parameter estimation algorithms used to verify the proposed methods.

**Appendix D:** Some of the Matlab code for implementation of the algorithms found in this thesis.

**Appendix E:** In this appendix, a linear Kalman filter is used to track harmonics and to show the complicated tuning process of such a filter.

**Appendix F:** The adaptive Kalman filter algorithm is found here.

**Appendix G:** Some additional plots relevant for the results in this thesis is appended here.

# Theory

## 2.1 Electrical Power Systems

The focus of this thesis will be on three-phase AC electrical power systems. The voltage and current which are rectified are here denoted DC side voltage or current. The AC side is the rest of of the system, where three-phase AC is used.

Three-phase systems are widely used as a way of distributing and generating electrical power because of the efficiency mainly related to voltage level transformers. Three-phase systems are used to provide power from source to load. Typically the source converts energy from one form to electrical energy and powers the loads. Three-phase systems may consist of equipment such as generators, rectifiers and filters. Several such components are connected to form a distributed power system where there is one or more sources which power the system and one or more loads which draw power from the system. The three-phase voltage is expressed in the  $abc$  frame in (4.6) where  $\omega(t)$  is the angular frequency,  $V_a(t)$ ,  $V_b(t)$ ,  $V_c(t)$  are the amplitude for each of the phases and  $\theta_a(t)$ ,  $\theta_b(t)$ ,  $\theta_c(t)$  are the phase angle for the phases.

$$v_a(t) = V_a(t)\sin(\omega(t)t + \theta_a(t)) \tag{2.1a}$$

$$v_b(t) = V_b(t)\sin(\omega(t)t + \theta_b(t)) \tag{2.1b}$$

$$v_c(t) = V_c(t)\sin(\omega(t)t + \theta_c(t)) \tag{2.1c}$$

In a balanced system, there is a relationship between the phase angles by stating them as time-invariant given by  $\theta_b = \theta_a - \frac{2\pi}{3}$  and  $\theta_c = \theta_a + \frac{2\pi}{3}$ , and for the amplitudes  $V = V_a = V_b = V_c$  summarized below:

$$v_a(t) = V \sin(\omega(t)t) \quad (2.2a)$$

$$v_b(t) = V \sin(\omega(t)t - \frac{2\pi}{3}) \quad (2.2b)$$

$$v_c(t) = V \sin(\omega(t)t + \frac{2\pi}{3}) \quad (2.2c)$$

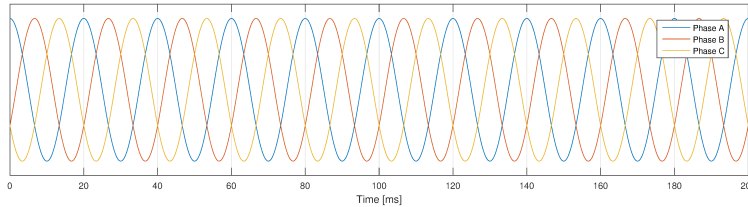


**Figure 2.1:** Balanced three-phase AC signals

In Figure 2.1 typical balanced three-phase signals are shown. Three-phase systems can be connected using Y ("star") configuration or in  $\Delta$  ("delta") configuration. For the Y configuration, a source connected in this form will have a common connection point from where a neutral connection is possible. For  $\Delta$  connected sources, there is no common defined node as the three sources are connected in series with the sum of the sources equal to zero.

### 2.1.1 Symmetrical Components

From the by Fortescue theorem in Fortescue (1918), an unbalanced system is described as a superposition of three balanced systems known as the symmetrical components. The components are the positive, negative and zero sequences.

### 2.1.2 Fault

A fault is an abnormal system state usually caused by a low impedance path to ground, which is not by design. For a three-phase system, there is the possibility of asymmetrical or symmetrical faults. Asymmetrical faults affect the phases in a different manner, and symmetrical is when all the phases are influenced the same way. Even in the presence of an asymmetrical fault the signals can be described using symmetrical components stated as the positive, negative and zero components. During a fault, the system will change the state rapidly during a period of transients before the system settles in a new steady state.

### 2.1.3 AC Generator

A very common power generator system is the three-phase synchronous generator known as the AC generator. An external force drives the rotor and the three identical stators coils generate three-phase voltages with equal magnitude but  $120^\circ$  apart, and usually the generator is connected as three-phase Y-connection. The rotor rotates with an angular

velocity of  $\omega$  which in a 2-pole rotor gives an instantaneous angular velocity of  $\omega$ . An electrical model of a generator is presented in Figure 2.2. The model consists of the  $E_f$  which is the induced voltage in the stator winding,  $R_a$  is the resistance in the winding and  $L_s$  is the inductance in the winding. The output voltage in frequency domain at the terminals of the load  $V$  is:

$$V = E_f - I(R_a + j\omega L) \quad (2.3)$$

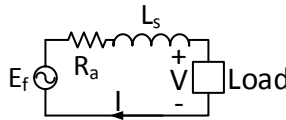


Figure 2.2: AC generator electrical model

### 2.1.4 Line-Commutated Rectifiers

A general model of a line-commutated rectifier based on diode technology with a general load is shown in Figure 2.3. The rectifiers are typically used for AC to DC conversion and based on a diode bridge because of the reliability and the ability to handle high power.

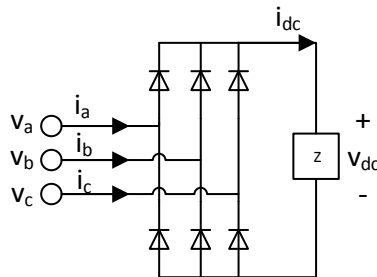


Figure 2.3: Three-phase line-commutated rectifier

In Figure 2.4 a balanced three-phase voltage signal with only the fundamental harmonic and the corresponding mapping function to the voltage on the DC side of the converter given by

$$v_{dc}(t) = s_a(t)v_a(t) + s_b(t)v_b(t) + s_c(t)v_c(t) \quad (2.4)$$

The mapping from the DC side current to the AC side is:

$$i_a(t) = s_a(t)i_{dc}(t) \quad (2.5a)$$

$$i_b(t) = s_b(t)i_{dc}(t) \quad (2.5b)$$

$$i_c(t) = s_c(t)i_{dc}(t) \quad (2.5c)$$

The diode on the upper side corresponding to the highest voltage potential will be in forward bias, but the others will be in reversed bias. For the lower diodes, the one with the

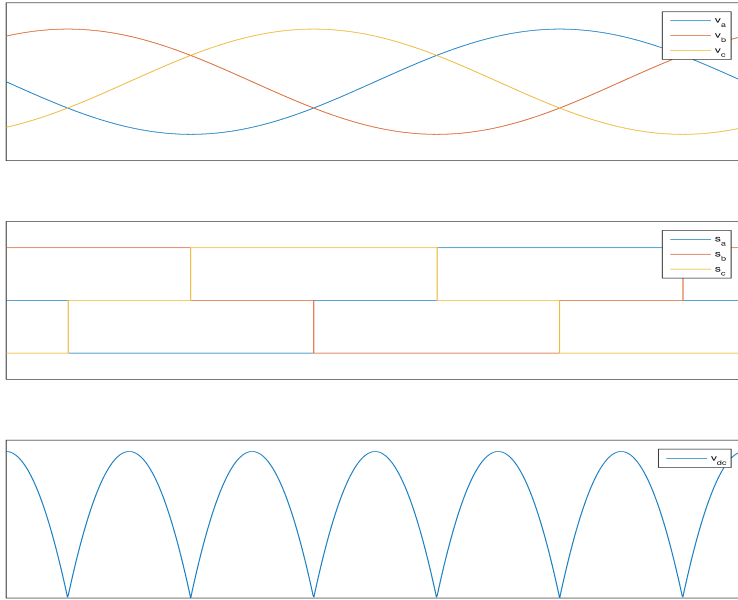


**Figure 2.4:** Typical balanced three-phase signal, mapping function for each phase and Dc side voltage

minimum voltage potential will be in forward bias and the other two in reversed. With this definition of the mapping function, the following is a compact mathematical description:

$$s_i(t) = \begin{cases} 1 & v_i(t) > v_j(t), i \neq j, i \in a, b, c, j \in a, b, c \\ -1 & v_i(t) < v_j(t), i \neq j, i \in a, b, c, j \in a, b, c \\ 0 & \text{else} \end{cases} \quad (2.6)$$

By calculating the Fourier Series of the three periodic mapping functions  $s_a(t)$ ,  $s_b(t)$ ,  $s_c(t)$ , it is possible to analyze the harmonic components of mapped signal with the Fourier Series defined in Kreyszig (2011), where  $2L$  is the period of the signal:

$$f(x) = a_0 + \sum_{n=1}^{\infty} (a_n \cos(\frac{n\pi}{L}x) + b_n \sin(\frac{n\pi}{L}x)) \quad (2.7)$$

The Fourier coefficients  $a_0, a_n, b_n$  are defined as follows:

$$a_0 = \frac{1}{2L} \int_{-L}^L f(x) dx \quad (2.8a)$$

$$a_n = \frac{1}{L} \int_{-L}^L f(x) \cos\left(\frac{n\pi x}{L}\right) dx \quad (2.8b)$$

$$b_n = \frac{1}{L} \int_{-L}^L f(x) \sin\left(\frac{n\pi x}{L}\right) dx \quad (2.8c)$$

By using the result from Bing et al. (2007) the complex Fourier coefficients are found for the phase a,b and c in (2.9), (2.10) and (2.11) respectively.

$$S_a[if_{nom}] = \begin{cases} -\frac{(-1)^k j\sqrt{3}}{\pi(6k\pm 1)} & i = (6k \pm 1), k \in \mathbb{Z}_{\geq 0} \\ 0 & i \neq (6k \pm 1), k \in \mathbb{Z}_{\geq 0} \end{cases} \quad (2.9)$$

$$S_b[if_{nom}] = \begin{cases} -\frac{(-1)^k j\sqrt{3}e^{\mp j2\pi/3}}{\pi(6k\pm 1)} & i = (6k \pm 1), k \in \mathbb{Z}_{\geq 0} \\ 0 & i \neq (6k \pm 1), k \in \mathbb{Z}_{\geq 0} \end{cases} \quad (2.10)$$

$$S_c[if_{nom}] = \begin{cases} -\frac{(-1)^k j\sqrt{3}e^{\pm j2\pi/3}}{\pi(6k\pm 1)} & i = (6k \pm 1), k \in \mathbb{Z}_{\geq 0} \\ 0 & i \neq (6k \pm 1), k \in \mathbb{Z}_{\geq 0} \end{cases} \quad (2.11)$$

From the (2.9), (2.10) and (2.11) the voltage phasor for the frequencies which are different from zero, also in Bing et al. (2007), given in (2.12) where  $V$  is the AC side voltage amplitude.

$$V_{dc}[6kf_{nom}] = \frac{(-1)^k 3\sqrt{3}V}{\pi(1-36k^2)}, k \in \mathbb{Z}_{\geq 0} \quad (2.12)$$

Based on (2.9) to (2.12) one can assume that the input AC current will have harmonic content at frequencies  $f_{nom}(6k \pm 1), k \in \mathbb{Z}_{\geq 0}$  and that the DC side voltage will have harmonics at frequencies  $f_{nom}6k, k \in \mathbb{Z}_{\geq 0}$ .

## 2.2 Clarke Transform

Defining the Clarke transformation  $T_{\alpha\beta 0}$  as the following:

$$\mathbf{T}_{\alpha\beta 0} = \begin{bmatrix} \frac{2}{3} & \frac{-1}{3} & \frac{-1}{3} \\ 0 & \frac{1}{\sqrt{3}} & \frac{-1}{\sqrt{3}} \\ \frac{1}{2} & \frac{1}{2} & \frac{1}{2} \end{bmatrix} \quad (2.13)$$

A three-phase signal in  $V_{\alpha\beta 0}$  is obtained by the following relation in (2.14).

$$V_{\alpha\beta 0}(t) = \mathbf{T}_{\alpha\beta 0} V_{abc}(t) \quad (2.14)$$

This transformation is useful because if the system is balanced, then the 0 component will always be zero. For a balanced three-phase, the method is a projection of the  $abc$

components to the static  $\alpha\beta$  reference frame. Given the balanced three-phase system in (2.2) this system can be described using only two components in the  $\alpha\beta$  frame given below:

$$v_\alpha = \sqrt{3}V \cos(\omega t + \phi) \quad (2.15a)$$

$$v_\beta = \sqrt{3}V \sin(\omega t + \phi) \quad (2.15b)$$

## 2.3 Small-Signal Methods

A three-phase AC system like (2.1) a DC operating point cannot be defined since the signal for each of the phases varies around the positive and negative peak value. The current state of the art to analyze the impedance of the system is with the use of the small-signal method (Familiant et al., 2009). The impedance is measured by injecting a signal with a low magnitude into the power grid with the system energized. The impedance for this type of system depends on the ratio of the small-signal injected voltage or current and the response voltage and current at the point of measurement.

A drawback of the small-signal methods is that large-signal perturbations are not covered by this approach, and the impedance is not correctly described in such cases. Such situations may occur during source fluctuation, transients or faults (Sun, 2000). Such conditions usually do not influence the stability of normal system operation, but it may be necessary to know how the grid operates in such events for systems where faults may have dramatic consequences for systems where grid outage can not be tolerated, for instance electrical systems on a marine ship or aviation.

A nonlinear AC component's AC impedance characteristic can only be obtained using small-signal operation (Bing et al., 2007). The problem is that there is no DC operation point in AC systems, where the DC component in almost all cases is zero. Small-signal impedance measurement is done by injecting a signal with low amplitude compared with the fundamental for different frequencies Familiant et al. (2009).

## 2.4 Generalized Nyquist Stability Criterion

The generalized Nyquist stability criterion was first described in Desoer and Wang (1980) with an application for power electronics in Sun (2011). The impedance-based stability analysis is done by dividing the system into two subsystems, namely the source and load and it is assumed a small-signal model. It is assumed that the source can be modeled as an ideal voltage in series with an output impedance  $Z_s(s)$ . The input impedance  $Z_l(s)$  for the load is defined as a function of the complex variable  $s$  with such a model in Figure 2.5. The transfer function is then defined as follows from  $V_s$  to  $V_{load}$ :

$$H = \frac{V_{load}}{V_s} = \frac{1}{1 + Z_s/Z_{load}} = \frac{1}{1 + H_0} \quad (2.16)$$

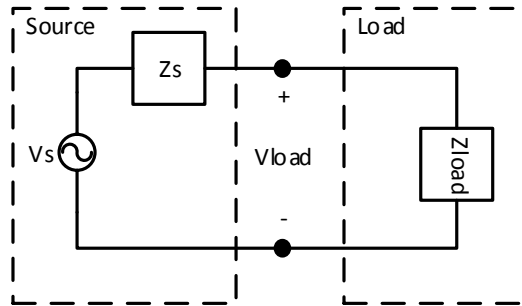


Figure 2.5: Impedance as source load system

By using linear control theory, the system is input-output stable if and only if  $H_0(s) = Z_s(s)/Z_l(s)$  satisfies the Nyquist stability criterion. Many algebraic methods regarding system stability exist where one can calculate the stability based on the closed loop system's poles in the frequency domain. The general Nyquist stability criterion can be viewed as a graphical method where no rational transfer function of the system is needed to determine the stability (Balchen et al., 2003). It is also possible to calculate the stability of such a system by looking at the amplitude and phase diagram for a system like (2.16). From Balchen et al. (2003) one can define  $\omega_{180}$  as the value which makes  $\angle H_0(j\omega) = -180^\circ$ . Using the  $\omega_{180}$  the system stability is determined if  $|H_0(j\omega_{180})| < 1$  holds. Based on this, a system like (2.16), if a  $H_0(j\omega)$  is found, one can calculate the stability of such a system. Here one uses the imaginary part of the complex variable  $s$  stated as  $j\omega$ , where  $\omega$  is the angular frequency and  $j = \sqrt{-1}$  the imaginary operator. This can be done for dynamical systems operating in steady state.

Stability of power systems is of high importance for systems which incorporate constant power loads due to the negative impedance instability (Emadi et al., 2006).

## 2.5 Total Harmonics Distortion

The total harmonics distortion (THD) of a signal is defined as the square root of the ratio of the sum of RMS values for all the harmonics and the RMS for the fundamental. If  $P_h$  is the power of all the harmonics in a signal  $x(t)$  and  $P_s$  is the power of the fundamental the THD is:

$$THD(x) = \sqrt{\frac{P_h}{P_s}} \quad (2.17)$$

The THD is an important property of a signal and the lower the value is, the closer the signal is to the ideal spectrum (Blagouchine and Moreau, 2011).

## 2.6 Kalman Filter

The basis for the Kalman filter (KF) was presented in Kalman (1960) with the focus on the discrete linear system as a new method of separating the signal from noise. The theory is still very much alive today with new application not only for signal and noise separation, but also as a parameter estimation tool for dynamical systems.

### 2.6.1 Discrete Kalman Filter

The problem formulation set up for the classical Discrete Kalman Filter is a state-space model like the one given in (2.18).

$$x[k+1] = Ax[k] + v[k] \quad (2.18a)$$

$$y[k] = Cx[k] + w[k] \quad (2.18b)$$

Here  $x[k]$  and  $y[k]$  are the states and measurements at time step  $k$ ,  $A$  is the system matrix relating  $x[k]$  to  $x[k+1]$  with an exact model without noise,  $C$  is the measurement matrix and  $v[k] \sim N(0, Q)$  and  $w[k] \sim N(0, R)$  are stochastic normal distributed error variables with zero mean and covariance matrices  $Q$  and  $R$ .

The objective of the KF is to minimize the diagonal on the error covariance matrix  $P[k]$  which represent the error between the estimated states and the actual state by choosing an optimal blending factor  $K[k]$  suitable for the problem statement. The  $K[k]$  is the Kalman-gain if it minimizes the error for a mean squared error estimate. The filter algorithm is provided in (2.19) given new measurements  $y[k]$  and an initial error matrix  $P[0]$  and state estimate  $\hat{x}^-[0]$ .

**Prediction:**

$$\hat{x}^-[k+1] = A\hat{x}[k] \quad (2.19a)$$

$$P^-[k+1] = AP[k]A^T + Q \quad (2.19b)$$

**Update:**

$$K[k+1] = P^-[k+1]C^T(CP^-C^T + R)^{-1} \quad (2.19c)$$

$$\hat{x}[k+1] = \hat{x}^-[k+1] + K[k+1](y[k] - C\hat{x}^-[k+1]) \quad (2.19d)$$

## 2.7 Recursive Online Parameter Estimation

Recursive online parameter estimation in its general form is given in (2.20) with the estimated parameters at each time step  $\hat{\Theta}[k]$ , a gain matrix  $K[k]$  and a regression vector  $\Psi[k]$ .

$$\hat{\Theta}[k+1] = \hat{\Theta}[k] + K[k](y[k+1] - \Psi^T[k+1]\hat{\Theta}[k]) \quad (2.20)$$

A recursive online parameter estimation algorithm based on forgetting factor  $\lambda$  where older measurements are discarded with a weight  $\lambda^k$  for time step  $k$  is shown in (2.21) with the algorithm based on the one from Ljung (1998) for single-input single-output systems.

$$\hat{\Theta}[k] = \hat{\Theta}[k-1] + K[k] \left( y[k] - \Psi^T[k] \hat{\Theta}[k-1] \right) \quad (2.21a)$$

$$Q[k] = \frac{P[k-1]}{\lambda + \Psi^T[k] P[k-1] \Psi[k]} \quad (2.21b)$$

$$K[k] = Q[k] \Psi[k] \quad (2.21c)$$

$$P[k] = \frac{1}{\lambda} \left( P[k-1] - \frac{P[k-1] \Psi[k] \Psi^T[k] P[k-1]}{\lambda + \Psi^T[k] P[k-1] \Psi[k]} \right) \quad (2.21d)$$

$$(2.21e)$$

This method works recursively by starting with an initial estimate of the  $\hat{\Theta}[0]$  and an initial error covariance matrix  $P[0]$ , and from this the procedure could run in an infinite loop by including new measurements. The method at hand works well when the assumption of white noise is correct. Else one ends up with a biased estimate. In Matlab Simulink, the algorithm is implemented in a Recursive Least Squares Estimator (RLSE) block where one specifies the estimation method recursive least squares with a forgetting factor  $\lambda$ .

## 2.8 Grid Synchronization Method

An overview of grid synchronization methods is presented in Timbus et al. (2005) where the main task of such a method is to measure the phase angle of the main voltage in the grid as accurate as possible. The state of the art for grid synchronization is to use a Phase Locked Loop (PLL). The PLL is used to track a signal by another. One implementation is to transform the three-phase signal into  $\alpha\beta$  frame and estimating the angle between  $\alpha$  and  $\beta$  component. An other is to convert the signal to the  $dq0$  frame using the Park transform where the Park transformation is defined as follows for a signal in  $abc$  frame to  $dq0$  frame:

$$\begin{bmatrix} s_d \\ s_q \\ s_0 \end{bmatrix} \sqrt{\frac{2}{3}} \begin{bmatrix} \cos(\theta) & \cos(\theta - \frac{2\pi}{3}) & \cos(\theta + \frac{2\pi}{3}) \\ -\sin(\theta) & -\sin(\theta - \frac{2\pi}{3}) & -\sin(\theta + \frac{2\pi}{3}) \\ \frac{\sqrt{2}}{2} & \frac{\sqrt{2}}{2} & \frac{\sqrt{2}}{2} \end{bmatrix} \begin{bmatrix} s_a \\ s_b \\ s_c \end{bmatrix} \quad (2.22)$$

## 2.9 Network Analysis

The transfer function  $Z(s)$ , defined in the frequency domain for a two-port system describes the relationship between voltage and current. The linear elements found in electrical circuits are the following:

- Resistor:  $R$
- Inductor:  $sL$

- Capacitor:  $\frac{1}{sC}$

Using the listed components in various parallel or series combinations complex transfer functions can be constructed. For a system operating in steady state driven by a sinusoidal with angular frequency  $\omega$  the impedances of the elements are functions of the imaginary angular frequency  $j\omega$ :

- Resistor:  $R$
- Inductor:  $j\omega L$
- Capacitor:  $\frac{1}{j\omega C}$

Given a linear transfer function  $H(s)$ , which is a rational function, the input-output relation for such a function is determined by its amplitude and phase at a given  $\omega$ . The output  $y$  of such a system, if the input is a sinusoidal as  $x(t) = A \cos(\omega t + \phi)$ , is  $y(t) = A|H(j\omega)| \cos(\omega t + \phi + \angle H(j\omega))$  when the system is in steady state. For nonlinear elements, such steady state solution may not exist, but it is possible to define the transfer function using small-signal methods.

## 2.10 Phasor Theory

The phasor carries information about the amplitude and the phase angle for a sinusoidal signal. Given a sinusoidal signal:

$$v = V \cos(\omega t + \phi) \quad (2.23)$$

This signal can be written using Euler's identity in (2.24) as the real part of such a function in (2.25).

$$e^{\pm j\theta} = \cos(\theta) \pm j \sin(\theta) \quad (2.24)$$

$$\mathbf{V} = \Re\{V e^{j\phi} e^{j\omega t}\} \quad (2.25)$$

By only keeping information about the phase one can state the phasor in polar form or rectangular form:

$$\mathbf{V} = V e^{j\phi} \quad (2.26a)$$

$$\mathbf{V} = V \cos \phi + jV \sin \phi \quad (2.26b)$$

A compact representation is only stating the amplitude and the phase angle, and is known as the angle representation:

$$V \angle \phi \equiv V e^{j\phi} \quad (2.27)$$

The phasor theory applies to linear systems operating in a steady state where all the frequencies in the response is also found in the source (Nilsson and Riedel, 2011). The

phasor carries only frequency domain information where the transient response observed in the time domain is not carried over into the phasor. Throughout this thesis, the transient response will be the brief period of a dynamic system before all the derivatives are zero and one is left with the steady state.

For phasors, the superposition principle holds for a set of phasors with the same frequency:

$$\mathbf{V} = \mathbf{V}_1 + \mathbf{V}_2 + \cdots + \mathbf{V}_n \quad (2.28)$$

When dealing with phasor dynamics, where the signal is not stationary in the time domain, there is an assumption that the phasor varies slowly and that the derivatives should be close to zero (Sun, 2009). The phasor can be stated as the information contained in a steady state sinusoidal system, where all the derivatives of such a system are zero.

## 2.11 Real-Time Systems

There is a need for defining the real-time concept since it has a broad range of definitions in literature (Burns and Wellings, 2010). Typically, it is defined as a concept for which the system reacts on the input by calculating the output inside well-defined period. One constructs deadlines for which the computation has to finish. Here one will define real-time as a system where the computational load for each time step is sufficiently low and that the computations have deterministic complexity.



## Summary of Previous Work

This thesis is a continuation of a specialization project which was done autumn 2015. The system that was used was similar to the microgrid in 7.1, but the loads were modeled as current sources with predefined harmonic components.

### 3.1 Mathematical Model

The grid is modeled in state-space form by the following differential equations with the following inputs and states where the generators are modeled as pure sinusoids. The harmonic loads are modeled as a sum of sinusoids with harmonic frequency components at the 1, 5, 7, 11 and 13 harmonics to emulate the harmonic components caused by a 6-pulse diode rectifier.

$$\dot{x} = Ax + Bu \quad (3.1a)$$

$$y = Cx \quad (3.1b)$$

$$x = [i_{s1}, i_{s2}, v_{c1}, v_{c2}, i_{mb}]^T \quad (3.1c)$$

$$u = [v_{s1}, v_{s2}, v_{load1}, v_{load2}]^T \quad (3.1d)$$

$$(3.1e)$$

$$v_{s1}(t) = A_{gen1} \sin(2\pi f_{nom}t) \quad (3.1f)$$

$$v_{s2}(t) = A_{gen2} \sin(2\pi f_{nom}t) \quad (3.1g)$$

$$i_{load1}(t) = \sum_i A_{load1,i} \sin(2\pi f_{load1,i}), \forall i \in [1, 5, 7, 11, 13] \quad (3.1h)$$

$$i_{load2}(t) = \sum_i A_{load2,i} \sin(2\pi f_{load2,i}), \forall i \in [1, 5, 7, 11, 13] \quad (3.1i)$$

$$(3.1j)$$

$$A = \begin{bmatrix} \frac{-R_{s1}}{L_{s1}} & 0 & 0 \\ 0 & \frac{-R_{s2}}{L_{s2}} & 0 \\ 0 & 0 & \frac{-R_{mb}}{L_{mb}} \end{bmatrix} \quad (3.1k)$$

$$B = \begin{bmatrix} \frac{1}{L_{s1}} & 0 & \frac{-1}{L_{s1}} & 0 \\ 0 & \frac{1}{L_{s2}} & 0 & \frac{-1}{L_{s2}} \\ 0 & 0 & \frac{1}{L_{mb}} & \frac{-1}{L_{mb}} \end{bmatrix} \quad (3.1l)$$

$$C = \mathbf{I} \quad (3.1m)$$

$$D = \mathbf{0} \quad (3.1n)$$

### 3.2 Estimating the Grid Equivalent Parameters with Augmented Kalman Filter

To estimate the parameters of the grid the system was discretized and a KF based parameter estimation method based on augmenting the state vector is given in (3.3) and with the parameters to estimate in (3.2).

$$\theta_{grid} = [R_{s1} \quad R_{s2} \quad L_{s1} \quad L_{s2} \quad R_{mb} \quad L_{mb}] \quad (3.2)$$

$$x[k+1] = \tilde{A}_x[k]\Theta[k] + V_x v_x[k] \quad (3.3a)$$

$$\Theta[k+1] = \mathbf{I}\Theta[k] + V v_\Theta[k] \quad (3.3b)$$

$$\tilde{x}[k] = [x[k]^T \quad \Theta[k]^T]^T \quad (3.3c)$$

$$\tilde{x}[k+1] = \tilde{A}\tilde{x} + V v[k] \quad (3.3d)$$

$$y[k] = C\tilde{x}[k] + R_y w[k] \quad (3.3e)$$

$$\tilde{A}_x(x, u) = \begin{bmatrix} x_1[k] & u_1[k] - u_3[k] & 0 & 0 & 0 & 0 & 0 & 0 \\ 0 & 0 & x_2[k] & u_2[k] - u_4[k] & 0 & 0 & 0 & 0 \\ 0 & 0 & 0 & 0 & x_3[k] & u_3[k] - u_4[k] & 0 & 0 \end{bmatrix} \quad (3.3f)$$

$$\tilde{A} = \begin{bmatrix} \mathbf{0} & \tilde{A}_x \\ \mathbf{0} & \mathbf{I} \end{bmatrix} \quad (3.3g)$$

$$\tilde{C} = \begin{bmatrix} \mathbf{I} & \mathbf{0} \\ \mathbf{0} & \mathbf{0} \end{bmatrix} \quad (3.3h)$$

$R_y$  is a 3x3 measurement noise matrix, and  $V$  is the 9x9 the model error matrix. A Simulink model was built to simulate the system and verify the method. In Figure 3.1 the parameters are shown when there is some measurement noise in the measurements.

The method can find the equivalent grid parameters, but the method is not general enough if the impedance model of the grid is changed. Then this linear method may not be possible to construct. The tuning process for such a system is also very painful where some tuning may not work for all operating points of the grid. This work only estimated

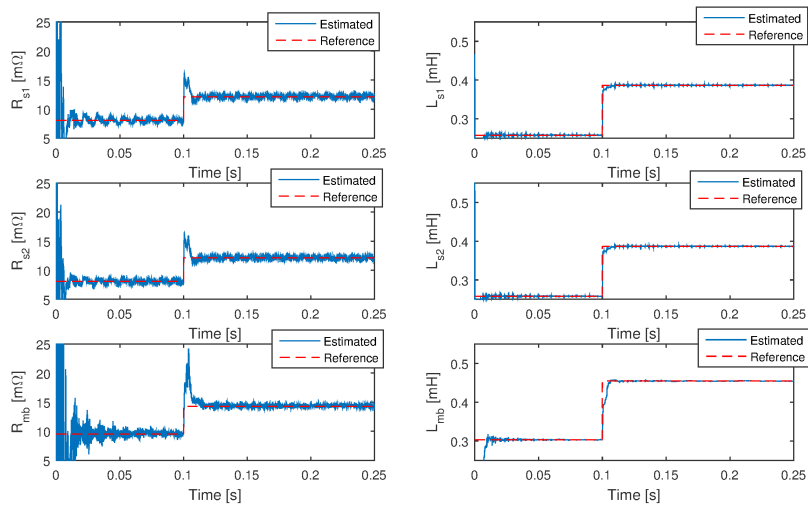


Figure 3.1: Estimated grid parameters

the parameters for the single-phase equivalent system which means that the concerns about symmetrical components with the positive and negative sequence are not part of this work.



# Harmonics Tracking Based on Kalman Filter

In this chapter, a method of tracking harmonics in a signal is presented. The method is based on Kalman theory where each harmonic is tracked with a magnitude and phase as a phasor. For single-phase signals, the method relies on Girgis et al. (1991) with an adaptive algorithm for self-tuning of the error model covariance matrix first presented in Macias and Gomez Exposito (2006). For the three-phase harmonics tracker, the model is an extension of the one presented in Sun and Sahinoglu (2011) where the authors present a method of grid synchronization based on tracking of the fundamental frequency for the positive and negative sequence using EKF. This approach is extended to track all harmonics in such a signal and combining this with the adaptive method in Macias and Gomez Exposito (2006). The three-phase harmonics tracking based on KF is the main work of the paper in Appendix B. The tracking of harmonics as phasors are a frequency domain defined problem, for which when the system is in the steady state all the derivatives are zero and the system can be described from the harmonics components at each frequency. When the system is not in steady state, the impact caused by the derivatives can play a significant role in the system for which the phasor information is not enough because of the presence of many other frequencies in the system.

The commonly applied methods relying on frequency scanning (Nagpal et al., 1998), require assumptions to be made about the signal such as the signal being stationary and periodic, where the sampling frequency is equal to the number of samples multiplied by the fundamental frequency. The Nyquist sampling theorem holds, and each frequency is an integer multiple of the fundamental frequency which will be the inverse of the window length (Girgis et al., 1991). These restrictions are rigid for this type of problem, and this is the primary motivation for developing a method to measure the harmonic components of a signal in the time domain.

## 4.1 Single-Phase Harmonics Tracking Based on Kalman Filter

The single-phase harmonics tracker is constructed by combining the KF for tracking harmonics from Girgis et al. (1991) by the adaptive algorithm for self-tuning of the model error covariance error in Macias and Gomez Exposito (2006). The tracker should be able to track fluctuations in the magnitude or phase of any harmonic component fast and with high accuracy. It is assumed that the input signal has the following form:

$$s(t) = \sum_{i=1}^n A_i(t) \cos(\omega_i t + \phi_i) \quad (4.1)$$

Here,  $A_i(t)$  is the amplitude of the  $i^{th}$  harmonic,  $\phi_i$  is the phase angle, and  $\omega_i$  is the angular frequency. By following the development in Girgis et al. (1991) this system could be stated as a linear system by defining the following state-space variables  $x_{i,1} = A_i(t) \cos(\phi_i)$  and  $x_{i,2} = A_i(t) \sin(\phi_i)$ . Then the following state vector can be constructed where all variables are functions of time.

$$\mathbf{x}[k] = [x_{1,1} \quad x_{1,2} \quad \dots \quad x_{n,1} \quad x_{n,2}]^T \quad (4.2)$$

When it is assumed that the harmonics do not change much, and the evolution follows a path similar to a random walk, then the state-space model could be written as follows:

$$\mathbf{x}[k+1] = \mathbf{I}x[k] + \mathbf{w}[k] \quad (4.3)$$

The state vector is now defined from one time step  $k$  to the next  $k+1$ .  $\mathbf{I}$  is the identity matrix and  $\mathbf{w}[k]$  is the model error input vector which is assumed to be normally distributed. The measurement equation is then given as:

$$y[k] = \mathbf{C}[k]\mathbf{x}[k] + \mathbf{v}[k] = \begin{bmatrix} \cos(\omega_1 k \Delta t) \\ -\sin(\omega_1 k \Delta t) \\ \dots \\ \cos(\omega_n k \Delta t) \\ -\sin(\omega_n k \Delta t) \end{bmatrix}^T \mathbf{x}[k] + \mathbf{v}[k] \quad (4.4)$$

Here,  $\Delta t$  is the time difference from one time step to the next. The input measurement vector  $\mathbf{v}[k]$  is also assumed to be normally distributed and one can see that the measurement matrix is time-varying with a known function.

The KF implementation is based on Macias and Gomez Exposito (2006) with an algorithm called Adaptive Kalman Filter (AKF) where the original algorithm is given in Appendix F.1. If one should implement a basic KF for this model, one have to provide the system model error covariance matrix  $\mathbf{Q}$  and the measurement error covariance matrix  $\mathbf{R}$ . The measurement matrix  $\mathbf{R}$  is directly related to the noise in the sensors which is possible to estimate from a physical system. The model error covariance matrix  $\mathbf{Q}$  is not linked to the sensor, but rather how fast the harmonics vary with time and deviates from the state transition matrix  $\mathbf{A} = \mathbf{I}$ . The assumption is that the harmonics from one time step to the next is a random walk with zero mean and covariance  $\mathbf{Q}$ . This assumption is accurate if

the harmonics do not vary much, but if they do, the model covariance matrix has to be modeled with this taken into account. For a general system where one can not assume a particular property of the signal, a method for adaptive updating the model covariance matrix is proposed in Macias and Gomez Exposito (2006). In Algorithm 1 the AKF is stated by adapting the algorithm in Macias and Gomez Exposito (2006) to include a maximum number of iterations and modifying the stopping criterion to be defined for a range of harmonics.

```

 $q^- = q[k-1];$ 
 $\mathbf{Q}[k] = q^- \mathbf{I};$ 
while  $i \leq N$  do
     $\mathbf{P}^-[k] = \mathbf{A}\mathbf{P}[k-1]\mathbf{A}^T + \mathbf{Q}[k];$ 
 $\mathbf{K}[k] = \mathbf{P}^-[k]\mathbf{C}[k]^T(\mathbf{C}[k]\mathbf{P}^-[k]\mathbf{C}[k]^T + \mathbf{R})^{-1};$ 
 $\hat{x}[k] = \hat{x}^-[k] + \mathbf{K}[k](y[k] - \mathbf{C}[k]\hat{x}^-[k]);$ 
 $\hat{w}[k] = \mathbf{K}[k](y[k] - \mathbf{C}[k]\hat{x}^-[k]);$ 
 $q = \sum_i \hat{w}_i[k]^2;$ 
    if  $|q| - |q^-| < \epsilon$  then
        break;
    end
     $\mathbf{Q}[k] = q\mathbf{I};$ 
 $q^- = q;$ 
 $i+ = 1;$ 
end
 $\mathbf{P}[k] = (\mathbf{I} - \mathbf{K}[k]\mathbf{C}[k])\mathbf{P}^-[k];$ 

```

**Algorithm 1:** AKF algorithm

Using this model the estimated error in the last time step  $\hat{w}[k]$  is used to calculate the next time step model error covariance matrix  $\mathbf{Q}$  which is calculated as a norm of the components of the estimated time step error. Using such a KF variation, the filter reacts quicker to transient changes in the signal. The filter will be easier to tune and will be, based on the authors, better at tracking harmonics.

From the state-space variables, the phasor for each harmonic component is found by calculating the magnitude and phase, and based on these variables constructing the complex phasor  $X_i$  in (4.5).

$$A_i = \sqrt{x_{i,1}^2 + x_{i,2}^2} \quad (4.5a)$$

$$\phi_i = \arctan\left(\frac{x_{i,2}}{x_{i,1}}\right) \quad (4.5b)$$

$$X_i = A_i e^{j\phi_i} \quad (4.5c)$$

### 4.1.1 Single-Phase Harmonics Tracker Implementation

The AKF for single-phase is implemented as a Matlab Simulink model shown in Figure C.1. The inputs to the system are the single-phase signal, assumed to have the same form as in (4.1), and the angular frequency multiplied with the time  $\omega t$ . The outputs are measured phasors  $X_i$ . The measurement matrix is implemented as a Matlab Function in Appendix D.2 and the parameters for the AKF block are gathered in a Matlab struct which is created by calling the function *single\_adaptive\_kalman\_struct(...)* which is given in Appendix D.5. The adaptive algorithm is the same for the three-phase system and the single-phase system and implemented as a Matlab Function in Appendix D.1. To calculate the phasor  $X_i$ , a Matlab Function in Appendix D.4 is implemented. The initialization method for the tracker is given in Appendix D.5 with the parameters for the tracker is given in Table 4.1 where a brief description is given.

Parameter	Brief description
$P_0$	Initial error covariance matrix
$R$	Measurement covariance matrix
$Q_0$	Initial input covariance matrix
$x_0$	Initial state
$H$	Set of harmonics to measure
$\epsilon_A$	Stopping criterion adaptive updating $Q$
$N_{max}$	Max iterations per time step

**Table 4.1:** Description of AKF parameters

## 4.2 Three-Phase Harmonics Tracking Based on Kalman Filter

The three-phase harmonic tracker is also based on the same AKF as in the single-phase harmonics tracker. The method builds on the work from Macias and Gomez Exposito (2006) where the AKF is introduced. In Sun and Sahinoglu (2011) a method for tracking the angular frequency  $\omega$  for a Smart Grid is proposed by following the positive and negative sequence fundamental frequency for a three-phase system. By restating the problem to track all harmonics and assume that the angular frequency is known, tracking of positive and negative sequence harmonics can be done with inspiration from the work in that paper. The development for such a tracker is given in this section.

Given a three-phase signal in the  $abc$  frame in (4.6) where  $\omega(t)$  is the angular frequency which is assumed to be known,  $A_a(t), A_b(t), A_c(t)$  are the amplitude for each of the phases,  $\phi_a, \phi_b, \phi_c$  are the initial phase angle for each phase, and  $\omega = 2\pi f$  is the angular frequency, and one define  $\theta_i(t) = \omega t + \phi_i$  for each phases  $i \in a, b, c$ .

$$S_a(t) = A_a(t)\cos(\omega(t)t + \phi_a(t)) \quad (4.6a)$$

$$S_b(t) = A_b(t)\cos(\omega(t)t + \phi_b(t)) \quad (4.6b)$$

$$S_c(t) = A_c(t)\cos(\omega(t)t + \phi_c(t)) \quad (4.6c)$$

In a balanced system, there is a relationship between the phase angles by stating them as time-invariant given by  $\phi_b = \phi_a - \frac{2\pi}{3}$  and  $\phi_c = \phi_a + \frac{2\pi}{3}$ , and for the amplitudes  $A_a = A_b = A_c = A$ . In an unbalanced system, no such assumptions can be made and one ends up with six variables for each time instant by stating the system in  $abc$  frame for tracking the components of such a signal. In order to reduce the number of variables, the unbalanced three-phase system is transformed into three balanced systems named the positive, negative and zero sequence by using the Fortescue Theorem Fortescue (1918). The system of the three balanced systems is given in (4.7).

$$S_a = S_{a,p} + S_{a,n} + S_{a,0} \quad (4.7a)$$

$$S_b = S_{b,p} + S_{b,n} + S_{b,0} \quad (4.7b)$$

$$S_c = S_{c,p} + S_{c,n} + S_{c,0} \quad (4.7c)$$

The unbalanced system  $S_{abc} = [S_a, S_b, S_c]^T$  is now stated as three balanced systems  $S_p = [S_{a,p}, S_{b,p}, S_{c,p}]^T$ ,  $S_n = [S_{a,n}, S_{b,n}, S_{c,n}]^T$  and  $S_0 = [S_{a,0}, S_{b,0}, S_{c,0}]^T$ . By using the phase sequence, one can state this problem in time domain form in (4.8) by using  $\theta_p = \omega t + \phi_p$  and  $\theta_n = \omega t + \phi_n$ .

$$\begin{bmatrix} S_a(t) \\ S_b(t) \\ S_c(t) \end{bmatrix} = S_p \begin{bmatrix} \cos(\theta_p(t)) \\ \cos(\theta_p(t) - \frac{2\pi}{3}) \\ \cos(\theta_p(t) + \frac{2\pi}{3}) \end{bmatrix} + S_n \begin{bmatrix} \cos(\theta_n(t)) \\ \cos(\theta_n(t) + \frac{2\pi}{3}) \\ \cos(\theta_n(t) - \frac{2\pi}{3}) \end{bmatrix} + S_0 \begin{bmatrix} 1 \\ 1 \\ 1 \end{bmatrix} \quad (4.8)$$

This signal is transformed using the Clarke transform to the  $\alpha\beta 0$  stationary frame with the transformation defined in (4.9).

$$\mathbf{T}_{\alpha\beta 0} = \begin{bmatrix} \frac{2}{3} & \frac{-1}{3} & \frac{-1}{3} \\ 0 & \frac{1}{\sqrt{3}} & \frac{-1}{\sqrt{3}} \\ \frac{1}{2} & \frac{1}{2} & \frac{1}{2} \end{bmatrix} \quad (4.9)$$

The three-phase signal in  $S_{\alpha\beta 0}$  is obtained by using the defined transformation (4.10).

$$S_{\alpha\beta 0}(t) = \mathbf{T}_{\alpha\beta 0} S_{abc}(t) \quad (4.10)$$

This transformation is useful because, if the system is balanced, the zero component will always be reduced to zero. Applying the  $T_{\alpha\beta 0}$  transformation on the system in (4.8) one obtains the following:

$$S_{\alpha\beta 0} = \mathbf{T}_{\alpha\beta 0} S_{abc} = \mathbf{T}_{\alpha\beta 0} S_p \begin{bmatrix} \cos(\theta_p) \\ \sin(\theta_p) \\ 0 \end{bmatrix} + \mathbf{T}_{\alpha\beta 0} S_n \begin{bmatrix} \cos(\theta_n) \\ -\sin(\theta_n) \\ 0 \end{bmatrix} + \mathbf{T}_{\alpha\beta 0} S_0 \begin{bmatrix} 0 \\ 0 \\ 0 \end{bmatrix} \quad (4.11)$$

By inspection of (4.11) one sees that all the zero components are zero, because of the assumption that the Fortescue's theorem holds. The reduced model with only the  $\alpha$  and  $\beta$  components is shown in (4.13) with the use of the reduced Clarke Transform as shown in (4.12).

$$\mathbf{T}_{\alpha\beta} = \begin{bmatrix} \frac{2}{3} & \frac{-1}{3} & \frac{-1}{3} \\ 0 & \frac{1}{\sqrt{3}} & \frac{-1}{\sqrt{3}} \end{bmatrix} \quad (4.12)$$

$$S_{\alpha\beta} = \mathbf{T}_{\alpha\beta} S_{abc} = \mathbf{T}_{\alpha\beta} S_p \begin{bmatrix} \cos(\theta_p) \\ \sin(\theta_p) \end{bmatrix} + \mathbf{T}_{\alpha\beta} S_n \begin{bmatrix} \cos(\theta_n) \\ -\sin(\theta_n) \end{bmatrix} \quad (4.13)$$

By remembering that  $\theta_p = \omega t + \phi_p$  and  $\theta_n = \omega t + \phi_n$  and using the sum and difference formulas for trigonometric functions,

$$\sin(a \pm b) = \sin(a)\cos(b) \pm \cos(a)\sin(b) \quad (4.14a)$$

$$\cos(a \pm b) = \cos(a)\cos(b) \mp \sin(a)\sin(b) \quad (4.14b)$$

one can write the (4.13) as (4.15). Here, all the harmonics of the system are included into one equation. By stating the fundamental angular frequency of the grid as  $\omega$ , other harmonics, but not limited to natural numbers  $i$ , have an angular frequency  $\omega i = i\omega$ . Here  $A_{i,p}$  and  $A_{i,n}$  are the magnitudes of the positive and negative sequence respectfully at the harmonic  $i$ .  $\phi_{i,p}$  and  $\phi_{i,n}$  are the initial phase angles for the positive and negative sequence for harmonic number  $i$ .

$$\begin{bmatrix} S_\alpha(t) \\ S_\beta(t) \end{bmatrix} = \sum_{i \in h_p} \begin{bmatrix} \cos(i\omega t) & -\sin(i\omega t) \\ \sin(i\omega t) & \cos(i\omega t) \end{bmatrix} \begin{bmatrix} A_{i,p} \cos(\phi_{i,p}) \\ A_{i,p} \sin(\phi_{i,p}) \end{bmatrix} + \sum_{i \in h_n} \begin{bmatrix} \cos(i\omega t) & -\sin(i\omega t) \\ -\sin(i\omega t) & -\cos(i\omega t) \end{bmatrix} \begin{bmatrix} A_{i,n} \cos(\phi_{i,n}) \\ A_{i,n} \sin(\phi_{i,n}) \end{bmatrix} \quad (4.15)$$

$S_i \cos(\phi_i)$  and  $S_i \sin(\phi_i)$  in (4.15) are written as  $x_{i,1}$  and  $x_{i,2}$  to make the formulation suitable for AKF. Using this formulation, one has separated the time-varying  $\omega t$  from the slowly varying part of the magnitude and the initial phase angle. The state-space and measurement equations are given in (4.16) and (4.17) which estimate the states  $x_{i,1}$  and  $x_{i,2}$  in which the states have information about the phase angle and amplitude of each harmonic number  $i$  which is analyzed by the AKF. The same AKF algorithm as for the single-phase case in Algorithm 1 is used.

$$y[k] = \sum_{h \in h_p} \begin{bmatrix} \cos(i\omega\Delta tk) & -\sin(i\omega\Delta tk) \\ \sin(i\omega\Delta tk) & \cos(i\omega\Delta tk) \end{bmatrix} \begin{bmatrix} x_{i,1} \\ x_{i,2} \end{bmatrix}_k + \sum_{i \in h_n} \begin{bmatrix} \cos(i\omega\Delta tk) & -\sin(i\omega\Delta tk) \\ -\sin(i\omega\Delta tk) & -\cos(i\omega\Delta tk) \end{bmatrix} \begin{bmatrix} x_{i,1} \\ x_{i,2} \end{bmatrix}_k \quad (4.16)$$

$$\begin{bmatrix} x_{i,1} \\ x_{i,2} \end{bmatrix}_{k+1} = \begin{bmatrix} 1 & 0 \\ 0 & 1 \end{bmatrix} \begin{bmatrix} x_{i,1} \\ x_{i,2} \end{bmatrix}_k \quad (4.17)$$

In the AKF, one can define the size of the system  $N$  as the twice the number of positive and negative harmonics. Then the  $\mathbf{A}$  is a  $N \times N$  system matrix,  $\mathbf{C}$  is a  $2 \times N$  measurement matrix. The  $\mathbf{Q}$  is a  $N \times N$  adaptively updated covariance matrix which is initialized to the zero matrix.  $\mathbf{R}$  is a  $2 \times 2$  measurement error matrix which needs to be tuned in agreement with the measurement noise of the system.

From the  $x_{i,1}$  and  $x_{i,2}$  the magnitude and phase angle are calculated in the same way as in (4.5) for the single-phase case and one obtains a complex phasor with the magnitude and phase angle information for each harmonic component.

### 4.2.1 Three-Phase Harmonics Tracker Implementation

The AKF Matlab Simulink model is shown in Figure C.2. Inputs to the block are the signal in the  $\alpha\beta$  frame from which the harmonic components for each of the defined harmonics should be extracted, and the  $wt$  input port which is the angular frequency of the fundamental harmonic multiplied with time.

The parameters for the AKF block are gathered in a Matlab struct which is created by calling the function *three\_adaptive\_kalman\_struct(...)* which is given in Appendix D.6. The parameters are presented in Table 4.2 with a brief description for each parameter is given. For the sets of the harmonics  $H_p$  and  $H_n$ , the angular frequency is given by  $\omega_p = H_p w$  and  $\omega_n = H_n w$ . The calculation of the measurement matrix is implemented as a Matlab function in Appendix D.3.

Parameter	Brief description
$P_0$	Initial error covariance matrix
$\mathbf{R}$	Measurement covariance matrix
$Q_0$	Initial input covariance matrix
$x_0$	Initial state
$H_p$	Set of positive sequence harmonics to measure
$H_n$	Set of negative sequence harmonics to measure
$\epsilon_A$	Stopping criterion adaptive updating $Q$
$N_{max}$	Max iterations per time step

**Table 4.2:** Description of AKF parameters

### 4.3 Performance Testing of the Three-Phase Tracking Method

In this section, a deterministic signal is used as input for the AKF to verify that the filter has the desired performance properties. It is desired that the filter can track harmonics with fluctuations which can happen during faults or when there are new components connected to the grid. In Experiment 1, there are no measurement noise or non-modeled harmonics. In Experiment 2, noise and non-modeled harmonics are added and in Experiment 3 the objective is to know how well the filter behaves when there is a deviation between the angular frequency of the signal and what the filter expects.

To compare the AKF with the linear KF a system based on the linear KF is also built, where the Matlab Simulink implementation of a KF as a block function from the Control System Toolbox is used. The results for the linear KF implementation are found in Appendix E.

The generator for the positive sequence signal in the  $abc$  frame is given in Figure C.4. The negative sequence is created by changing the bias for each phase from  $[0, -\frac{2\pi}{3}, \frac{2\pi}{3}]$  to  $[0, \frac{2\pi}{3}, -\frac{2\pi}{3}]$ . By providing an input signal to the frequency, phase angle or magnitude port, the three-phase output signal is created. The base frequency  $f_{nom}$  is set to 50Hz and the frequency of the harmonics is stated relatively to this frequency.

The error at each time step is defined as the sum of difference of each estimated harmonic from the reference, squared and taken the square root for the magnitude and phase. The magnitude from the estimation is  $|\hat{H}_i|$  for each harmonic  $i$  and the reference  $H_i$ ; then the error is per time step is:

$$|E_i| = \sqrt{\sum_{\forall i} (|\hat{H}_i| - |H_i|)^2} \quad (4.18)$$

For the phase angle the error is defined in a similar way:

$$\angle E_i = \sqrt{\sum_{\forall i} (\angle \hat{H}_i - \angle H_i)^2} \quad (4.19)$$

#### 4.3.1 Experiment 1: Tracking Without Noise

The signal has no noise; all harmonics are modeled. The AKF block is initialized with the parameters in Table 4.3.

A reference signal to vary the magnitude and phase angle of the harmonic components are created as an input for the sequence generator in Figure C.4. The phasor for the positive sequence harmonics are  $\mathbf{H}_p$  and for the negative sequence  $\mathbf{H}_n$ . The angular frequency is for the sets  $H_p$  and  $H_n$  equal to  $\omega_p = 2\pi f_{nom} H_p$  and  $\omega_n = 2\pi f_{nom} H_n$ . The initial parameters are given in Table 4.4. The system is simulated for 350 time steps and with a step change in the magnitude of the positive harmonic components down to zero at time step 100, and then back up again at the time step 150. The phase angle is set accordingly to the Table 4.4 and the phase angle reference set down to zero at time step 200 and back up again at time step 250. The results are shown in Figure 4.1 for the AKF and Figure E.3 for the KF. Both filter implementations are able to track such a signal with good accuracy and decent time response.

Parameter	Value
$H_p$	[1, 3, 5]
$H_n$	[7, 3, 10]
$\mathbf{P}_0$	$1 \times 10^3 \mathbf{I}$
$\mathbf{R}$	$1 \times 10^{-4} \mathbf{I}$
$\mathbf{Q}_0$	$\mathbf{0}$
$\mathbf{x}_0$	$\mathbf{0}$
$\epsilon_A$	$1 \times 10^{-5}$
$N_{max}$	10

**Table 4.3:** Initialization of the AKF parameters for Experiment 1

Parameter	Value
$\mathbf{H}_p$	[50∠1, 30∠10, 20∠−30]
$\mathbf{H}_n$	[15∠5, 25∠40, 35∠−60]
$\omega_p$	$2\pi f_{nom}$ [1, 3, 5]
$\omega_n$	$2\pi f_{nom}$ [3, 7, 10]

**Table 4.4:** Reference harmonics signal

### 4.3.2 Experiment 2: Noise and Non-Modeled Harmonics

In this experiment, non-modeled harmonics and measurement noise will also be added to the system. The system is simulated for 500 time steps. A positive harmonic component at the 4th harmonic with the magnitude set to 5 and phase angle to 0 and a negative sequence harmonic at the 9th harmonic with the magnitude set to 10 and phase angle set to 0 is added from time step 0 to 100 and from 200 to 500. A measurement noise is added to each of the phases with variance on 10 for both the  $\alpha$  and the  $\beta$  component. The  $\mathbf{R}$  matrix is set to the diagonal matrix with 100 on its diagonal. The results are shown in Figure 4.2 for the AKF, in Figure E.4 for the KF with a static  $\mathbf{Q} = \mathbf{I}$  and in Figure E.5 for the KF with  $\mathbf{Q} = 1 \times 10^{-3} \mathbf{I}$ .

Sample set [ <i>from</i> , <i>to</i> ]	Noise Process
[0, 100]	Non-modeled harmonics
[100, 200]	Measurement noise
[200, 500]	Non-modeled and noise
[350, 400]	$\mathbf{H}_p = 0 \angle 0$

**Table 4.5:** Test 2 setup

Based on the result the AKF can track such a signal influenced by non-modeled harmonics and measurement noise when there is a sudden change in the signal. The KF can track the stationary signal given no sudden variations with appropriate tuning of the  $\mathbf{Q}$  matrix. However, when tuning the filter to follow the signal without sudden changes, the filter will perform with a very slow response when an abrupt variation in the signal is present as shown in Figure E.5. When tuning the filter to track the sudden change in Figure E.4 the

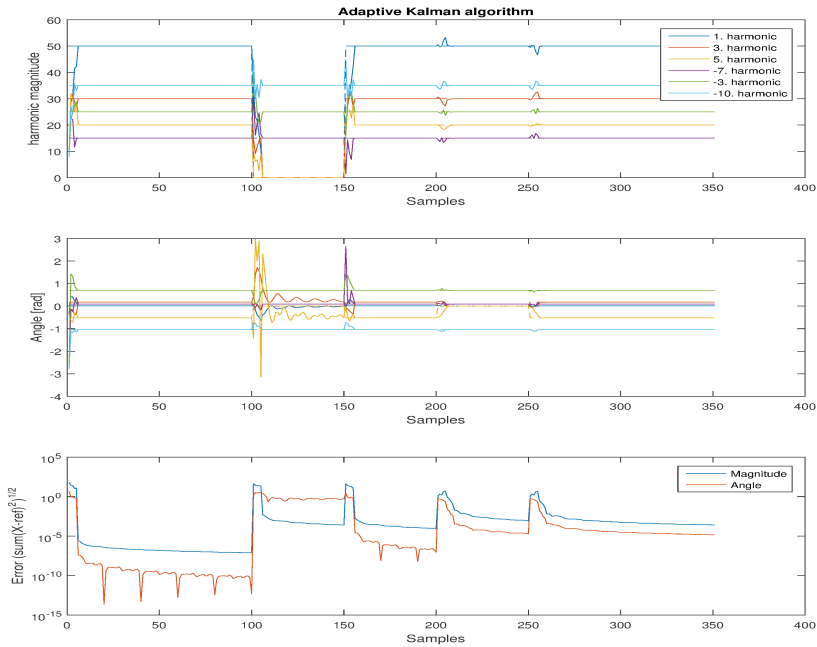


**Figure 4.1:** Experiment 1: Magnitude, phase angle and error for the AKF

filter will not track the stationary signal with high accuracy but have a faster tracking dynamic when the signal is changing rapidly. In Figure 4.3 the  $q_a$  evolution is shown where  $\mathbf{Q} = q_a \mathbf{I}$ . Based on the AKF for experiment 2 of such a signal, there are multiple optimal  $\mathbf{Q} = q \mathbf{I}$  tuning values based on which noise process is present. Based on Figure 4.3 a table of optimal  $q$  values can be defined in Table 4.6.

Sample set [ <i>from</i> , <i>to</i> ]	Optimal $q$
[0, 100]	$2 \times 10^{-2}$
[100, 200]	$3 \times 10^{-4}$
[200, 500]	$2 \times 10^{-3}$
350	1
450	1

**Table 4.6:** Optimal  $q$  for experiment 2

In Table 4.6 one can see that there is a considerable variation in the optimal  $q$  value for a simple experiment like the one in Experiment 2. Based on this there will be a difficult task to tune the KF for such a signal.

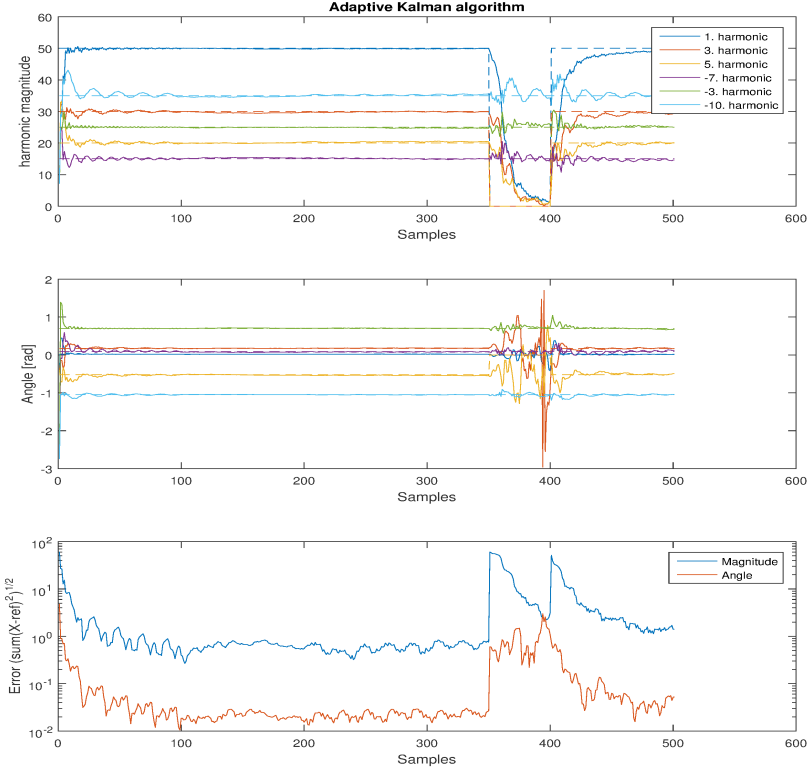


**Figure 4.2:** Experiment 2: Magnitude, phase angle, and error for the AKF

### 4.3.3 Experiment 3: Tracking with Angular Frequency Deviation

The objective of Experiment 3 is to know how deviation from the estimated angular frequency of the 1st harmonic  $\hat{\omega}$  to the angular frequency of the signal  $\omega$  is propagated to the estimation result. This is to know how the desired accuracy for frequency measurement devices such as PLL for the AKF and KF to measure the harmonics with sufficient precision. In this experiment, the same harmonics as in Experiment 1 are used, with no measurement noise nor non-modeled harmonics. The angular frequency is increased in steps of 0.1% increments from 98% of the modeled angular frequency to 102%.

The results are shown in Figure 4.4, Figure E.6 and Figure 4.5. In this setup, there is not much difference between the AKF and KF method. The phase reference for this experiment is for each harmonic component  $\angle \check{\mathbf{H}}_i$  with harmonic number  $i$  is given below.

$$\angle \check{\mathbf{H}}_i = i \int \omega - \hat{\omega} dt + \angle \mathbf{H}_i \quad (4.20)$$

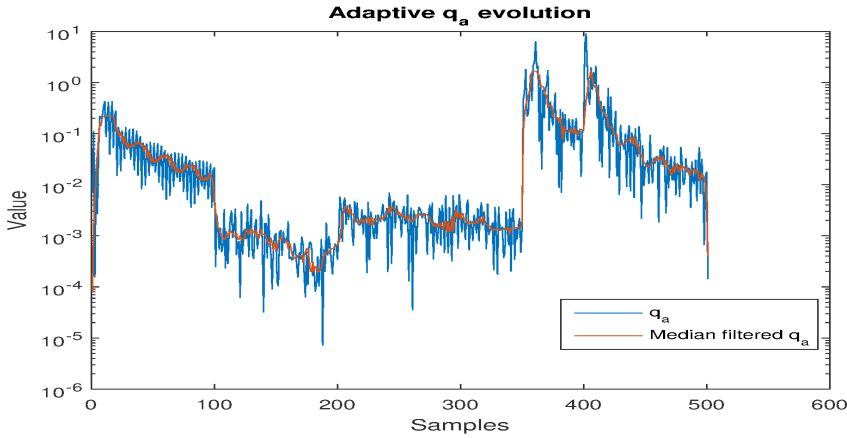


**Figure 4.3:** Evolution of  $q_a$  per sample and the median filtered  $q_a$  for 10 samples

In Figure 4.4 one can see that the measurement of the magnitude is done with decreasing accuracy with higher frequency deviation. The measurement of the phase angle is not much affected by frequency difference for following the reference, but the reference is here also a function of the frequency deviation which means it is not possible to detect the phase angle  $\angle H$  without making any changes to the algorithm.

In Figure 4.6 the frequency deviation is in the range from -10% to 10% with 0.1% increments. A linear regression line is fitted to the error with the assumption of a linear relation given by  $e = \beta_0 + \beta_1 \hat{f}$  with  $\hat{f}$  is the deviation from the frequency in %. The regression gives  $\beta_0 = 0.32$  and  $\beta_1 = 1.60$  for AKF and  $\beta_0 = -0.02$  and  $\beta_1 = 1.42$  for KF.

## 4.4 Discussion

In these experiments, one can see that the AKF and the KF very efficiently measure the harmonic positive and negative components of a three-phase signal in the  $\alpha\beta$  frame with no noise or non-modeled harmonics. When adding noise and harmonics, the AKF is developed to cope with this by adapting the model error covariance matrix  $\mathbf{Q}$  to the filter depending on the error in the model. As shown in Figure 4.3 one can see that there are significant variations in which  $q_a$  value that is appropriate to minimize the error of the filter. The stopping criterion for the AKF also needs to be determined to have a deterministic calculation time for the system to be implemented in a real-time setting. The main argument for using the AKF instead of the KF is that one would like to use the filter regardless of what one can assume of the signal in the sense of noise, rapid changes, or non-modeled harmonics. In a microgrid system, however, if the magnitude changes the derivatives are not equal to zero and the proposed method may not be able to measure harmonics with the desired accuracy.

During faults, there may be rapid changes in the signal for some of the harmonics on one or more symmetrical component. This kind of faults will be captured by this method

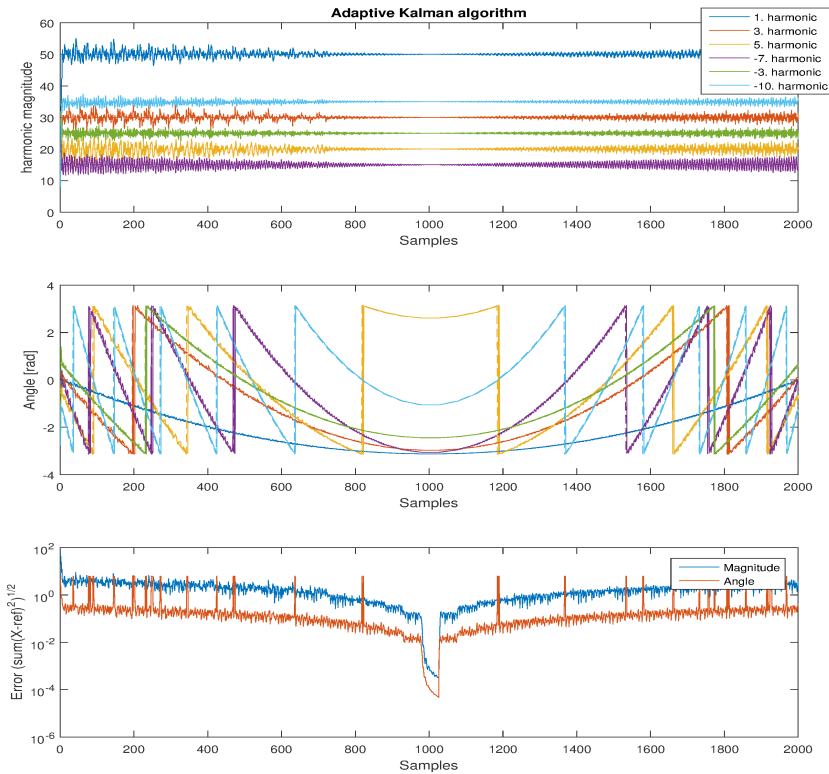


**Figure 4.4:** Experiment 3: Magnitude, phase angle and error for the AKF

because it naturally describes the system by its symmetrical components. The harmonic estimation, however, requires that the system is in the steady state and with the presence of large changes in a dynamic system there are transients and the derivatives are far from zero. In this system, as it is not a dynamic system but rather a generated signal without dynamics, the presence of transients remains untested.

Even though the proposed method works well for measuring harmonics in steady state, there is room for improvements. From Figure 4.4 one can see that even with a deviation in the angular frequency, the method can track the phase angle. To track the amplitude part of the phasor, the system needs an accurate frequency estimation. From phase tracking capabilities, one could argue that it would be possible to let the harmonics tracker estimate the angular frequency and by this, the method would be more self-sustained. The frequency estimation is done in Sun and Sahinoglu (2011) where the authors propose to use an Extended Kalman Filter where one of the states is the estimated angular frequency. If one would implement a system for measuring the angular frequency for the fundamental, this could lead to an additional improvement where the method could add more harmonics to

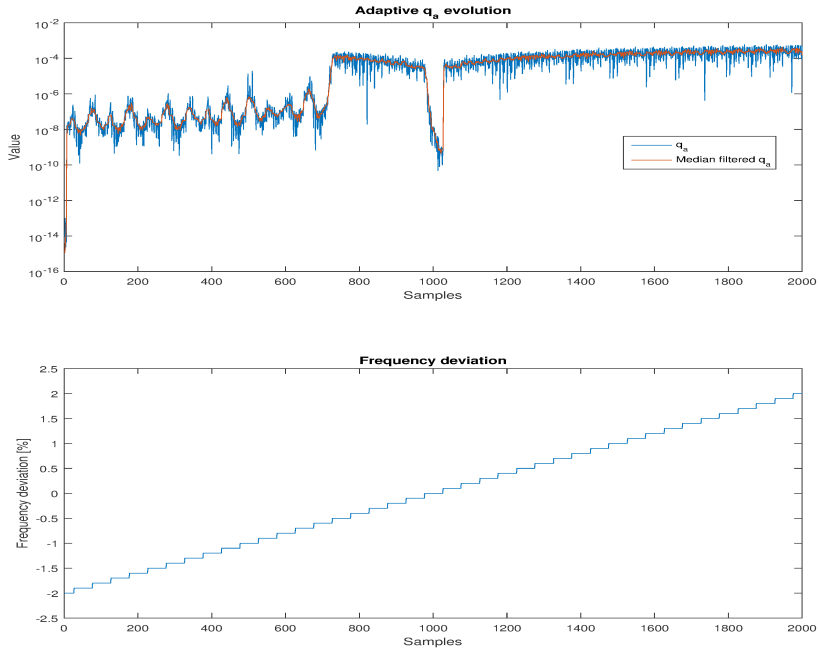


**Figure 4.5:** Evolution of  $q_a$  per sample and the median filtered  $q_a$  for 10 samples and the frequency deviation for each sample

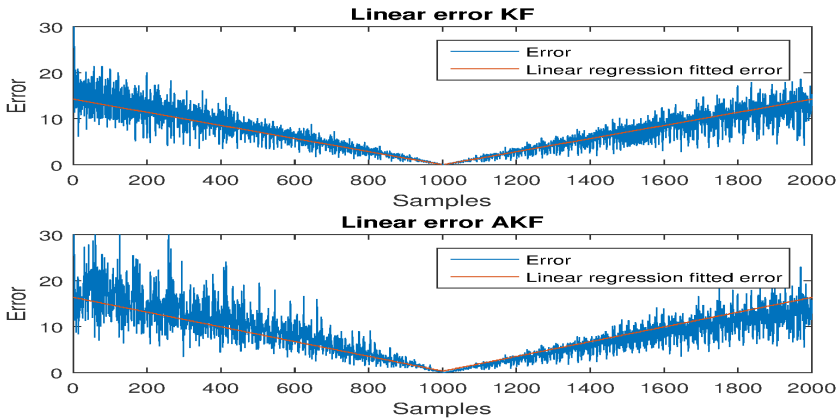


**Figure 4.6:** Linear error with increased frequency deviation

measure on the fly. How this could be done will not be discussed any further but a puzzle for future work.

## Proposed Method

This chapter is a detailed walkthrough of the proposed method to estimate parameters for AC side linear impedance and DC side impedance where the AC side and the DC side is separated by a three-phase full wave rectifying device. The two main components that will be described are:

- AC side parameter estimator
- DC side parameter estimator

The main stage of these elements is the harmonics analyzer which consists of an AKF implementation for tracking harmonics in a three-phase signal for the positive and negative sequence for the three-phase case, and the same AKF but for single-phase in the single-phase case presented in Chapter 4. First, the AC side real-time parameter estimator will be described, then the similar one for the DC side.

The time domain property of a KF is important, and another desired feature of the proposed measurement is that it is possible to do the impedance measurement in a non-invasive way. For an isolated microgrid structure, it can be costly to implement a frequency scanning injection device in the system. More equipment usually means more equipment which can fail. If the microgrid is a complex structure, the perturbation has to be done in multiple areas of the grid which may not be feasible to implement. These motivate for doing an analysis in a non-invasive way based on the present information in the system. One possible solution for system implementation is to do extensive impedance estimation by frequency scanning of the microgrid during production, and in use, the microgrid is monitored by a non-invasive measurement method like the one proposed. This approach can be utilized for online calculation of the impedances of a grid where the parameters vary with time due to aging or temperature rise. This information is useful for detecting irregularities in the grid operation, optimal tuning of grid-connected devices and stability.

## 5.1 AC Side Real-Time Parameter Estimator

In Figure 5.1 a flowchart of AC side parameter estimator is shown. The system has two main inputs for three-phase voltage and three-phase current, and the impedance parameters as output. The main processing stages are listed below and will be described more in detail later in this chapter.

- Pre-processing
- Three-phase harmonics analyzer
- Phase correction
- Complex division per harmonic component
- Parameter estimation

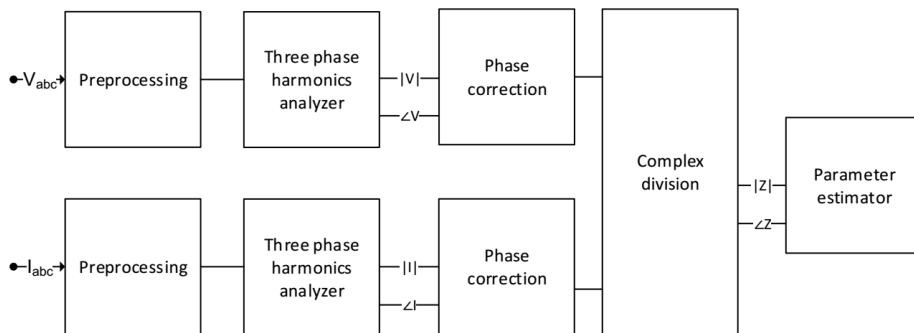


**Figure 5.1:** AC side real-time parameter estimator

### 5.1.1 Pre-Processing

The pre-processing stage consists of low-pass filtering the input voltage and current signal, down sampling and transforming the signal into  $\alpha\beta$  frame with the use of the Clarke transform.

#### Low-Pass Filtering

Based on the theory about the line-commuted rectifier loads, the loads will create higher harmonic disturbances. A low-pass filter is added before the AKF to attenuate high frequencies. Each phase of the signal in the  $abc$  frame is low-pass filtered using a low-pass block from the Digital Signal Processing Toolbox in Simulink. This block implements a low-pass filter where the type is Finite Impulse Response (FIR) filter and designed to have a minimum phase for linear phase response in the passband for easy phase correction.

### 5.1.2 Three-Phase Harmonics Analyzer

The three-phase harmonics analyzer is presented in Section 4.2. For each AC side parameter estimator it is used two three-phase harmonics analyzers where one is for input voltage and the other for current, where they come from the low-passed signal in the  $\alpha\beta$  frame. The other input is the angular frequency times the time  $\omega t$  which could be estimated using, for instance, a PLL or assumed to be a constant multiplied with the time.

### 5.1.3 Phase Correction

Because of the pre-processing stage where one of the operations is to low-pass filter the signal, the phase angle of the measured phasor is not correct with the input signal because of the phase response of the low-pass filter. The phase angle is then corrected by calculating of the phase response of the low-pass filter and making the inverse response for each harmonic component with a Simulink model built as shown in Figure C.5. Because it is used a low-pass filter with linear phase in the passband of the filter, the response is a linear function of frequency. Given that the linear phase response is described by:

$$H_{LP}(f) = C_{LP}f \quad (5.1)$$

The phase correction coefficient is  $C_{LP}$  for frequency  $f$ . The estimated phase corrected phase angle  $\theta_{ph}(f)$  at frequency  $f$  from an estimated phase angle  $\theta(f)$  is calculated by the following equation where the phase is corrected to the range of  $[0, 2\pi]$ :

$$\theta_{ph}(f) = (\theta(f) - H_{LP}(f)) \mod 2\pi \quad (5.2)$$

### 5.1.4 Complex Division per Harmonic Component

Impedance in the frequency domain is defined as the complex division of voltage by current for phasors at the same frequency as follows:

$$Z(\omega) = \frac{V(\omega)}{I(\omega)} \quad (5.3)$$

This is valid for linear elements when in steady state. The output will be a new phasor with magnitude and phase for a given frequency.

### 5.1.5 Parameter Estimation

The parameter estimation block estimates the impedance parameters from the measured impedance phasors. Given a set of measured phasors, an impedance model is constructed. This stage is implemented using RLSE blocks from the System Identification Toolbox for Matlab Simulink. This block is an implementation of the Recursive Online Parameter Estimation problem defined in Section 2.7. To use this method, one has to define an impedance model which in some sense is linear with the parameters, usually for linear circuits the parameters together with the angular frequency is linear with the impedance. For instance, the line impedance in microgrids usually is modeled as a series inductor  $L$

and resistor  $R$  where the impedance is defined as  $Z_{RL}(\omega) = j\omega L + R$  where the regression vector  $[j\omega, 1]$  is linear with the parameter vector  $[L, R]$ . In cases where such a relationship is found, methods based on least squares will be a very well known method to extract the parameters.

## 5.2 DC Side Real-Time Parameter Estimator

For the DC side parameter estimation the similar flowchart is shown in Figure 5.2 which has the same inputs and outputs as the previous component. The similar processing stages are listed below.

- Pre-processing
- Single-phase harmonics analyzer
- Phase correction
- Complex division per harmonic component
- Parameter estimation

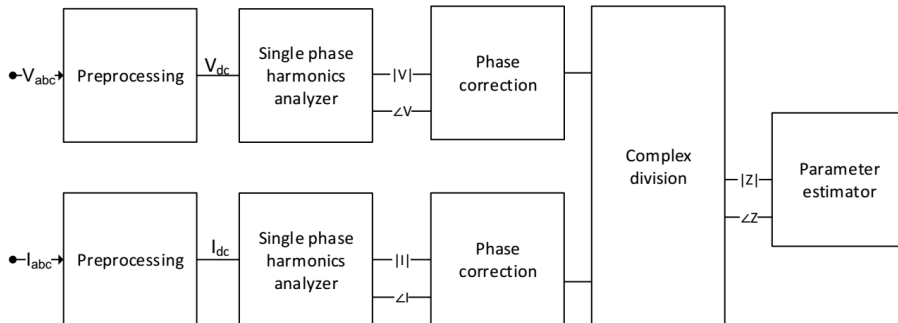


Figure 5.2: DC side real-time parameter estimator

### 5.2.1 Pre-Processing

The first step for the DC side parameter estimator is to estimate the DC side voltage and current from the AC side three-phase input voltage and current. Given a three-phase system with voltage

$$v_{abc}(t) = [v_a(t) \quad v_b(t) \quad v_c(t)]^T \quad (5.4)$$

and three-phase current:

$$i_{abc}(t) = [i_a(t) \quad i_b(t) \quad i_c(t)]^T \quad (5.5)$$

The DC side voltage from an ideal diode bridge rectifier is then given by:

$$v_{dc}(t) = \max(v_a(t), v_b(t), v_c(t)) - \min(v_a(t), v_b(t), v_c(t)) \quad (5.6)$$

and the current given by

$$i_{dc}(t) = \max(|i_a|, |i_b|, |i_c|) \quad (5.7)$$

This holds when one can assume that the diodes are ideal with Simulink model in Figure C.9. As for the AC side parameter estimator, the pre-processing step also consists of the same low-pass filtering of the signal.

### **5.2.2 Single-Phase Harmonics Analyzer**

The Single-Phase Harmonics Analyzer is presented in 4.1; else this is very similar to the three-phase case.

### **5.2.3 Phase Correction**

Same as in Section 5.1.3.

### **5.2.4 Parameter Estimation**

The parameter estimation will also here be in the same form as in Section 5.1.5.



# Impedance Model of a Harmonic Source

More use of switching devices since the 1970s in power networks where such loads have a nonlinear relation between input voltage and current and is known as harmonic sources Yifei et al. (2007). These sources create harmonic frequencies which distort the bus line. There are many different types of such harmonic sources, but in this work the loads are limited to the line-commuted rectifier with a DC load consisting of an RLC circuit given in Figure 6.1 and mathematical model of the DC side impedance in (6.1) One will also restrict the work to the small-signal analysis of the loads where one can assume that the fundamental frequency component is much larger than the rest of the harmonic components. The diode rectifier is modeled with ideal diodes. For such a model the current should be continuous for such an impedance model to make sense.

This chapter is focused on deciding on a small-signal input impedance model to be used for modeling the nonlinear loads. A presentation of the models will first be given, how to obtain the parameters for the models online, and finally, some experiments to compare them before a decision on which model to use.

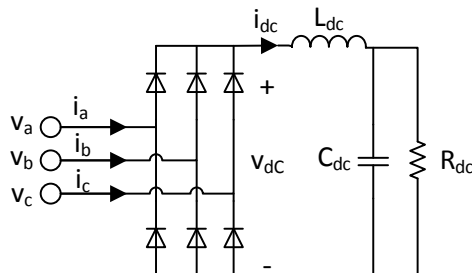


**Figure 6.1:** Diode bridge with RLC load

$$Z_{dc}(\omega) = j\omega L_{dc} + \frac{R_{dc}}{1 + j\omega C_{dc}R_{dc}} \quad (6.1)$$

## 6.1 AC input impedance model

The diode bridge and the DC side load together defines the load impedance. The goal for this model is to capture the main dynamics of the load accurately and have an analytic model of the impedance as a function of the angular frequency  $\omega$  to be used in stability analysis. In this section, two earlier works on modeling the impedance will be presented and verified using simulation in addition to the microgrid system defined in the case study in Chapter 7.

In Sun (2009), impedance modeling for microgrids with the focus on electric ship power systems are presented. In that paper, three models are presented, namely based on transformation to the DQ reference frame and do the analysis in this frame, using phasor based modeling, and lastly describe the system using harmonic linearization. There are some advantages to all methods, but the paper concludes that the one using DQ reference or harmonic linearization are most useful for such loads based on rectifiers. This project will analyze the stability in the  $abc$  reference frame, and because of this, the harmonic linearization is most applicable. The paper proposes an analytic expression for the positive and negative sequence impedance where the small-signal input impedance for the positive and negative sequence are given in (Bing et al., 2007, Eq. 19,20) where the DC side impedance is  $Z_{dc}(\omega)$  and the fundamental angular frequency  $\omega_0$ :

$$Z_{ac-p}(\omega) = \frac{\pi^2}{9} \left[ \frac{1}{Z_{dc}(0)} + \frac{1}{Z_{dc}(\omega - \omega_0)} \right]^{-1} \quad (6.2a)$$

$$Z_{ac-n}(\omega) = \frac{\pi^2}{9} \left[ \frac{1}{Z_{dc}(0)} + \frac{1}{Z_{dc}(\omega + \omega_0)} \right]^{-1} \quad (6.2b)$$

In Sun (2009), the same model is used for small isolated power grids found in ships. The conclusion of the author is that the model is general and compared to the one using transformation to the DQ reference frame, the model can also decompose the impedance into the positive and negative sequence harmonics. One can have any number of harmonics, balanced and unbalanced system dynamics are captured, the frequency range of the model can be valid for both above and below the fundamental, and the impedances are defined per phase which has a clear physical interpretation. There are some shortcomings such that if the system small-signal injection is a superimposed signal of multiple sinusoidal signals with the different frequency the impedance may be different from this model. The design also needs an expression for the DC side impedance, which may not be straightforward to develop in many converter systems. This model is named "Bing" for the rest of this thesis.

The other impedance model, which is used is presented in Lei et al. (2013), is a generalized input impedance model for a three-phase diode rectifier with an analytic expression

in the frequency domain. This model has the same objective as the one in Bing et al. (2007) where the model should be developed for stability analysis of source and load connected power electronic systems. The paper proposes an analytic expression for the input impedance  $Z_{ac}(\omega)$  which is a function of the angular frequency  $\omega$ . This model is named "Lei" for the rest of the thesis and is given in (6.3) with a description of the parameters in Table 6.1.

$$Z_{ac}(\omega) = -j \left[ \begin{aligned} & \sum_{l=0, n=6l+1}^{\infty} \frac{\frac{3}{4} [A_{sn}(l)^2 + B_{sn}(l)^2]}{Z_0(n\omega_0 - \omega) + Z_{dc}(n\omega_0 - \omega)} \\ & + \sum_{l=1, n=6l-1}^{\infty} \frac{\frac{3}{4} [A_{sn}(l)^2 + B_{sn}(l)^2]}{Z_0(n\omega_0 + \omega) + Z_{dc}(n\omega_0 + \omega)} \\ & + \frac{\sqrt{3}}{\pi E} \left[ I_d + \frac{1}{2} \sum_{k=1, m=6k}^{\infty} \frac{A_d(k) e^{j3k\pi}}{Z_{dc}(m\omega_0)} \right] \end{aligned} \right]^{-1} \quad (6.3)$$

This model is more complicated than the one in Bing et al. (2007). The definition of the variables are defined in Lei et al. (2014), Lei et al. (2013) and the paper which Lei et al. (2013) is based on, Sakui and Fujita (1994). The model was developed in these papers as well as a more descriptive information on the variables.

$u$	Overlap angle in the diode rectifier commutation
$\phi$	Firing angle
$A_{sn}$ and $B_{sn}$	Fourier series coefficients for the switching function for the commutation
$A_d$	Fourier coefficient for the DC side voltage real part
$I_d$	The DC current on the DC side of the rectifier
$Z_{dc}(\omega)$	DC side impedance
$Z_0(\omega)$	AC impedance on the AC side of the load
$E$	pu amplitude of the AC side voltage

**Table 6.1:** Description of parameters for the impedance model in Lei et al. (2013)

The Fourier coefficients for the switching function is provided here.

$$A_{sn}(l) = 2\sqrt{3}(-1)^l \sin(nu + n\phi) + \sin(n\phi) \quad (6.4a)$$

$$B_{sn}(l) = 2\sqrt{3}(-1)^l \cos(nu + n\phi) + \cos(n\phi) \quad (6.4b)$$

$$n = 6l \pm l \quad (6.4c)$$

The expression for  $A_d(k)$  is found in Eq. (2) in Lei et al. (2014) and is a function of  $E$ ,  $u$ ,  $\phi$ ,  $I_d$  and  $R_s$ .

The DC impedance has the same form as in (6.1). The AC side impedance is given by

$$Z_0(\omega) = \left(2 - \frac{3u}{2\pi}\right)(R_s + j\omega L_s) \quad (6.5)$$

where the line impedance is modeled as a series resistor and inductor.

To use the models one have to provide a method to obtain the parameters necessary to calculate the impedance. Most of the parameters can be found trivially except for the DC side impedance. The following sections will investigate this problem further, primarily to provide a real-time estimate of the DC side impedance.

## 6.2 DC Side Impedance

In this section three test systems will be stated. The three test cases systems are System 1 in Lei et al. (2013) System 2 in Bing et al. (2007) and the shipboard case study System 3. The parameters for the DC side impedance is given in Figure 6.2.

Parameters	System 1	System 2	System 3
$R_{dc}[\Omega]$	8	10	2.89
$L_{dc}[H]$	$1.59 \times 10^{-4}$	0.05	$1 \times 10^{-3}$
$C_{dc}[F]$	$9.55 \times 10^{-5}$	$1 \times 10^{-3}$	0.084
$f_{nom}[Hz]$	400	60	50
E[V]	326	89.76	563.04

**Table 6.2:** DC side impedance parameters

In Figure 6.2 the real and imaginary part of the DC side impedance is shown and the generated harmonics at  $6kf_{nom}$ ,  $k \in 0, 1, 2, 3, \dots$  is marked with circles. These are the only measurable outputs when the grid is in normal operation with no perturbation mechanism attached. The problem formulation to estimate the parameters of the DC side by only using the harmonic information in the  $6kf_{nom}$  harmonics is a hard problem for one of the parameters. The generated harmonics will also typically decrease with a frequency such that the signal to noise level is much higher for the lower harmonics, especially the DC component and rapidly decreases with frequency.

The parameter estimation is done by stating the problem as one of Recursive Least Squares to recursively update the parameters as new information is obtained. Starting with the  $R_{dc}$  it could be calculated by using the DC component of the impedance first described in (6.1),  $Z_{dc}(0) = R_{dc}$ . The  $L_{dc}$  could be estimated by using the imaginary part of the impedance

$$\Im\{Z_{dc}(\omega)\} = \omega L_{dc} - \frac{\omega C_{dc} R_{dc}^2}{1 + (\omega C_{dc} R_{dc})^2} \quad (6.6)$$

which is reduced to  $\Im\{Z'_{dc}(\omega)\} = \omega L_{dc}$  for frequencies at  $kf_{nom}$ . This holds as long that the area that is influenced by the  $-\frac{\omega C_{dc} R_{dc}^2}{1 + (\omega C_{dc} R_{dc})^2}$  part is between the harmonic frequencies at  $6kf_{nom}$ . This means that the  $L_{dc}$  can be solved using a linear least squares estimate with  $\omega$  as regressors. For the  $C_{dc}$  parameter, it is difficult to estimate since the dynamics are in between the harmonic points. Simulations have shown that if the dynamic is placed before the  $f_{nom}$  then this parameter does not cause any significant difference.

### 6.2.1 DC Side Impedance Estimation Method

In Section 5.2 the proposed method to estimate the DC side parameters by using the three-phase voltage and current measurements close to the diode rectifier. Here it is assumed that the AC side impedance is a short circuit such that it is possible to measure the voltage and current directly fed to the diode rectifier. If such measurements are not possible, methods for estimating the input voltage could be based on Lei et al. (2013).

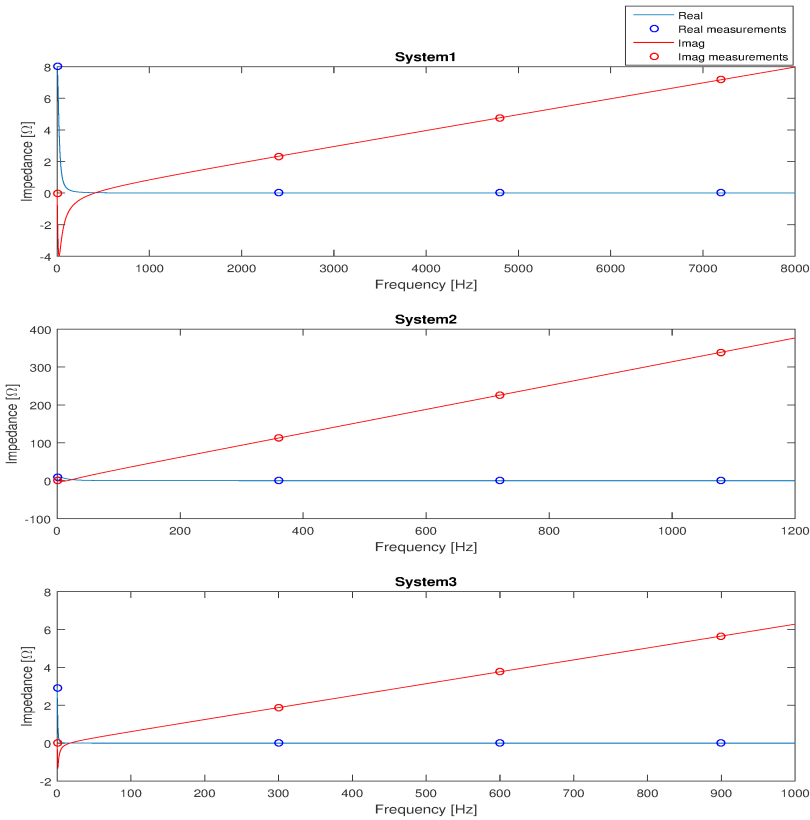


**Figure 6.2:** Real and imaginary part of impedance for the three test systems

The model consists of an ideal diode bridge rectifier model stage, DC impedance measurement stage, and a parameter estimation stage. In the first stage the input three-phase current and measurements are converted into the DC side voltage and current by modeling the diode bridge rectifier using ideal components. The model of such a device is implemented in Simulink as an approximation for the diode bridge where an implementation is in the Simscape Power Systems library. The model assumes a rectifier consisting of ideal diodes.

In the final stage, the parameters are estimated using RLSE. The RLSE block in the Systems Identification Toolbox in Matlab Simulink implements a solution to the regression problem  $y(t) = H(t)\Theta(t)$  with known output  $y(t)$  and regressors  $H(t)$ . For the  $R_{dc}$  parameter  $y_R(t) = \Re(Z_{dc}(0))$  and  $H_R(t) = 1$ . For the  $L_{dc}$  parameter the  $y_L(t, k) = \Im(Z_{dc}(kw_0))$  and  $H_L(t, k) = k\omega$  where  $k \in 0, 6, 12, \dots$ . For each time step  $t$ , the input to the estimator block is all the values  $k$  in which the previous stage estimates harmonics at. This means that the sample rate at the inductor estimator is faster than the one for estimating the resistor value.

### 6.3 Small-Signal Measurement by Voltage Perturbation

To verify that the small-signal input impedance models for the loads are accurate, a circuit for measuring the small-signal impedance by injecting a small voltage perturbation into relevant components of the grid and measuring the response is shown. As in Lei et al. (2013), a three-phase voltage source is connected in series with the input voltage signal generator to create a perturbation with frequency  $f_h$  and amplitude  $A_h$ . The input impedance is measured by Fourier transformation of the input voltage signal and the input current signal, and complex dividing the voltage by the current at the perturbation frequency (Familiant et al., 2009). The three-phase signal is created with the positive sequence by injecting single frequency components.

In Figure C.7 a model for measuring the input impedance by injecting a positive sequence perturbation voltage which is superimposed on the source voltage. A small resistor is connected in series between the load and the voltage sources with value  $R_s = 1 \times 10^{-3}\Omega$ .

### 6.4 Simulation Results

The parameters for the three test systems are given in Table 6.2. The perturbation voltage is set to 2% of the magnitude of the voltage source, and the perturbation frequency is swept from 5Hz up to  $1 \times 10^4 Hz$  where frequencies at a multiple of the fundamental frequency are not included. In Figure G.1, Figure G.2 and Figure 6.3 the results of the impedance measurement by small-signal injection are shown for System 1, System 2 and System 3 respectively. For System 1 both of the models provides accurate results for the magnitude response, where the Lei model can capture the regular spikes for magnitude and phase between 2000Hz and 10000Hz, but the Bing model only estimates the impedance as a smooth curve. For the phase angle, neither of the models can capture the phase dynamics under 80Hz where the measured impedance is shown to tend rapidly toward zero in this region. For this system, the Lei model is more accurate because it can capture the regular spikes for high frequencies and this is also the system which is used as verification in Lei et al. (2013) where the author is showing the result from 100Hz up to  $1 \times 10^4 Hz$  where the model is accurate. For System 2, this is a similar system as found in Bing et al. (2007). The simulated result shows that there is a good agreement for magnitude for the whole frequency range. For some of the measured impedance values for the magnitude above 250Hz is not modeled accurately may be outliers and caused by measurement errors in the measurement process. The model of Lei is consistently estimating a lower magnitude than the measured and the one of the Bing. For the phase, there is an excellent agreement between the Bing model and the measured impedance up to 1000Hz. For System 2 the Bing model is more accurate. For the System 3, the same spikes as System 1 show up starting at a frequency about 300Hz and are persistent at about  $6kf_{nom}$ ,  $k \in \{1, 2, 3, \dots\}$  which is the same harmonic components as found in the DC side voltage.

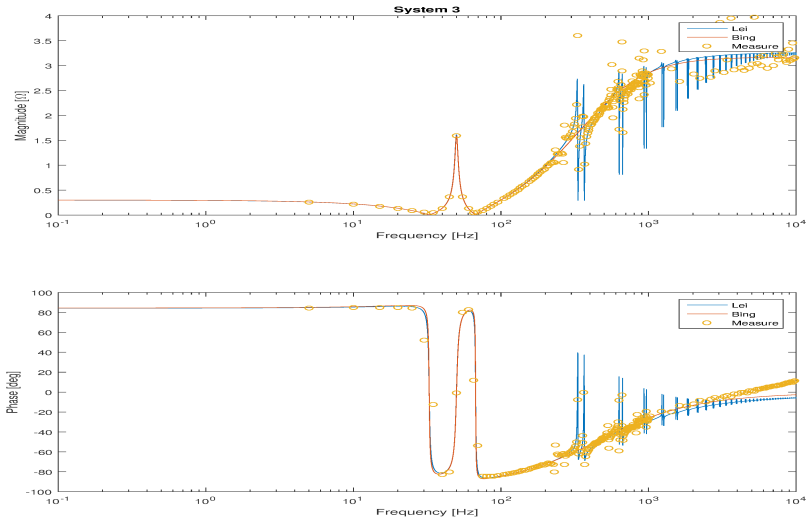


**Figure 6.3:** Measured impedance using Figure C.7 and compared to the model Bing in Bing et al. (2007) and Lei in Lei et al. (2013) for System 3

## 6.5 Discussion

Based on the simulation results one has to decide which small-signal model to use as the input impedance model. One can argue that the model of Lei provides more accurate results when the spikes are also included in the model. However, the Lei model is more complicated and does not capture the main dynamics of the System 3, which will be used in the case study better than the Bing model. The model of Lei also needs more parameters and has more complex calculations. Because of this, the Bing model will be used for the case study in Chapter 7.



# Case Study: Real-Time Stability Analysis of a Shipboard Microgrid

In this chapter a case study where the components from Chapter 5 will be used to calculate the source and load impedance of a microgrid for which can be used to calculate input-output stability of such a grid using the generalized Nyquist criterion.

The objective is to calculate the transfer functions related to stability for the grid in Figure 7.1 where only the voltage is measured at the main bus, current measurement at the small circles in the figure, nominal generator voltage, and nominal frequency for the grid are assumed all measured.

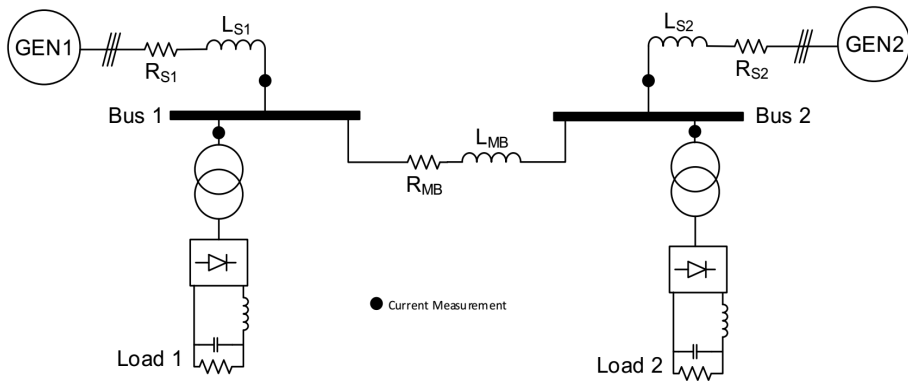


**Figure 7.1:** Power grid model for case study

With the use of the measurements available, the objective is to know as much as possible of the grid and based on this information calculate stability properties of the grid.

## 7.1 Mathematical Model

From the Specialization Project, where a summary is given in Chapter 3, a mathematical model of the grid is found. Using Kirchhoff's circuit laws, the following set of differential equations is found in (7.1).

$$L_{s1} \frac{di_{s1}}{dt} = v_{s1} - R_{s1}i_{s1} - v_{bus1} \quad (7.1a)$$

$$L_{s2} \frac{di_{s2}}{dt} = v_{s2} - R_{s2}i_{s2} - v_{bus1} \quad (7.1b)$$

$$L_{mb} \frac{di_{mb}}{dt} = v_{bus1} - v_{bus1} - R_{mb}i_{mb} \quad (7.1c)$$

$$i_{load1} = i_{s1} - i_{load1} \quad (7.1d)$$

$$i_{load2} = i_{s2} - i_{load2} \quad (7.1e)$$

$$\frac{di_{load1}}{dt} = f_L(v_{bus1}, i_{load1}) \quad (7.1f)$$

$$\frac{di_{load2}}{dt} = f_L(v_{bus2}, i_{load2}) \quad (7.1g)$$

Here  $i_{s1}$  and  $i_{s2}$  are the currents in generator 1 and 2, and  $i_{mb}$  is the current passing in the main bus. The system in (7.1) is a nonlinear model because of the function  $f_L$ . In Skjong et al. (2015) the loads are modeled as a harmonic current source in parallel with a resistor, but the current source still has to be defined.

## 7.2 Microgrid Implementation

The model is built using the SimPowerSystems software for Matlab Simulink with the use of the Specialized Technology library which has components for building and simulating electrical power systems. The library includes three-phase components such as generators, rectifiers and passive elements. It also provides tools to do harmonics analysis, frequency domain tools, and impedance measurements. The library supports fast and accurate simulation methods to simulate complex electrical components. The implemented Simulink model of the grid in Figure 7.1 can be seen in Figure C.3. Some parameters to initialize the model are found in Table 7.1.

The SimPowerSystems setup is done by using the Powergui block, where the model is simulated using discrete time simulation and the solver type is the Tustin/Backward Euler and sampling period  $T_s = 2 \times 10^{-6} s$ .

## 7.3 Bus Line Voltage

In Figure 7.2 the three-phase ideal source voltage from the identical  $V_{s1}$  and  $V_{s2}$  together with the bus voltage on bus 1 and bus 2 are shown. The voltages is measured from phase to ground which means that the RMS input source voltage is  $\sqrt{\frac{2}{3}}V_{LL} = 563, 38V$ .

Parameter	Brief description
<b>Generators</b>	
$V_{LL1} = V_{LL2} = 690V$	RMS voltage phase to phase for the generator 1 and 2
$f_{nom} = 50Hz$	Fundamental frequency
<b>Line impedance</b>	
$R_{s1} = R_{s2} = 8.1 \times 10^{-3}\Omega$	Line resistance for the generator 1 and 2
$L_{s1} = L_{s2} = 2.6 \times 10^{-4}H$	Line inductance for the generator 1 and 2
$R_{MB} = 9.5 \times 10^{-3}\Omega$	Line resistance for the main bus
$L_{MB} = 3.0 \times 10^{-4}H$	Line inductance for the main bus
<b>Loads</b>	
$C_{dc1} = C_{dc2} = 0.084F$	DC rectifier diode for the loads 1 and 2
$L_{dc1} = L_{dc2} = 1 \times 10^{-3}H$	DC rectifier series inductance
$R_{L1} = 2.89\Omega$	Resistance for the load 1
$R_{L2} = 1.74\Omega$	Resistance for the load 2

Table 7.1: Description of grid parameters

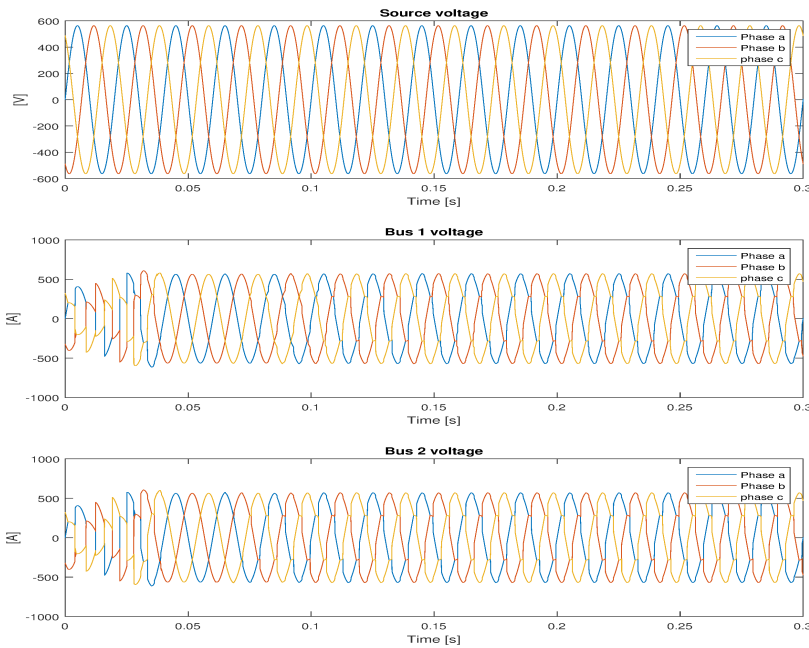


Figure 7.2: Input source voltages and voltages at bus 1 and bus 2

From Section 2.1.4, harmonic loads are modeled as harmonic sources which cause perturbation on the bus line with harmonic components on the  $kf_{nom}$ ,  $k = (6n \pm 1)n \in$

$\mathbb{Z}_{\geq 0}$  where  $\mathbb{Z}_{\geq 0}$  is all integers greater or equal to zero. In this microgrid system, there are no filters for eliminating the harmonic content so that the THD will be quite high. For some chosen measured values the THD content is shown in 7.2. Without filtering the bus, to which the nonlinear loads are connected, there are considerably high harmonic distortions.

Measurement Point	THD
<b>Voltage</b>	
$V_{bus1}$	9.37%
$V_{bus2}$	11.55%
<b>Current</b>	
$I_{s1}$	24.04%
$I_{s2}$	23.58%

**Table 7.2:** THD content for some measured values given in % of the fundamental

## 7.4 DC Side Voltage and Current of the Three-Phase Rectifier Load

In Figure 7.3 the DC side currents and voltages of the harmonics loads are shown. From Section 2.1.4 the current and voltage signal should have a large DC component and harmonic components on the  $6kf_{nom}$ ,  $k \in \mathbb{Z}_{\geq 0}$ .

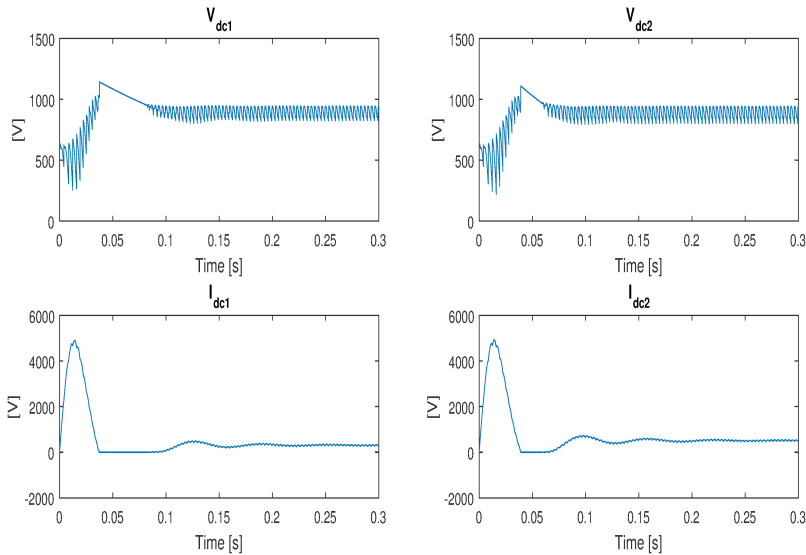


**Figure 7.3:** Measured DC side voltages and currents

From Figure 7.3 one can see that it takes some time before the system settles to the steady state. During this transition, there are, especially large currents on the DC side of the rectifiers. These currents are not found in steady state and have frequency components in frequencies not found in the steady state.

## 7.5 Limitation to the Steady State

The KF approach for measuring harmonics is based on the assumption that there are distinct harmonic components with defined frequencies where this is tested on a static system in Chapter 4 and no dynamics involved. For the AC side, it is assumed for this type of system that there is a three-phase full wave rectifier which distorts the bus with frequency component on only the  $6kf_{nom} \pm 1$  and the rest is zero in steady state. In this case study, the system dynamics are introduced. In Figure G.4 the difference in frequency content is evident from the transient response to the steady state. The transient response period is here defined as from the start of the simulation until all the transients of the system have died out. It is easiest to determine when the system settles based on the currents in the system, for instance using Figure 7.3 the system is more or less settled at  $t = 0.2s$ . when the system is in steady state, where all the derivatives are zero, there are distinct frequency components as predicted. In the transient response, however, the frequency content is not limited to the stated frequency components, but rather the system has frequency content on frequencies.

In Figure G.5 this is shown how the harmonics tracker is incapable of tracking  $i_{s1}$  when the system is not in steady state. The frequency content caused by the transients cause the natural occurring harmonics in steady state to be overshadowed and not tracked. The fundamental harmonic is still higher than the rest of the frequency components, as shown in Figure G.4d, and because of this that frequency component is still tracked. The higher harmonics are noise and carries no useful information. Another observation is the time lag from the variation in the three-phase signal to the change is detected in the harmonics tracker, this time, the difference is about  $0.02s$  which agrees with the period of the fundamental frequency.

Recalling that when the system is not in the steady state, the impedance has the following form described by transfer function  $H(s) = V(s)/I(s)$ . The system is reduced from the function of the complex variable  $s$  to only the imaginary angular frequency  $j\omega$  such that the transfer functions have the form  $H(j\omega) = V(j\omega)/I(j\omega)$  when the system is in steady state. The harmonics tracker can track the fundamental frequency, but comes to short estimating the rest of the frequency components as they come in a smooth band containing all frequencies and not only those which are a multiple of the fundamental frequency. From a parameter estimation perspective, since the method is not able to measure the function  $H(s)$  accurately during transients, the method will neither be able to estimate the impedance parameters. For this reason, the parameter estimation only gives reliable results in the steady state.

## 7.6 Building the Impedance Model

To model the grid, subsystems of the grid are modeled as input-output impedance systems defined according to Table 7.3. For the linear loads, the impedance is a simple linear model where the estimated model can be directly compared with the model used in the simulation. For the nonlinear loads, there are no exact models for comparison. The way of comparison is here done by injecting a small perturbation voltage and measuring the input current as in Section 6.3.

System	Parameters	Brief description
$Z_{s1}(\omega)$	$L_{s1}$ and $R_{s1}$	Linear model with $Z_{s1}(\omega) = j\omega L_{s1} + R_{s1}$
$Z_{s2}(\omega)$	$L_{s2}$ and $R_{s2}$	Linear model with $Z_{s2}(\omega) = j\omega L_{s2} + R_{s2}$
$Z_{mb}(\omega)$	$L_{mb}$ and $R_{mb}$	Linear model with $Z_{mb}(\omega) = j\omega L_{mb} + R_{mb}$
$Z_{load1}(\omega)$	$L_{dc1}$ , $R_{dc1}$ and $C_{dc}$	Nonlinear model
$Z_{load2}(\omega)$	$L_{dc2}$ , $R_{dc2}$ and $C_{dc}$	Nonlinear model

**Table 7.3:** Grid impedance subsystems

For the system in Figure 7.1, when dividing the system into source and load when using  $V_{s1}$  as input and Vload as output the system is shown in 7.4. Here all the load impedances are modeled as linear loads with voltage potential from the bus to the same negative potential as the generators.

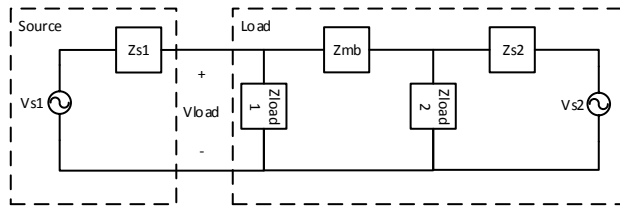


**Figure 7.4:** Equivalent impedance model represented as a source load system

From the equivalent impedance model in Figure 7.4, the next step is to define the equivalent source impedances  $Z_{s1}$  and  $Z_{s2}$  and equivalent load impedances  $Z_{eq1}$  and  $Z_{eq2}$ . For all frequencies which are not the fundamental frequency, the voltage sources  $V_{s1}$  and  $V_{s2}$  will be a short circuit to the negative voltage potential since they are modeled as an ideal voltage sources in the frequency domain. The equivalent source and load impedance is then found by defining either the  $V_{s1}$  or  $V_{s2}$  as the input of the system. The impedances are valid for  $\omega \neq 2\pi f_{nom}$ , and because the load impedances are nonlinear, and a model is only valid for small-signal injection the entire model is a small-signal accurate model. The equivalent impedance model for the equivalent load seen from Vload1 is (7.2), and from Vload2, when defining the  $V_{s2}$  and  $Z_{s2}$  as the source the equivalent load is (7.3).

$$Z_{eq1} = \frac{Z_{load1}(Z_{load2} + Z_{s2})}{Z_{load2} + Z_{s2} + Z_{load1}Z_{load2}Z_{mb} + Z_{load1}Z_{load2}Z_{s2} + Z_{load1}Z_{mb}Z_{s2}} \quad (7.2)$$

$$Z_{eq2} = \frac{Z_{load2}(Z_{load1} + Z_{s1})}{Z_{load1} + Z_{s1} + Z_{load1}Z_{load2}Z_{mb} + Z_{load1}Z_{load2}Z_{s1} + Z_{load2}Z_{mb}Z_{s1}} \quad (7.3)$$

For the equivalent source impedances, these are simply  $Z_{s1}$  for Source 1 and  $Z_{s2}$  for Source 2. By recalling from the theory that by stating the transfer function from  $V_{s1}$  to  $V_{l1}$  and from  $V_{s2}$  to  $V_{l2}$  a function  $H_0$  can be found. For such source load systems the function  $H_0$  which will determine the stability is found to be  $H_0 = \frac{Z_s}{Z_l}$  by recalling the following transfer function:

$$\frac{V_l}{V_s} = \frac{1}{1 + Z_s/Z_l} = \frac{1}{1 + H_0} \quad (7.4)$$

Then the transfer function from  $V_{s1}$  to  $V_{l1}$  could be found as

$$\frac{V_{l1}}{V_{s1}} = H_{sys1} = \frac{Z_{load1}(Z_{load2} + Z_{s2})}{Z_{s1}(Z_{load2} + Z_{s2}) + Z_{load1}(Z_{s2} + Z_{mb}Z_{s1}Z_{s2} + Z_{load2}(1 + Z_{mb}Z_{s1} + Z_{s1}Z_{s2}))} \quad (7.5)$$

and the transfer function from  $V_{s2}$  to  $V_{l1}$

$$\frac{V_{l2}}{V_{s2}} = H_{sys2} = \frac{Z_{load2}(Z_{load1} + Z_{s1})}{Z_{s2}(Z_{load1} + Z_{s1}) + Z_{load2}(Z_{s1} + Z_{mb}Z_{s2}Z_{s1} + Z_{load1}(1 + Z_{mb}Z_{s2} + Z_{s2}Z_{s1}))} \quad (7.6)$$

Finally the function  $H_0$  can be defined for the systems  $V_{s1}$  to  $V_{l1}$  and  $V_{s2}$  to  $V_{l2}$  as  $H_{01}$  and  $H_{02}$  in (7.7) and (7.8)

$$H_{01} = \frac{Z_{s1}}{Z_{l1}} = \frac{Z_{load1}(Z_{s2} + Z_{load2})}{Z_{s1}(Z_{s2} + Z_{load2} + Z_{load1}(Z_{mb}Z_{s2} + Z_{load2}(Z_{mb} + Z_{s2})))} \quad (7.7)$$

$$H_{02} = \frac{Z_{s2}}{Z_{l2}} = \frac{Z_{load2}(Z_{s1} + Z_{load1})}{Z_{s2}(Z_{s1} + Z_{load1} + Z_{load2}(Z_{mb}Z_{s1} + Z_{load1}(Z_{mb} + Z_{s1})))} \quad (7.8)$$

From the defined  $H_{01}$  and  $H_{02}$  functions the input-output stability is calculated by using the Nyquist stability criterion.

In Chapter 6, a decision for small-signal input model for the diode rectifier was done. The model is the one in Bing described in Bing et al. (2007). Below the model is given again for the positive sequence perturbation signal, where the negative sequence perturbation is not included in this thesis.

$$Z_{ac-p}(\omega) = \frac{\pi^2}{9} \left[ \frac{1}{Z_{dc}(0)} + \frac{1}{Z_{dc}(\omega - \omega_0)} \right]^{-1} \quad (7.9)$$

## 7.7 Parameter Estimation Model

In this section the parameter estimation models for the AC side, and DC side parameters are given where one strives to find a regression vector and output vector as input for the RLSE block which solve the problem.

### 7.7.1 DC Side Parameters

From Section 6.2.1 the parameter estimation problem is defined as  $y(t) = H(t)\Theta(t)$  with known output  $y(t)$  and regressors  $H(t)$ . For the  $R_{dc}$  parameter  $y_R(t) = \Re(Z_{dc}(0))$  and  $H_R(t) = 1$ . For the  $L_{dc}$  parameter the  $y_L(t, k) = \Im(Z_{dc}(kw_0))$  and  $H_L(t, k) = k\omega$  where  $k \in 0, 6, 12, \dots$ . In Figure C.8 the entire proposed system is shown where the final parameter estimation stage also is found.

### 7.7.2 AC Side Parameters

For the AC side parameters, the same parameter estimation problem is defined as  $y(t) = H(t)\Theta(t)$  with known output  $y(t)$  and regressors  $H(t)$ . For the  $R$  parameter  $y_R(t) = \Re(Z_{ac}(2\pi f_{nom}))$  and  $H_R(t) = 1$ . For the  $L$  parameter the  $y_L(t, k) = \Im(Z_{ac}(2\pi f_{nom}))$ . This means that the parameter estimation is only estimated with the information contained in the fundamental harmonic. The implemented Simulink model of this estimation process is shown in Figure C.6.

## 7.8 Initialization of the Estimation Method

To use the method, a set of parameters is passed to initialize the parameter estimation algorithm for estimating the AC side and DC side parameters. The initialization values together with a description is found in Table 7.4.

The grid has to be simulated for some time to get the system into the steady state for which the phasor theory applies. The parameter estimation will not give an useful estimate before all the derivatives in the grid system is close to zero. Since this grid has static parameters the forgetting factor is set to 1, which means that the model does not forget. The forgetting factor could be lowered to a value close to 1 if there is a need for a method which follows the change in parameters. From the Table 7.3 the impedance

Parameter	Value	Description
<b>Adaptive Kalman Filter</b>		
$H_p$	[1, 7, ..., 37]	Positive sequence harmonics
$H_n$	[5, 12, ..., 35]	Negative sequence harmonics
$N_p$	7	Number of positive sequence harmonics
$N_n$	6	Number of negative sequence harmonics
$H_s$	[6, 12, ..., 36]	Single-phase harmonics
$N_s$	7	Number of single-phase harmonics
$\mathbf{P}_0$	$1 \times 10^3 \mathbf{I}$	Initial error covariance matrix
$\mathbf{R}$	$1 \times 10^{-4} \mathbf{I}$	Measurement covariance matrix
$\mathbf{Q}_0$	$\mathbf{0}$	Initial input covariance matrix
$\mathbf{x}_0$	$\mathbf{0}$	Initial state
$\epsilon_A$	$1 \times 10^{-5}$	Stopping criterion adaptive update Q
$N_{max}$	10	Number of max iterations per time step
<b>Low pass filter</b>		
$T_s$	$1 \times 10^6 \text{Hz}$	Sample Rate
$f_{pass}$	$37 f_{nom} = 1850 \text{Hz}$	Passband Frequency
$f_{stop}$	$41 f_{nom} = 2050 \text{Hz}$	Stopband Frequency
Ripple	$1 \times 10^{-4} \text{dB}$	Passband ripple
Attenuation	$100 \text{dB}$	Stopband attenuation
<b>Phase correction</b>		
$C_{LP}$	$0.0319 \frac{\text{rad}}{\text{Hz}}$	Phase correction coefficient
<b>Recursive Least Squares Estimator</b>		
$\lambda$	1	Forgetting factor

Table 7.4: Description grid parameters

models are shown and based on these the total system to estimate the grid parameters from the measurable input is shown in Figure C.10.

## 7.9 Results

With the defined microgrid structure, impedance model and initialization of the parameter estimation method, the results are given here where the performance for the parameter estimation, the fit of the impedance model and the transfer functions for stability will be compared with measurements using small-signal injection.

### 7.9.1 Parameter Estimation

In this section, the results from the parameter estimation are shown in Figure 7.5. As shown in the figure the parameters are estimated with good accuracy, both the AC side and the DC side parameters. To estimate the parameters, the Power Grid is simulated for one second, where the estimation starts at  $t = 0.2 \text{s}$  for the grid to stabilize before the estimation process starts.

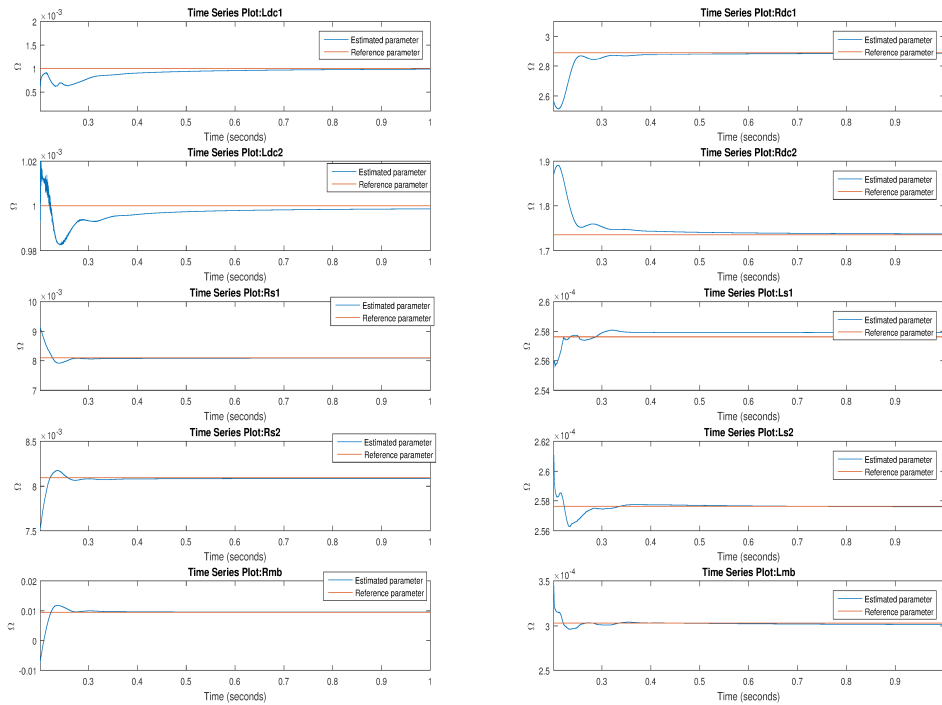


Figure 7.5: Estimated power grid parameters with the use of AKF and RLSE

## 7.9.2 AC Side Impedance Estimation

In Figure 7.6 the models with the estimated impedance values are compared to the ones of parameters used in the simulation. The estimator can detect the parameters correctly and build the correct impedance models. The microgrid in this study has a simple line impedance model which easily is estimated using the proposed method.

## 7.9.3 Harmonic Load Impedance Estimation

In Figure 7.7 the estimated model for Load 1 and Load 2 are compared to the small-signal perturbation impedance measurement. The model of (7.9) is added a small resistor to have a better fit between the measurement and the model. By using the model of (7.9) there are some non-modeled peaks at high frequencies, which is the biggest downside of using the chosen load model. One can, however, see that the model fit the measurements with good accuracy from very low to high frequency especially for the magnitude. The phase is harder to measure correctly, but the main dynamics are captured using this model.

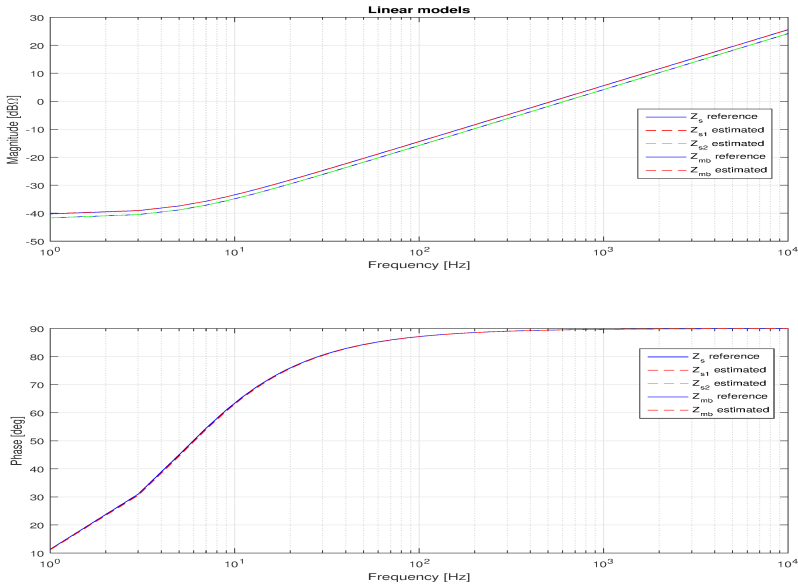


**Figure 7.6:** Estimated linear impedance model using AKF and RLSE compared to the reference impedance for  $Z_{mb}$ ,  $Z_{s1}$  and  $Z_{s2}$ .

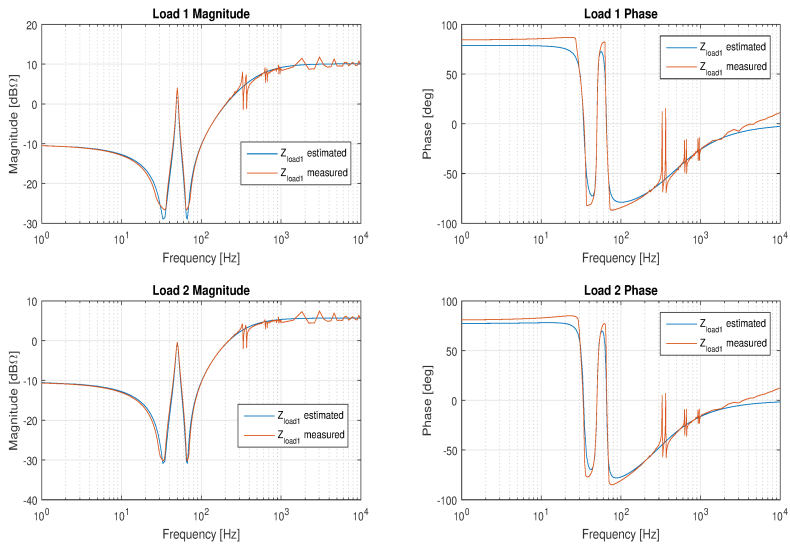


**Figure 7.7:** Estimated impedance model of Load 1 and Load 2 with use of AKF, RLSE and the Bing small-signal impedance model, compared to the measured impedance using small-signal injection.

## 7.9.4 System Transfer Function Estimation Result

In Figure 7.8 the transfer function  $H_{sys1} = \frac{V_{I1}}{V_{s1}}$  and  $H_{sys2} = \frac{V_{I2}}{V_{s2}}$  is shown by using the estimated parameters in Figure 7.5 and compared with signal injection a small perturbation voltage on the positive sequence from  $V_{s1}$  for System 1 and and  $V_{s2}$  for system 2.

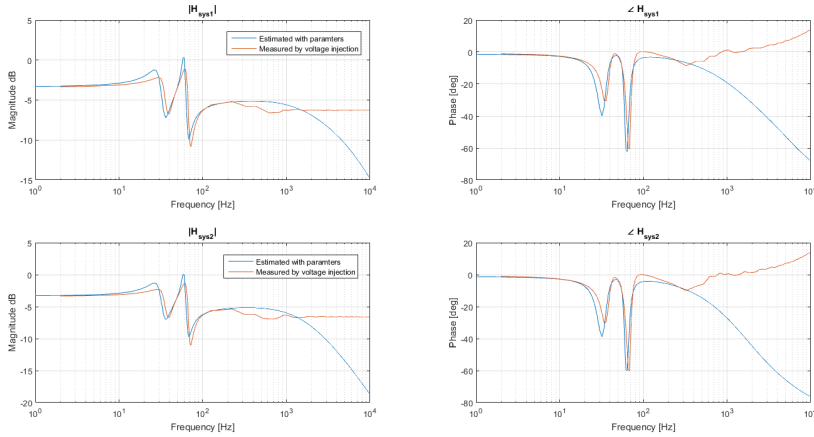


**Figure 7.8:** Estimated  $H_{sys1}$  and  $H_{sys2}$  with use of AKF, RLSE and the Bing small-signal impedance model, compared to the measured impedance using small-signal injection.

The result shows good agreement between the estimated transfer functions and the measured by injecting a small perturbation voltage up to about  $1 \times 10^3 Hz$ . For frequencies above this, the estimated model show a decrease in the magnitude, but the model measured by signal injection show a static gain at about 6dB for frequencies above  $1 \times 10^3 Hz$ . From Figure 7.8 the system dampens all frequencies with the measured method and all frequencies except for a small region between 58Hz to 60Hz.

## 7.9.5 Stability Analysis

In Figure 7.9 The  $H_{01}$  and  $H_{02}$  functions are shown where the functions are based on the estimated parameters in Figure 7.5. To get a good fit between the measured impedance based on small-signal injection and the estimated impedance based on the model in (7.9). From the plot one can see that the estimated impedance has a good matching with the measured by small-signal injection. The main dynamics are captured well, but there are spikes at about each  $k6f_{nom}$ . These spikes should not cause any difference in this system regarding stability. For other systems, such spikes may be larger and a different model, for instance, the model in (6.3). From the Nyquist stability criterion, it is possible to calculate the stability of a  $H_0$  function based on the magnitude and phase information for such a function. The first step is to find the  $\omega_{180}$  which is the point where the function crosses the  $\omega = -180^\circ$  line. For neither of the functions, this is possible, and one can conclude that the system is stable.

One can also do the analysis by defining input and output differently for instance by looking at the transfer functions from the voltage of entry to current at different parts

of the system. For example, there is a low impedance path from one generator to the other for low frequencies since it consists of only low-value resistors and inductors, which have low impedance for low frequency. From this analysis, one could argue that a small perturbation voltage with low frequency will cause high currents through the main bus which propagates to the other generator and could be harmful to such equipment.

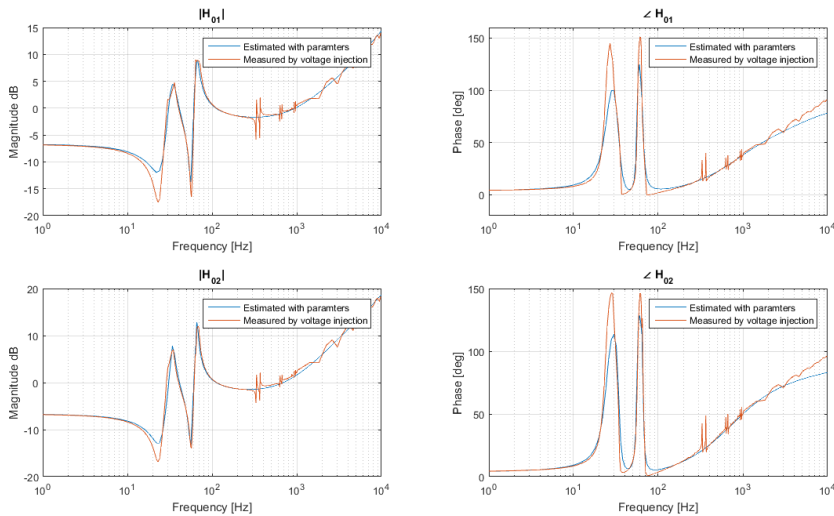


**Figure 7.9:** Estimated  $H_{01}$  and  $H_{02}$  with use of AKF, RLSE and the Bing small-signal impedance model, compared to the measured transfer function using small-signal injection.

## 7.10 Discussion

In this chapter, a case study where the proposed methods have been tested on a simplified microgrid system meant for a marine vessel. Small-signal impedance model of such a system is introduced, and stability calculations were done. From the result, one can see that the resulting models have a good accuracy for a broad range of frequencies.

However, the tested system is stable, and because of this, the stability calculations are not that interesting since unstable modes cannot be tested. One can see that the proposed method for doing stability analysis works for this stable system, but it is not verified that the technique can find instabilities in relevant systems.

The method of splitting the microgrid into a source and load subsystem could be done in multiple ways. One could, for instance, divide the system by the main bus and assign each side as the source and load respectively. If this would yield a different stability conclusion is not determined in this thesis.

Limitations with the use of a KF approach which measures only frequency is presented, and it is evident that this method does not work during in the transient response because one then would have to add many more frequency components to measure if the method were to track harmonics in during the transient response. Then it follows that the positive

attributes with using a KF approach vanish as it would be close to a pure frequency domain tool. How to measure the transient response due to dynamics in the system without adding many more harmonics is not in the scope of this thesis. One would have to assume that the transients disappear soon from the system and that the system, for the most part, can be said to operate in the steady state and therefore, is a steady state analysis tool.

When dealing with nonlinear loads, they may have different impedance characteristics, not solely based on the frequency for linear passive elements. The loads may not be linear on the voltage. It has not been verified that the impedance model is suitable when the system is in different operating points for instance by moving the grid operating point to a higher or lower voltage level.

## Discussion

The primary research question of this thesis was to determine if it is possible to calculate the stability of a microgrid structure by only measuring information contained in the grid during normal operation by using a non-invasive approach. Literature has shown many ways to measure impedances of a system in an invasive way, but there is still no methods which work well for every system. Non-invasive measurement is also extensively studied in literature, but in this case also, no superior method exists. In this work the focus has been on Kalman filtering, where there are multiple ways of measuring harmonics. The choice of Kalman filter implementation is an approach where an adaptive filter which adaptively changes the parameters of the Kalman filter depending on the state of the system. The Kalman filter implementation using this method leads to better tracking in the presence of variations in the signal, but additional calculations have to be done which means that this filter is more computationally demanding. One can see that this leads to a trade-off where the accurate measurement vs. computational complexity has to be decided.

Nonlinear loads distort the distribution bus with harmonic distortion. Equipment connected to such a distribution bus will show a performance degradation because of the present harmonics. The measurement of such harmonics is done, online, in this thesis with good accuracy. There are, however, some limitations for which the Kalman based algorithm will provide accurate results. If the system is not in steady state, the information contained in phasors are not sufficient to describe the system accurately because of the present derivatives.

The system stability of a microgrid is mainly due to the characteristics of the nonlinear loads. This thesis only concerns with small-signal methods, but such loads are not entirely described by such a method. The impedance is only valid for injections of single tone frequencies and measured when the system is in steady-state. Outside this narrow, but important range, the proposed method does not tell much about the stability properties of the grid. If the small-signal is a technique which accurately states the stability properties of the microgrid is an important question which is left unanswered. However, stability

properties when such grid is perturbed by a small in amplitude sinusoidal is an important characteristic and useful information.

The only way of verification is by simulation in this thesis. If the methods proposed here are suitable for real microgrid systems is not concluded. This may be the most critical part for the next steps for these methods to prove their usefulness.

The proposed stability calculation is only based on the positive sequence perturbation. There are different impedance characteristics based on which symmetrical component the analysis is done for, for the nonlinear loads. The used impedance model for the loads also has a negative sequence input impedance model, but this is not verified with simulations in this thesis and will be a task for future work.

In the Chapter 4 it was shown that the Kalman based harmonics tracker was able to track harmonics when the magnitude and phase changes with time. However, for a static system these variations will not create any transients because the system does not have any dynamics. The tracker used in a system with dynamics was tested in Chapter 7 where during the transient response the system has frequency components at a broad range of frequencies and not only those found in the steady state. One of the main arguments for using the Kalman filter method for tracking harmonics was that it has better properties for tracking time-varying signals. However, when the signals in a dynamic system change this causes transients to occur before the system settles at a new operating point. During this phase, only the fundamental frequency is tracked with reasonable accuracy. For parameter estimation, which is only defined in the steady state in this thesis, the system will only detect slowly varying changes in the system and do stability analysis based on this.

## Conclusion

In this master's thesis, a proposed method for real-time stability analysis for a microgrid by parameterizing the source and load impedance and estimating the parameters of the naturally occurring harmonic components in the grid is developed and verified by numerical simulations.

First, a method for tracking positive and negative sequence harmonics in a three-phase signal and harmonics for a single-phase signal are proposed. The methods can track variations in the magnitude and phase of such signals when the signals are composed of sinusoidals with a limited set of frequencies which is typically found in the steady state. The adaptive Kalman filter implementation for the problem of tracking harmonics shows promising results both regarding accuracy and response time. When the method was tested on a system with dynamics, it was evident that this is a method for use in the steady state. Nevertheless, the method is still able to measure the fundamental frequency component during transients, but additional frequency components are usually needed for the parameter estimation algorithm.

A small-signal impedance model for the grid in the steady state has been parameterized based on the AC side impedance subsystems and DC side impedance. By using small-signal analysis for such a system, the subsystems are treated as impedance models by functions of the angular frequency. From the naturally observed harmonics in such a system, the parameters for the AC side and DC side impedance subsystems are estimated. From the extracted impedance parameters, the equivalent source and load impedances are estimated in good accordance with measured impedance where a small-signal injection is used. The small-signal impedance model is then used to assess the system stability of the grid.



# Chapter 10

## Future Work

This master's thesis has laid the foundation for analysis and improvements of methods for real-time tracking of harmonics and impedance estimation for stability analysis. Still, there is room for improvements.

- In this thesis, only one nonlinear load is analyzed, namely the 6-pulse diode rectifier. More nonlinear loads and sources could be analyzed and parameterized. For the rectifier in this model, an AC side impedance could also be added.
- By enabling new grid connected equipment, this adds new frequency components to the grid. In this master's thesis, one assumes that the harmonics are known in advance, but if this is not possible, the method could provide a way for automatically add more harmonics on the fly.
- The fundamental frequency component is in this type of grid always is the most prominent and tracking of the phase and magnitude is done with good accuracy even during transients. The tracking of the frequency for grid synchronization could be done by developing the method further and will make the method more self-sustained.



# Bibliography

- Balchen, J. G., Andresen, T., Foss, B. A., 2003. Reguleringssteknikk. Institutt for teknisk kybernetikk, NTNU.
- Bing, Z., Karimi, K. J., Sun, J., June 2007. Input impedance modeling and analysis of line-commutated rectifiers. In: 2007 IEEE Power Electronics Specialists Conference. pp. 1981–1987.
- Blagouchine, I. V., Moreau, E., 2011. Analytic method for the computation of the total harmonic distortion by the cauchy method of residues. *Communications, IEEE Transactions on* 59 (9), 2478–2491.
- Burns, A., Wellings, A. J., 2010. Real-time systems and programming languages. Addison-Wesley.
- Cespedes, M., Sun, J., April 2014. Adaptive control of grid-connected inverters based on online grid impedance measurements. *IEEE Transactions on Sustainable Energy* 5 (2), 516–523.
- Cobreces, S., Bueno, E., Pizarro, D., Rodriguez, F., Huerta, F., Sept 2009. Grid impedance monitoring system for distributed power generation electronic interfaces. *IEEE Transactions on Instrumentation and Measurement* 58 (9), 3112–3121.
- Desoer, C., Wang, Y.-T., Apr 1980. On the generalized nyquist stability criterion. *IEEE Transactions on Automatic Control* 25 (2), 187–196.
- Emadi, A., Khaligh, A., Rivetta, C. H., Williamson, G. A., July 2006. Constant power loads and negative impedance instability in automotive systems: definition, modeling, stability, and control of power electronic converters and motor drives. *IEEE Transactions on Vehicular Technology* 55 (4), 1112–1125.
- Familiant, Y. A., Huang, J., Corzine, K. A., Belkhatay, M., July 2009. New techniques for measuring impedance characteristics of three-phase ac power systems. *IEEE Transactions on Power Electronics* 24 (7), 1802–1810.

## BIBLIOGRAPHY

---

- Feng, X., Liu, J., Lee, F. C., Mar 2002. Impedance specifications for stable dc distributed power systems. *IEEE Transactions on Power Electronics* 17 (2), 157–162.
- Fortescue, C. L., July 1918. Method of symmetrical co-ordinates applied to the solution of polyphase networks. *Transactions of the American Institute of Electrical Engineers* XXXVII (2), 1027–1140.
- Girgis, A., Chang, W., Makram, E., Jul 1991. A digital recursive measurement scheme for online tracking of power system harmonics. *IEEE Transactions on Power Delivery* 6 (3), 1153–1160.
- Hoffmann, N., Fuchs, F. W., Feb 2014. Minimal invasive equivalent grid impedance estimation in inductive-resistive power networks using extended kalman filter. *IEEE Transactions on Power Electronics* 29 (2), 631–641.
- Huang, J., Corzine, K. A., Belkhat, M., Feb 2009. Small-signal impedance measurement of power-electronics-based ac power systems using line-to-line current injection. *IEEE Transactions on Power Electronics* 24 (2), 445–455.
- Kalman, R. E., 1960. A new approach to linear filtering and prediction problems. *Journal of Fluids Engineering* 82 (1), 35–45.
- Kreyszig, E., 2011. *Advanced Engineering Mathematics*. John Wiley & Sons.
- Lei, Q., Shen, M., Blasko, V., Liang, S., Peng, F. Z., March 2014. A generalized dq impedance model of a three phase system. In: 2014 IEEE Applied Power Electronics Conference and Exposition - APEC 2014. pp. 1874–1881.
- Lei, Q., Shen, M., Blasko, V., Peng, F. Z., March 2013. A generalized input impedance model of three phase diode rectifier. In: Applied Power Electronics Conference and Exposition (APEC), 2013 Twenty-Eighth Annual IEEE. pp. 2655–2661.
- Ljung, L., 1998. *System identification, Theory for the User*. Springer.
- Macias, J., Gomez Exposito, A., Jan 2006. Self-tuning of kalman filters for harmonic computation. *IEEE Transactions on Power Delivery* 21 (1), 501–503.
- Nagpal, M., Xu, W., Sawada, J., Jan 1998. Harmonic impedance measurement using three-phase transients. *IEEE Transactions on Power Delivery* 13 (1), 272–277.
- Nilsson, J. W., Riedel, S. A., 2011. *Electric Circuits*. Pearson Education, Inc.
- Rhode, J. P., Kelley, A. W., Baran, M. E., Oct 1995. Line impedance measurement: a nondisruptive wideband technique. In: Industry Applications Conference, 1995. Thirtieth IAS Annual Meeting, IAS '95., Conference Record of the 1995 IEEE. Vol. 3. pp. 2233–2240 vol.3.
- Sakui, M., Fujita, H., Nov 1994. An analytical method for calculating harmonic currents of a three-phase diode-bridge rectifier with dc filter. *IEEE Transactions on Power Electronics* 9 (6), 631–637.

- Skjong, E., Molinas, M., Johansen, T., March 2015. Optimized current reference generation for system-level harmonic mitigation in a diesel-electric ship using non-linear model predictive control. In: Industrial Technology (ICIT), 2015 IEEE International Conference on. pp. 2314–2321.
- Sumner, M., Palethorpe, B., Thomas, D. W. P., July 2004. Impedance measurement for improved power quality-part 1: the measurement technique. *IEEE Transactions on Power Delivery* 19 (3), 1442–1448.
- Sun, J., 2000. Unified averaged switch models for stability analysis of large distributed power systems. In: Applied Power Electronics Conference and Exposition, 2000. APEC 2000. Fifteenth Annual IEEE. Vol. 1. pp. 249–255 vol.1.
- Sun, J., April 2009. Small-signal methods for electric ship power systems. In: 2009 IEEE Electric Ship Technologies Symposium. pp. 44–52.
- Sun, J., Nov 2011. Impedance-based stability criterion for grid-connected inverters. *IEEE Transactions on Power Electronics* 26 (11), 3075–3078.
- Sun, M., Sahinoglu, Z., Jan 2011. Extended kalman filter based grid synchronization in the presence of voltage unbalance for smart grid. In: Innovative Smart Grid Technologies (ISGT), 2011 IEEE PES. pp. 1–4.
- Sørffonn, I., 2007. Power management control of electrical propulsion systems. In: Dynamic Positioning Conference, Wartsila NA Inc.
- Timbus, A., Liserre, M., Teodorescu, R., Blaabjerg, F., June 2005. Synchronization methods for three phase distributed power generation systems - an overview and evaluation. In: 2005 IEEE 36th Power Electronics Specialists Conference. pp. 2474–2481.
- Wildrick, C. M., Lee, F. C., Cho, B. H., Choi, B., May 1995. A method of defining the load impedance specification for a stable distributed power system. *IEEE Transactions on Power Electronics* 10 (3), 280–285.
- Xiao, P., Venayagamoorthy, G., Corzine, K., June 2007. A novel impedance measurement technique for power electronic systems. In: 2007 IEEE Power Electronics Specialists Conference. pp. 955–960.
- Yifei, W., Chen, S., Choi, S. S., Dec 2007. An overview of various approaches to power system harmonic analysis. In: 2007 International Power Engineering Conference (IPEC 2007). pp. 338–343.
- Ådnanes, A. K., Sørensen, A. J., Hackman, T., 1997. Essential characteristics of electrical propulsion and thruster drives in dp vessels. In: Proc. DP Conference. Houston, Texas.



# Appendices



# Appendix **A**

## Submitted digest for COMPEL

In this appendix the digest submission for the IEEE Power Electronics Society's Seventeenth IEEE Workshop on Control and Modeling for Power Electronics, COMPEL 2016 in Trondheim, Norway.

# Instantaneous Frequency Tracking of Harmonic Distortions for Grid Impedance Identification based on Kalman Filtering

## Abstract

This paper presents a non-invasive approach for real-time grid impedance identification based on the principle of instantaneous frequency tracking of voltage and current harmonics by the use of Kalman Filtering(KF). The KF based technique is compared to the FFT frequency domain approach highlighting the advantages and disadvantages of each method. The KF based approach can be used as basis for a real-time grid stability assessment based on impedance identification.

## I. INTRODUCTION

Knowledge of the source and load impedances in an electrical grid is essential in order to estimate the stability of the grid using the impedance-base method with the generalized Nyquist stability criterion first described in [1] with an application for AC systems in [2]. The impedance-based method requires however the injection of small signals in a wide range of frequency to obtain a good estimate of the stability of the grid. This frequency scanning technique does not allow for a real-time estimation of the impedances and stability. The real-time identification of the impedances of the grid can be relevant considering the non-stationary environment where the impedance may vary with the operating conditions and with parameter variations over time [3]. This paper is proposing a non-invasive method to identify the impedances of the grid based on the use of the information of the distortions already present in the current and voltage waveforms, without resorting to any small signal injection. Modern electrical systems are including more and more non-linear loads that are a frequent source of harmonic distortions. Electrical grids that are already affected by distorted voltages and currents can readily benefit from a non-invasive approach of impedance identification that makes use of the information provided by such distortions and can lead to a straightforward grid stability assessment in time-domain. The tracking, at a given node, of each of the harmonic components present in the voltage and current can enable the identification of the grid impedances in a non-invasive way, by simply calculating the ratio  $V(\omega)/I(\omega) = Z(\omega)$  at each harmonic distortion.

The commonly applied methods relying on frequency scanning [4], generally require assumptions to be made about the signal such as the signal being stationary and periodic, where the sampling frequency is equal to the number of samples multiplied by the fundamental frequency, the Nyquist sampling theorem holds and each frequency is an integer multiple of the fundamental frequency which will be the inverse of the window length [5].

Harmonics estimation in the time-domain using Kalman theory will track the phase and amplitude of the harmonics of a distorted signal (voltage and current) using state space form and has potential for real-time processing due to

the low computational load. The use of KF for this problem is proposed in [5] using a linear KF as first described in [6]. These methods concludes that KF theory is able to estimate accurately harmonic components even during high power system disturbance conditions.

In the following, this paper will present how a linear KF can be used for combined harmonic identification and impedance estimation based on a linear state-space model and best fitting curve. The impedance identified with the KF based approach will be used in the final paper to assess the stability of the grid and it will be compared to the frequency scanning method in terms of real-time properties.

## II. POWER SYSTEM OVERVIEW

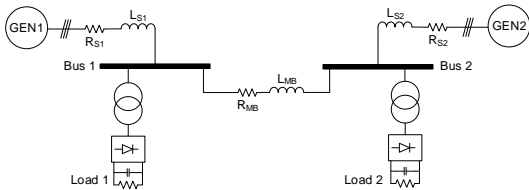


Fig. 1: Power Grid model

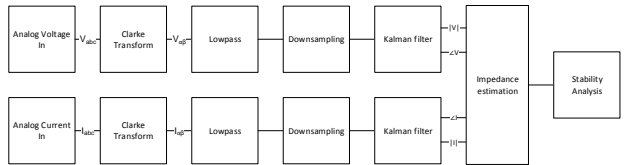


Fig. 2: Signal acquisition and signal processing

The system under investigation in this paper is a shipboard power system with two generators and two loads based on 6-pulse diode rectifiers. The 6-pulse diode rectifier will distort the AC side of the converter currents with higher order harmonics because of the non-linear relation between voltage and currents [7]. These harmonics currents will propagate through the electrical grid and distort the source voltage for other grid-connected equipment.  $N_d$ -pulse diode rectifiers will create harmonic distortions on the positive sequence in the harmonic components in the set  $h_p = \{1, N_d k + 1 | k = 1, 2, \dots\}$  and in the negative sequence  $h_n = \{N_d k - 1 | k = 1, 2, \dots\}$ .

## III. PROBLEM FORMULATION FOR HARMONIC IDENTIFICATION

For the system in Fig. 1, unbalanced three-phase current and voltage signals are assumed. Applying the Clarke, transform without the zero sequence components, and the Fortescue Theorem [8], such a signal is described in the  $\alpha\beta$  frame as a balanced system in (1) with  $X_i$  is the magnitude for the harmonic  $i$  in positive or negative sequence, and similar for the angle  $\theta_i$ .

$$x_{\alpha\beta}(t) = \begin{bmatrix} x_\alpha \\ x_\beta \end{bmatrix} = \sum_{i \in h_p} \begin{bmatrix} \cos(i\omega t) & -\sin(i\omega t) \\ \sin(i\omega t) & \cos(i\omega t) \end{bmatrix} \begin{bmatrix} X_{i,p} \cos(\theta_{i,p}) \\ X_{i,p} \sin(\theta_{i,p}) \end{bmatrix} + \sum_{i \in h_n} \begin{bmatrix} \cos(i\omega t) & -\sin(i\omega t) \\ -\sin(i\omega t) & -\cos(i\omega t) \end{bmatrix} \begin{bmatrix} X_{i,n} \cos(\theta_{i,n}) \\ X_{i,n} \sin(\theta_{i,n}) \end{bmatrix} \quad (1)$$

### A. Signal Acquisition and Processing

In the system described in Fig.1, three-phase voltage and current measurements in the abc frame,  $\mathbf{V}_{abc}$  and  $\mathbf{I}_{abc}$  are taken. In order to ease the extraction of the phase and amplitude of the phasors, the Clarke transform is used to obtain the signal in the  $\alpha\beta\gamma$  frame with the  $\gamma$  component omitted. In Fig. 2 an overview of the signal acquisition and processing is shown.

### B. Instantaneous Frequency Tracking

In KF based estimation, the states are estimated using an adaptive KF in linear state space form with random walk for the states which corresponds to the  $\alpha$  and  $\beta$  signal magnitude at each time instant. The tuning of a KF is a difficult task when tracking signals with sudden changes, hence an adaptive KF filter based on [9] is implemented. For adaptively changing the model error covariance  $\mathbf{Q}$  depending on the errors and changes in the system to comply with a real-time application with additional step given in (2). This reformulation of the KF will yield much better estimation for a non-stationary system.

$X_i \cos(\theta_i)$  and  $X_i \sin(\theta_i)$  in (1) are written as  $x_{i,1}$  and  $x_{i,2}$  for making the formulation suitable for KF. The state space and measurement equations is given in (3) which estimate the states  $x_{i,1}$  and  $x_{i,2}$  in which states have information about the phase and amplitude of each harmonic  $i$  analyzed by the KF.

$$\hat{\mathbf{w}}[k] = \mathbf{K}[k](y[k] - \mathbf{C}[k]\hat{\mathbf{x}}^-[k]) \quad (2a)$$

$$\mathbf{Q}[k] = \sum_i \hat{w}_i[k]^2 \quad (2b)$$

$$\begin{bmatrix} x_{i,1} \\ x_{i,2} \end{bmatrix}_{k+1} = \begin{bmatrix} 1 & 0 \\ 0 & 1 \end{bmatrix} \begin{bmatrix} x_{i,1} \\ x_{i,2} \end{bmatrix}_k + \begin{bmatrix} w_{i,1} \\ w_{i,2} \end{bmatrix}_k \quad i \in h_p, h_n \quad (3)$$

With the states estimated, the phasor information for the positive and negative sequence are obtained by calculating the magnitude and phase. Furthermore, the impedance could be calculated by voltage over current phasor division of  $\mathbf{V}_i$  and  $\mathbf{I}_i$  for each harmonic  $i$  estimated.

### C. Comparison to the sequence analyzer in MATLAB

The KF based identification results shown in Fig. 3 and 5 are compared to a Fourier-based method of [10] where a waveform  $x(t)$  can be approximated by estimating all harmonics with angular frequency  $\omega_k = k \frac{2\pi}{T}$ ,  $k \in 1, 2, \dots$  and  $T$  is the sliding window length. This estimation method will provide a dynamical phasor with high accuracy when the harmonic is an integer multiple of the inverse of the window function length which in most applications are one period of the fundamental frequency.

## IV. PRELIMINARY RESULTS

### A. Power Grid and Measured Signals

A simulation model is built in MATLAB Simulink using the SimPowerSystems library components. The first step is to estimate the phasor of the harmonics for the currents and voltages. The voltage is measured at Bus 1 and the current through Generator 1 in Fig. 1. The grid is simulated for 100ms before the estimation starts in order for the grid to stabilize. The signal is filtered with a low-pass filter with cut-off frequency at the 13th harmonic component.

### B. Harmonic detection

The KF based method in Fig. 3 and the sequence analyzer in Fig. 4 give both very similar results when tracking components of periodic signals. The KF has slightly faster response as it does not need one fundamental period before meaningful results are obtained. When adding a non-characteristic harmonic, the Fourier method is not able to track the harmonic with sufficient accuracy. This is because the signal is not an integer multiple of the inverse of the window length. However, the KF based method is unaffected by the presence of non-characteristic harmonics, resulting in a good identification in Fig. 5 and Fig. 6. This is simulated by injecting two non-characteristic harmonics on 75Hz and 175Hz, (1.5 and 3.5 harmonics) in the grid from Generator 1.

Both methods are able to track non-stationary signals but the KF based method has a slightly faster response compared to the Fourier method with dynamics faster than the inverse of the window length. These results are seen in Fig. 8 with amplitude variation on the fundamental harmonic in addition to a 5th and 13th order harmonics with no time-variation. In this case the non-stationary signal is not generated by the grid, but artificially generated signals so that the time variation is better viewed and not the transient after step change in the grid.

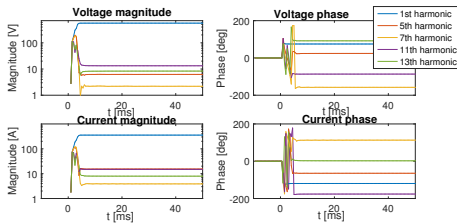


Fig. 3: Current and voltage harmonics estimated with Kalman filter

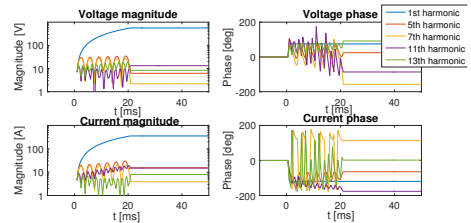


Fig. 4: Current and voltage harmonics estimated with Sequence Analyzer in MATLAB Simulink

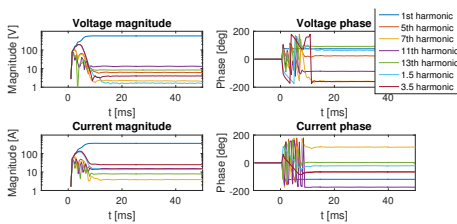


Fig. 5: Non-characteristics harmonics current and voltage phasor estimated with Kalman filter

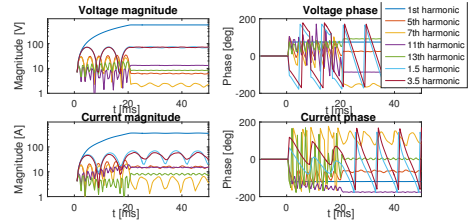


Fig. 6: Non-characteristics harmonics current and voltage phasor estimated with Sequence Analyzer in MATLAB Simulink

## V. REAL-TIME IMPEDANCE IDENTIFICATION

Based on the identified impedance values for each given harmonic distortion, the Least Squares method is used to best fit the identified points in order to estimate the best fitting equivalent impedance curve following technique described in [11]. The proposed method utilizes the harmonics present in the system to obtain all the operating points in each time step. By modeling the portion of the grid under investigation as a pure series R-L branch in series

with a voltage source with component only on the fundamental frequency, the impedance is  $Z = R_g + j\omega L_g$  and is equal for each harmonic where  $R_g$  and  $L_g$  is the sum of impedance in the generator and in the distributional lines [12]. The estimated impedance magnitudes and phases with respect to frequency is presented in Fig. 7 where the estimations from the Kalman filtering, the estimated impedance from the Least Squares method and the analytical expression for the impedance are shown. The result is promising when assuming an impedance model of the grid.

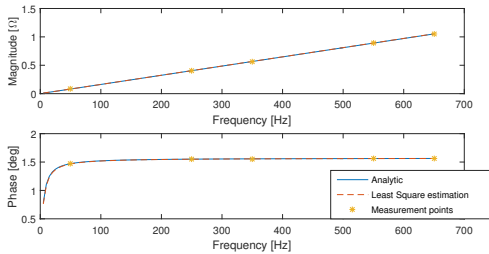


Fig. 7: Estimated impedance with Least Squares compared to analytically calculated impedance

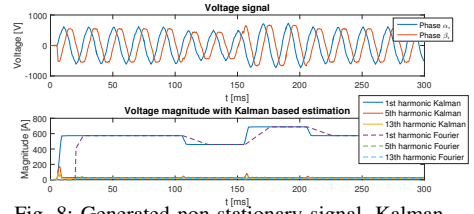


Fig. 8: Generated non-stationary signal, Kalman harmonics tracking compared to Fourier based tracking

## REFERENCES

- [1] C. Desoer and Y.-T. Wang, "On the generalized nyquist stability criterion," *IEEE Transactions on Automatic Control*, vol. 25, no. 2, pp. 187–196, Apr 1980.
- [2] J. Sun, "Impedance-based stability criterion for grid-connected inverters," *IEEE Transactions on Power Electronics*, vol. 26, no. 11, pp. 3075–3078, Nov 2011.
- [3] M. Cespedes and J. Sun, "Adaptive control of grid-connected inverters based on online grid impedance measurements," *IEEE Transactions on Sustainable Energy*, vol. 5, no. 2, pp. 516–523, April 2014.
- [4] M. Nagpal, W. Xu, and J. Sawada, "Harmonic impedance measurement using three-phase transients," *IEEE Transactions on Power Delivery*, vol. 13, no. 1, pp. 272–277, Jan 1998.
- [5] A. Girgis, W. Chang, and E. Makram, "A digital recursive measurement scheme for online tracking of power system harmonics," *IEEE Transactions on Power Delivery*, vol. 6, no. 3, pp. 1153–1160, Jul 1991.
- [6] R. E. Kalman, "A new approach to linear filtering and prediction problems," *Journal of Fluids Engineering*, vol. 82, no. 1, pp. 35–45, 1960.
- [7] "Modeling and simulation of the propagation of harmonics in electric power networks. i. concepts, models, and simulation techniques," *IEEE Transactions on Power Delivery*, vol. 11, no. 1, pp. 452–465, Jan 1996.
- [8] C. L. Fortescue, "Method of symmetrical co-ordinates applied to the solution of polyphase networks," *Transactions of the American Institute of Electrical Engineers*, vol. XXXVII, no. 2, pp. 1027–1140, July 1918.
- [9] J. Macias and A. Gomez Exposito, "Self-tuning of kalman filters for harmonic computation," *IEEE Transactions on Power Delivery*, vol. 21, no. 1, pp. 501–503, Jan 2006.
- [10] S. Sanders, J. Noworolski, X. Liu, and G. C. Verghese, "Generalized averaging method for power conversion circuits," *IEEE Transactions on Power Electronics*, vol. 6, no. 2, pp. 251–259, Apr 1991.
- [11] S. Cobrecas, E. Bueno, D. Pizarro, F. Rodriguez, and F. Huerta, "Grid impedance monitoring system for distributed power generation electronic interfaces," *IEEE Transactions on Instrumentation and Measurement*, vol. 58, no. 9, pp. 3112–3121, Sept 2009.
- [12] M. R. Patel, *Shipboard Electrical Power Systems*. CRC Press, 2011.

# Appendix **B**

## Submitted paper for COMPEL

In this appendix the paper submission for the IEEE Power Electronics Society's Seventeenth IEEE Workshop on Control and Modeling for Power Electronics, COMPEL 2016 in Trondheim, Norway.

# Instantaneous Frequency Tracking of Harmonic Distortions for Grid Impedance Identification based on Kalman Filtering

Anders Kjekja Broen<sup>\*†</sup>, Mohammad Amin<sup>\*</sup>, Espen Skjong<sup>\*</sup> and Marta Molinas<sup>\*</sup>

<sup>\*</sup> Department of Engineering Cybernetics  
Norwegian University of Science and Technology

<sup>†</sup> Email: anders.kjekja.broen@gmail.com

**Abstract**—This paper presents a non-invasive approach for real-time grid impedance identification based on the principle of instantaneous frequency tracking of voltage and current harmonics by the use of Kalman filter(KF). The KF based technique is compared to the FFT frequency domain approach highlighting the advantages and disadvantages of each method. The KF based approach can be used as basis for a real-time grid stability assessment based on impedance identification.

## I. INTRODUCTION

Knowledge of the source and load impedances in an electrical grid is essential to estimate the stability of the grid using the impedance-base method with the generalized Nyquist stability criterion first described in [1] with an application for AC systems in [2]. The impedance-based method requires, however, the injection of small signals in a wide range of frequency to obtain a good estimate of the stability of the grid. This frequency scanning technique does not allow for a real-time estimation of the impedances and stability. The real-time identification of the impedances of the grid can be relevant considering the non-stationary environment where the impedance may vary with the operating conditions and with parameter variations over time [3]. This paper is proposing a non-invasive method to identify the impedances of the grid based on the use of the information of the distortions already present in the current and voltage waveforms, without resorting to any small-signal injection.

Modern electrical systems are including more and more non-linear loads that are a frequent source of harmonic distortions. Electrical grids that are already affected by distorted voltages and currents can readily benefit from a non-invasive approach of impedance identification that makes use of the information provided by such distortions and can lead to a straightforward grid stability assessment in time-domain. The tracking, at a given node, of each of the harmonic components present in the voltage and current, can enable the identification of the grid impedances in a non-invasive way, by simply calculating the ratio  $V(\omega)/I(\omega) = Z(\omega)$  at each harmonic distortion.

The commonly applied methods relying on frequency scanning [4], generally require assumptions to be made about the signal such as the signal being stationary and periodic, where the sampling frequency is equal to the number of samples

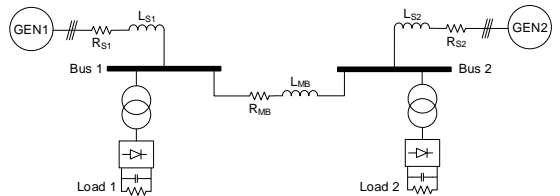


Fig. 1. Power Grid model

multiplied by the fundamental frequency, the Nyquist sampling theorem holds and each frequency is an integer multiple of the fundamental frequency which will be the inverse of the window length [5].

Harmonics estimation in the time-domain using Kalman theory will track the phase and amplitude of the harmonics of a distorted signal (voltage and current) using state space form and has the potential for real-time processing due to the low computational load. The use of KF for this problem is proposed in [5] using a linear KF as first described in [6]. These methods conclude that KF theory can estimate accurately harmonic components even during high power system disturbance conditions.

In the following, this paper will present how a linear KF can be used for combined harmonic identification and impedance estimation based on a linear state-space model and best fitting curve.

## II. POWER SYSTEM OVERVIEW

The system under investigation in this paper is a shipboard power system with two generators and two loads based on 6-pulse diode rectifiers. The 6-pulse diode rectifier will distort the AC side of the converter currents with higher order harmonics because of the non-linear relation between voltage and currents [7]. These harmonics currents will propagate through the electrical grid and distort the source voltage for other grid-connected equipment.  $N_d$ -pulse diode rectifiers will create harmonic distortions on the positive sequence in the harmonic components in the set  $h_p = \{1, N_d k + 1 | k = 1, 2, \dots\}$  and in the negative sequence  $h_n = \{N_d k - 1 | k = 1, 2, \dots\}$ .

### III. PROBLEM FORMULATION FOR HARMONIC IDENTIFICATION

The method for harmonic detection builds on the work from [8] where an Adaptive Kalman Filter (AKF) is introduced. In [9] a method for tracking the angular frequency  $\omega$  for a Smart Grid is proposed by following the positive and negative sequence fundamental frequency for a three-phase system. By restating the problem to track all harmonics and assume that the angular frequency is known, tracking of positive and negative sequence harmonics can be done with inspiration from the work in that paper. The development for such a tracking is given in this section.

Given a three-phase signal in the  $abc$  frame in (1) where  $\omega(t)$  is the angular frequency which is assumed to be known,  $A_a(t), A_b(t), A_c(t)$  are the amplitude for each of the phases and  $\phi_a, \phi_b, \phi_c$  are the initial phase angle for each phase.  $\omega = 2\pi f$  is the angular frequency, and one define  $\theta_i(t) = \omega t + \phi_i$  for each phases  $i \in a, b, c$ .

$$S_a(t) = A_a(t)\cos(\omega(t)t + \phi_a(t)) \quad (1a)$$

$$S_b(t) = A_b(t)\cos(\omega(t)t + \phi_b(t)) \quad (1b)$$

$$S_c(t) = A_c(t)\cos(\omega(t)t + \phi_c(t)) \quad (1c)$$

In a balanced system there is a relationship between the phase angles by stating them as time-invariant given by  $\phi_b = \phi_a - \frac{2\pi}{3}$  and  $\phi_c = \phi_a + \frac{2\pi}{3}$ , and for the amplitudes  $A_a = A_b = A_c = A$ . In an unbalanced system, no such assumptions can be made, and one ends up with six variables for each time instant by stating the system in the  $abc$  frame for tracking the components of such a signal. To reduce the number of variables, the unbalanced three-phase system is transformed into three balanced systems named the positive, negative and zero sequence by using the Fortescue Theorem [10]. The system of the three balanced systems is given in (2).

$$S_a = S_{a,p} + S_{a,n} + S_{a,0} \quad (2a)$$

$$S_b = S_{b,p} + S_{b,n} + S_{b,0} \quad (2b)$$

$$S_c = S_{c,p} + S_{c,n} + S_{c,0} \quad (2c)$$

The unbalanced  $S_{abc} = [S_a, S_b, S_c]^T$  is now stated as 3 balanced systems  $S_p = [S_{a,p}, S_{b,p}, S_{c,p}]^T$ ,  $S_n = [S_{a,n}, S_{b,n}, S_{c,n}]^T$  and  $S_0 = [S_{a,0}, S_{b,0}, S_{c,0}]^T$ . By using the phase sequence one can state this problem in time domain form in (3) by using  $\theta_p = \omega t + \phi_p$  and  $\theta_n = \omega t + \phi_n$ .

$$\begin{bmatrix} S_a(t) \\ S_b(t) \\ S_c(t) \end{bmatrix} = S_p \begin{bmatrix} \cos(\theta_p(t)) \\ \cos(\theta_p(t) - \frac{2\pi}{3}) \\ \cos(\theta_p(t) + \frac{2\pi}{3}) \end{bmatrix} + S_n \begin{bmatrix} \cos(\theta_n(t)) \\ \cos(\theta_n(t) + \frac{2\pi}{3}) \\ \cos(\theta_n(t) - \frac{2\pi}{3}) \end{bmatrix} + S_0 \begin{bmatrix} 1 \\ 1 \\ 1 \end{bmatrix} \quad (3)$$

This signal is transformed using the Clarke transform to the  $\alpha\beta 0$  stationary frame with the transformation defined in (4).

$$\mathbf{T}_{\alpha\beta 0} = \begin{bmatrix} \frac{2}{3} & \frac{-1}{3} & \frac{-1}{3} \\ 0 & \frac{1}{\sqrt{3}} & \frac{-1}{\sqrt{3}} \\ \frac{1}{2} & \frac{1}{2} & \frac{1}{2} \end{bmatrix} \quad (4)$$

The three-phase signal in  $S_{\alpha\beta 0}$  is obtained by using the defined transformation (5).

$$S_{\alpha\beta 0}(t) = \mathbf{T}_{\alpha\beta 0} S_{abc}(t) \quad (5)$$

This transformation is useful because if the system is balanced, then the 0 component will always be reduced to zero. Applying the  $T_{\alpha\beta 0}$  transformation on the system in (3) one obtains the following.

$$S_{\alpha\beta 0} = \mathbf{T}_{\alpha\beta 0} S_{abc} = \mathbf{T}_{\alpha\beta 0} S_p \begin{bmatrix} \cos(\theta_p) \\ \sin(\theta_p) \\ 0 \end{bmatrix} + \mathbf{T}_{\alpha\beta 0} S_n \begin{bmatrix} \cos(\theta_n) \\ -\sin(\theta_n) \\ 0 \end{bmatrix} + \mathbf{T}_{\alpha\beta 0} S_0 \begin{bmatrix} 0 \\ 0 \\ 0 \end{bmatrix} \quad (6)$$

By inspection of (6) one sees that all the zero components are zero, because of the assumption that the Fortescue's theorem holds. The reduced model with only the  $\alpha$  and  $\beta$  component is shown in (8) using the reduced Clarke Transform as shown in (7).

$$\mathbf{T}_{\alpha\beta} = \begin{bmatrix} \frac{2}{3} & \frac{-1}{3} & \frac{-1}{3} \\ 0 & \frac{1}{\sqrt{3}} & \frac{-1}{\sqrt{3}} \end{bmatrix} \quad (7)$$

$$S_{\alpha\beta} = \mathbf{T}_{\alpha\beta} S_{abc} = \mathbf{T}_{\alpha\beta} S_p \begin{bmatrix} \cos(\theta_p) \\ \sin(\theta_p) \end{bmatrix} + \mathbf{T}_{\alpha\beta} S_n \begin{bmatrix} \cos(\theta_n) \\ -\sin(\theta_n) \end{bmatrix} \quad (8)$$

By remembering that  $\theta_p = \omega t + \phi_p$  and  $\theta_n = \omega t + \phi_n$  and using the sum and difference formulas for trigonometric functions:  $\sin(a \pm b) = \sin(a)\cos(b) \pm \cos(a)\sin(b)$  and  $\cos(a \pm b) = \cos(a)\cos(b) \mp \sin(a)\sin(b)$  one can write the (8) as (9). Here all the harmonics of the system are included into one equation. By stating the fundamental angular frequency of the grid as  $\omega$  other harmonics, but not limited to natural numbers  $i$ , is a harmonic with angular frequency  $\omega i = i\omega$ . Here  $A_{i,p}$  and  $A_{i,n}$  are the magnitudes of the positive and negative sequence respectively at the harmonic  $i$ .  $\phi_{i,p}$  and  $\phi_{i,n}$  are the initial phase angles for the negative and the positive sequence for harmonic  $i$ .

$$\begin{bmatrix} S_\alpha(t) \\ S_\beta(t) \end{bmatrix} = \sum_{i \in h_p} \begin{bmatrix} \cos(i\omega t) & -\sin(i\omega t) \\ \sin(i\omega t) & \cos(i\omega t) \end{bmatrix} \begin{bmatrix} A_{i,p} \cos(\phi_{i,p}) \\ A_{i,p} \sin(\phi_{i,p}) \end{bmatrix} + \sum_{i \in h_n} \begin{bmatrix} \cos(i\omega t) & -\sin(i\omega t) \\ -\sin(i\omega t) & -\cos(i\omega t) \end{bmatrix} \begin{bmatrix} A_{i,n} \cos(\phi_{i,n}) \\ A_{i,n} \sin(\phi_{i,n}) \end{bmatrix} \quad (9)$$

$S_i \cos(\phi_i)$  and  $S_i \sin(\phi_i)$  in (9) are written as  $x_{i,1}$  and  $x_{i,2}$  for making the formulation suitable for KF. Using this formulation one has separated the time-varying  $\omega t$  and the slow varying part of magnitude and initial phase angle. The

state-space and measurement equations is given in (10) and (11) which estimate the states  $x_{i,1}$  and  $x_{i,2}$  in which states have information about the phase and amplitude of each harmonic  $i$  analyzed by the KF.

$$y[k] = \sum_{h \in h_p} \begin{bmatrix} \cos(i\omega\Delta tk) & -\sin(i\omega\Delta tk) \\ \sin(i\omega\Delta tk) & \cos(i\omega\Delta tk) \end{bmatrix} \begin{bmatrix} x_{i,1} \\ x_{i,2} \end{bmatrix}_k + \quad (10)$$

$$\sum_{i \in h_n} \begin{bmatrix} \cos(i\omega\Delta tk) & -\sin(i\omega\Delta tk) \\ -\sin(i\omega\Delta tk) & -\cos(i\omega\Delta tk) \end{bmatrix} \begin{bmatrix} x_{i,1} \\ x_{i,2} \end{bmatrix}_k$$

$$\begin{bmatrix} x_{i,1} \\ x_{i,2} \end{bmatrix}_{k+1} = \begin{bmatrix} 1 & 0 \\ 0 & 1 \end{bmatrix} \begin{bmatrix} x_{i,1} \\ x_{i,2} \end{bmatrix}_k \quad (11)$$

In the AKF, one can define the size of the system  $N$  as the twice the number of positive and negative harmonics. Then the  $\mathbf{A}$  is a  $N \times N$  system matrix,  $\mathbf{C}$  is a  $2 \times N$  measurement matrix. For the KF, the  $\mathbf{Q}$  is a  $N \times N$  adaptively updated covariance matrix which is initialized to the zero matrix.  $\mathbf{R}$  is a  $2 \times 2$  measurement error matrix which needs to be tuned in agreement with the measurement noise of the system.

#### A. Instantaneous Frequency Tracking

In contrast to the frequency domain approach of the FFT, the Kalman filter identification operates directly in the time domain, and there is no lag from measurements to the estimation result. Using frequency domain approach there is a minimum lag of one fundamental period before the estimation has meaningful data. In KF based estimation, the states are estimated using an adaptive KF in linear state space form with a random walk for the states which corresponds to the  $\alpha$  and  $\beta$  signal magnitude at each time instant. The tuning of a KF is a difficult task when tracking signals with sudden changes; hence, an adaptive KF filter based on [8] is implemented. For adaptively changing the model error covariance  $\mathbf{Q}$  depending on the errors and variations in the system the update law for adaptive Kalman filter algorithm is given in (12).

$V_i \cos(\phi_i)$  and  $V_i \sin(\phi_i)$  in (9) are written as  $x_{i,1}$  and  $x_{i,2}$  for making the formulation suitable for KF. Using this formulation one has separated the the time-varying  $\omega t$  and the slow varying part of magnitude and initial phase angle. The state space and measurement equations is given in (10) and (11) which estimate the states  $x_{i,1}$  and  $x_{i,2}$  in which states have information about the phase and amplitude of each harmonic  $i$  analyzed by the KF.

$$\hat{\mathbf{x}}^- [k] = \mathbf{A} \hat{\mathbf{x}} [k-1] \quad (12a)$$

$$\mathbf{P}^- [k] = \mathbf{A} \mathbf{P} [k-1] \mathbf{A}^T + \mathbf{Q} [k-1] \quad (12b)$$

$$\mathbf{K} [k] = \mathbf{P}^- [k] \mathbf{C} [k]^T (\mathbf{C} [k] \mathbf{P}^- [k] \mathbf{C} [k]^T + \mathbf{R})^{-1} \quad (12c)$$

$$\hat{\mathbf{x}} [k] = \hat{\mathbf{x}}^- [k] + \mathbf{K} [k] (y[k] - \mathbf{C} [k] \hat{\mathbf{x}}^- [k]) \quad (12d)$$

$$\hat{\mathbf{w}} [k] = \mathbf{K} [k] (y[k] - \mathbf{C} [k] \hat{\mathbf{x}}^- [k]) \quad (12e)$$

$$\mathbf{Q} [k] = \sum_i \hat{\mathbf{w}}_i [k]^2 \quad (12f)$$

$$\mathbf{P} [k] = (\mathbf{I} - \mathbf{K} [k] \mathbf{C} [k]) \mathbf{P}^- [k] \quad (12g)$$

In the adaptive Kalman filter, one can define the size of the system  $N$  as the twice the number of positive and negative harmonics. Then the  $\mathbf{A}$  is a  $N \times N$  system matrix,  $\mathbf{A}$  is a  $2 \times N$  measurement matrix. For the Kalman filter, the  $\mathbf{Q}$  is a  $N \times N$  adaptively updated covariance matrix which is initialized to the zero matrix.  $\mathbf{R}$  is a  $2 \times 2$  measurement error matrix which needs to be tuned by the measurement noise of the system.

With the states estimated, the phasor information for the positive and negative sequence are obtained by calculating the magnitude and phase. Furthermore, the impedance could be calculated by voltage over current phasor division of  $\mathbf{V}_i$  and  $\mathbf{I}_i$  for each harmonic  $i$  estimated by using (13).

$$A_i = \sqrt{x_{i,1}^2 + x_{i,2}^2} \quad (13a)$$

$$\theta_i = \arctan\left(\frac{x_{i,2}}{x_{i,1}}\right) \quad (13b)$$

#### B. Signal Acquisition and Processing

In the system described in Fig.1, three-phase voltage and current measurements in the  $abc$ -frame,  $\mathbf{V}_{abc}$  and  $\mathbf{I}_{abc}$  are taken. To ease the extraction of the phase and amplitude of the phasors, the Clarke transform is used to obtain the signal in the  $\alpha\beta\gamma$  frame with the  $\gamma$  component omitted.

#### C. Comparison to the sequence analyzer in MATLAB

The KF based identification results shown in Fig. 2 and 4 are compared to a Fourier-based method of [11] where a waveform  $x(t)$  can be approximated by estimating all harmonics with angular frequency  $\omega_k = k \frac{2\pi}{T}$ ,  $k \in 1, 2, \dots$  and  $T$  is the sliding window length. This estimation method will provide a dynamical phasor with high accuracy when the harmonic is an integer multiple of the inverse of the window function length which in most applications are one period of the fundamental frequency.

#### D. Prerequisites for method

For the proposed method to function correctly, the assumption of zero sequences is negligible has to hold. If not, this could easily be added to the algorithm by changing the Clarke transform. For the method to measure impedances at multiple frequencies, the system must be distorted with harmonic frequencies. This assumption holds when using line commuted rectifiers which distort the grid with higher harmonic frequencies above the fundamental frequency. One of the limitation with this is that impedance below the fundamental frequency is not detected. In the Kalman measurement equation (10) it is an assumption that the waveform can be structured into harmonic sinus functions with a given frequency and phase angle. If the signal does not have this characteristic, this equation have to change accordingly.

## IV. EXPERIMENTS

The method is verified by using two models, one simple grid model where a source impedance of the line and a generator is found and a more complex system of an MMC.

### A. Power Grid and Measured Signals

A simulation model is built in MATLAB Simulink using the SimPowerSystems library components. The first step is to estimate the phasor of the harmonics for the currents and voltages. The voltage is measured at Bus 1 and the current through Generator 1 in Fig. 1. The grid is simulated for 100ms before the estimation starts for the grid to stabilize. The signal is filtered by a low-pass filter with cut-off frequency at the 13th harmonic component.

### B. Simulation of grid

The grid is simulated for 50ms with a sampling time of  $1 \times 10^{-5}$ . This signal is low passed filtered using a Finite Impulse Response filter and down sampled to accordingly to the Nyquist sampling theorem. The grid has a nominal frequency of 50Hz. The Kalman filter is

### C. Harmonic detection

The KF based method in Fig. 2 and the sequence analyzer in Fig. 3 give both very similar results when tracking components of periodic signals. The KF has slightly faster response as it does not need one fundamental period before meaningful results are obtained. When adding a non-characteristic harmonic, the Fourier method is not able to track the harmonic with sufficient accuracy. This is because the signal is not an integer multiple of the inverse of the window length. However, the KF based method is unaffected by the presence of non-characteristic harmonics, resulting in a good identification in Fig. 4 and Fig. 5. This is simulated by injecting two non-characteristic harmonics on 75Hz and 175Hz, (1.5 and 3.5 harmonics) in the grid from Generator 1.

Both methods can track non-stationary signals, but the KF based method has a slightly faster response compared to the Fourier method with dynamics faster than the inverse of the window length. These results are seen in Fig. 10 with amplitude variation on the fundamental harmonic in addition to a 5th and 13th order harmonics with no time-variation. In this case, the non-stationary signal is not generated by the grid, but artificially generated signals so that the time variation is better viewed and not the transient after a step change in the grid.

For tracking of non-stationary signals in systems with dynamics, the assumption that there are only frequency components at the given frequencies does not hold outside of the steady state. The derivatives of such dynamical system are not equal to zero in the transient response. One can by this, argue that the method is a steady state method. In steady state, the impedance is simply a function of the imaginary angular frequency  $j\omega$  for linear systems  $Z(j\omega)$ , but outside the steady state the impedance is a function of the complex variable  $s$ ,  $Z(s)$ . This gives a smooth band of frequencies, which means that this is a steady state method where the signals are assumed to vary slowly.

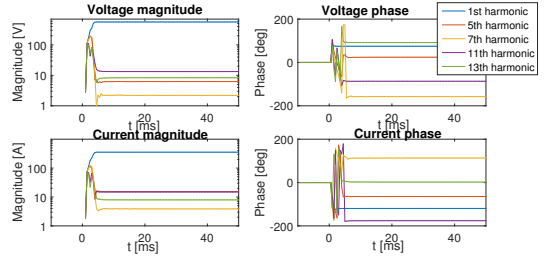


Fig. 2. Current and voltage harmonics estimated with Kalman filter

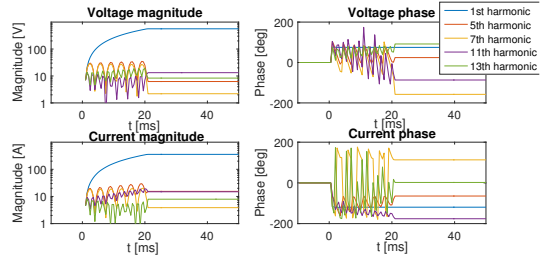


Fig. 3. Current and voltage harmonics estimated with Sequence Analyzer in MATLAB Simulink

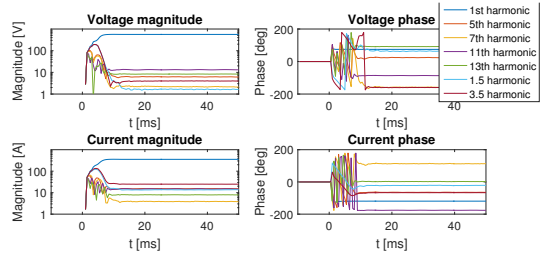


Fig. 4. Non-characteristics harmonics current and voltage phasor estimated with Kalman filter

### D. Impedance estimation of MMC model

The method is verified using a MATLAB Simulink model of a MMC model shown in 6 with the setup in Tab. IV-D. In Fig. 7 the estimated impedance as a time series is shown and the impedance at a given time step is shown in Fig. 8. Using this model, the method can identify the impedance at each higher harmonic component and converges quickly. The impedance of the each component is verified by doing an FFT analysis and also compared to the analytically obtained impedance.

### V. REAL-TIME IMPEDANCE IDENTIFICATION

Based on the identified impedance values for each given harmonic distortion, the Least Squares method is used to best

MMC setup	
$A_{gen1}$	$A_{gen2}$ 690V
$f_{nom}$	50Hz

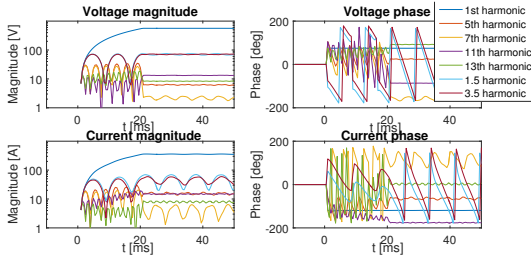


Fig. 5. Non-characteristics harmonics current and voltage phasor estimated with Sequence Analyzer in MATLAB Simulink

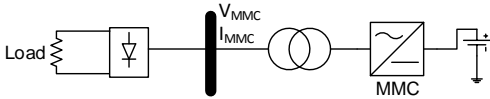


Fig. 6. MMC model

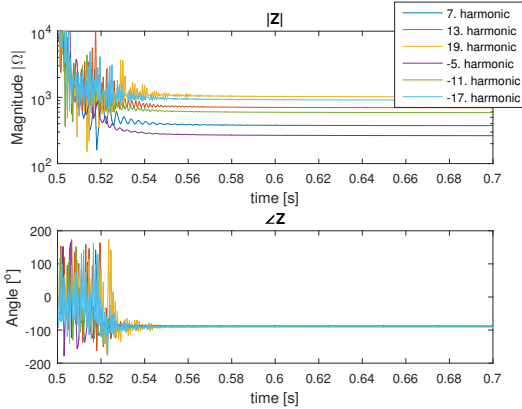


Fig. 7. Estimated impedance of the MMC with Kalman filter

fit the identified points to estimate the best fitting equivalent impedance curve following technique described in [12]. The proposed method utilizes the harmonics present in the system to obtain all the operating points in each time step. By modeling the portion of the grid under investigation as a pure series R-L branch in series with a voltage source with component only on the fundamental frequency, the impedance is  $Z = R_g + j\omega L_g$  and is equal for each harmonic where  $R_g$  and  $L_g$  is the sum of impedance in the generator and the distributional lines [13]. The estimated impedance magnitudes and phases on frequency are presented in Fig. 9 where the estimations from the Kalman filtering, the estimated impedance from the Least Squares method and the analytical expression for the impedance are shown. The result is promising when

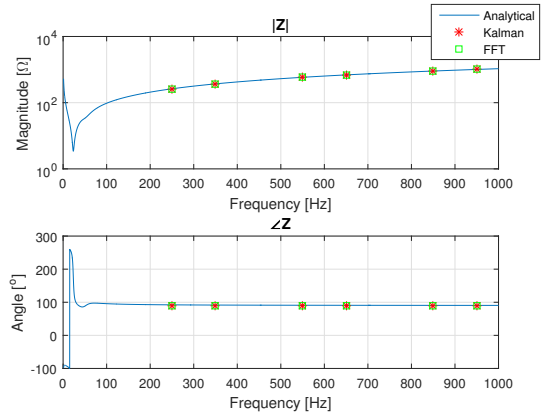


Fig. 8. Estimated impedance of the MMC with Kalman filter at a time step compared to

assuming an impedance model of the grid. For doing this estimation in real-time and recursive least squares estimator could be used to fit the parameters to the measured impedance.

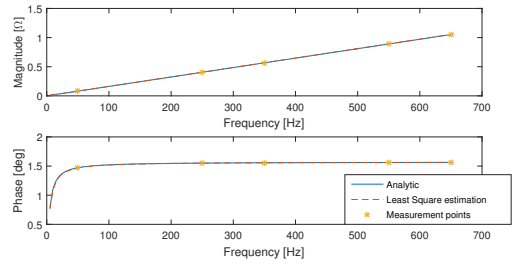


Fig. 9. Estimated impedance with Least Squares compared to analytically calculated impedance

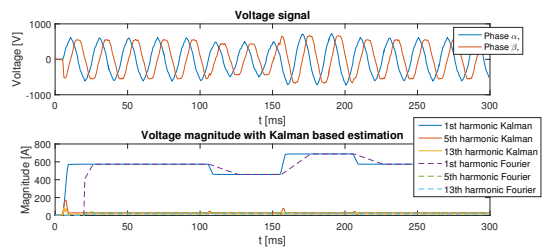


Fig. 10. Generated non-stationary signal, Kalman harmonics tracking compared to Fourier based tracking

## VI. RESULTS

By using the proposed method, the positive and negative sequence harmonic is detected with the Kalman based harmonics tracker for systems in the steady state. To estimate

the parameters correctly based on the harmonics, a model for the impedance in the steady state has to be known. From the estimated parameters for the impedance for different parts of a grid, one can do stability analysis with the use of Nyquist stability criterion. The method can track harmonics and relate those to the real grid parameters with good accuracy.

## VII. CONCLUSION

A method for tracking magnitude and phase of harmonics is proposed in this paper. The method yields good results for systems in the steady state where certain frequencies naturally are occurring but comes to short for estimation in the transient response. From the measured harmonics, one can estimate the parameters specifying the impedance of a system by fitting them in real-time using a recursive least squares estimator. When the impedance can be parameterized from for instance linear elements such as a resistor, capacitor, and inductor, this method can estimate the impedance in real-time based on the harmonics in the grid in a non-invasive way.

## REFERENCES

- [1] C. Desoer and Y.-T. Wang, "On the generalized nyquist stability criterion," *IEEE Transactions on Automatic Control*, vol. 25, no. 2, pp. 187–196, Apr 1980.
- [2] J. Sun, "Impedance-based stability criterion for grid-connected inverters," *IEEE Transactions on Power Electronics*, vol. 26, no. 11, pp. 3075–3078, Nov 2011.
- [3] M. Cespedes and J. Sun, "Adaptive control of grid-connected inverters based on online grid impedance measurements," *IEEE Transactions on Sustainable Energy*, vol. 5, no. 2, pp. 516–523, April 2014.
- [4] M. Nagpal, W. Xu, and J. Sawada, "Harmonic impedance measurement using three-phase transients," *IEEE Transactions on Power Delivery*, vol. 13, no. 1, pp. 272–277, Jan 1998.
- [5] A. Girgis, W. Chang, and E. Makram, "A digital recursive measurement scheme for online tracking of power system harmonics," *IEEE Transactions on Power Delivery*, vol. 6, no. 3, pp. 1153–1160, Jul 1991.
- [6] R. E. Kalman, "A new approach to linear filtering and prediction problems," *Journal of Fluids Engineering*, vol. 82, no. 1, pp. 35–45, 1960.
- [7] "Modeling and simulation of the propagation of harmonics in electric power networks. i. concepts, models, and simulation techniques," *IEEE Transactions on Power Delivery*, vol. 11, no. 1, pp. 452–465, Jan 1996.
- [8] J. Macias and A. Gomez Exposito, "Self-tuning of kalman filters for harmonic computation," *IEEE Transactions on Power Delivery*, vol. 21, no. 1, pp. 501–503, Jan 2006.
- [9] M. Sun and Z. Sahinoglu, "Extended kalman filter based grid synchronization in the presence of voltage unbalance for smart grid," in *Innovative Smart Grid Technologies (ISGT), 2011 IEEE PES*, Jan 2011, pp. 1–4.
- [10] C. L. Fortescue, "Method of symmetrical co-ordinates applied to the solution of polyphase networks," *Transactions of the American Institute of Electrical Engineers*, vol. XXXVII, no. 2, pp. 1027–1140, July 1918.
- [11] S. Sanders, J. Noworolski, X. Liu, and G. C. Verghese, "Generalized averaging method for power conversion circuits," *IEEE Transactions on Power Electronics*, vol. 6, no. 2, pp. 251–259, Apr 1991.
- [12] S. Cobreces, E. Bueno, D. Pizarro, F. Rodriguez, and F. Huerta, "Grid impedance monitoring system for distributed power generation electronic interfaces," *IEEE Transactions on Instrumentation and Measurement*, vol. 58, no. 9, pp. 3112–3121, Sept 2009.
- [13] M. R. Patel, *Shipboard Electrical Power Systems*. CRC Press, 2011.



# Appendix C

## Matlab Simulink Models

In this appendix, some of the Matlab Simulink model implementations are shown.

### C.1 AKF Simulink Model for Single-Phase Signal

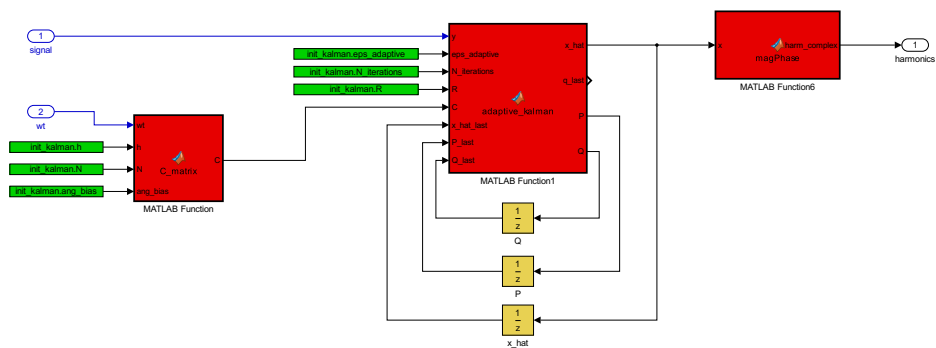


Figure C.1: AKF Simulink Model for Single-Phase Signal

## C.2 AKF Simulink Model for Three-Phase Signal

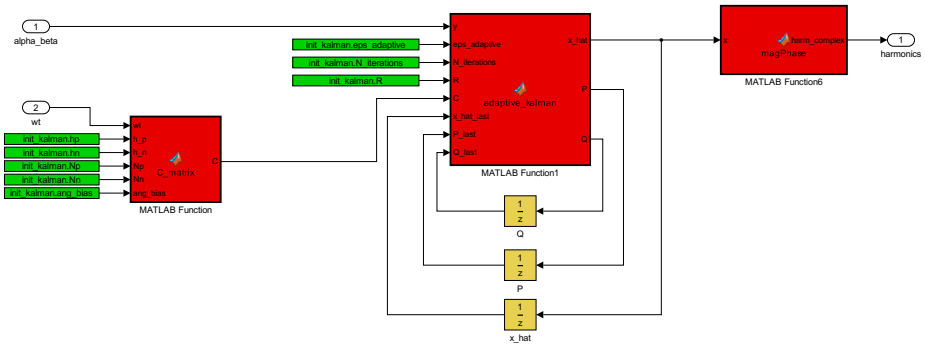


Figure C.2: AKF Simulink Model for Three-Phase Signal

## C.3 Distributional Power Grid Model

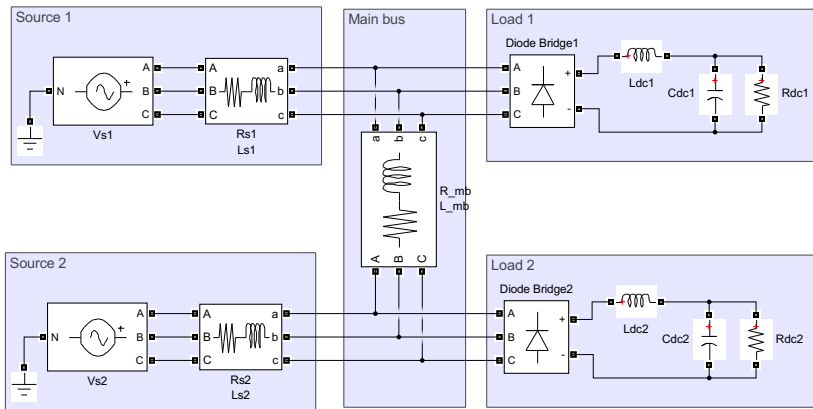


Figure C.3: Power Distributional Grid Model

## C.4 Ideal Three-Phase Sequence Generator

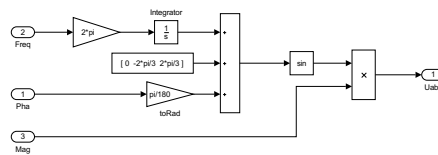


Figure C.4: Ideal Three-Phase Sequence Generator

## C.5 Phase correction Simulink model

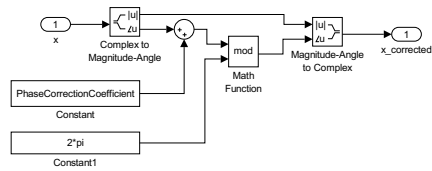


Figure C.5: Phase correction

## C.6 AC side parameter estimation Simulink model

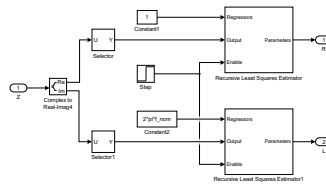


Figure C.6: AC side parameter estimation Simulink model

## C.7 Small-signal measurement of input impedance of rectifier load

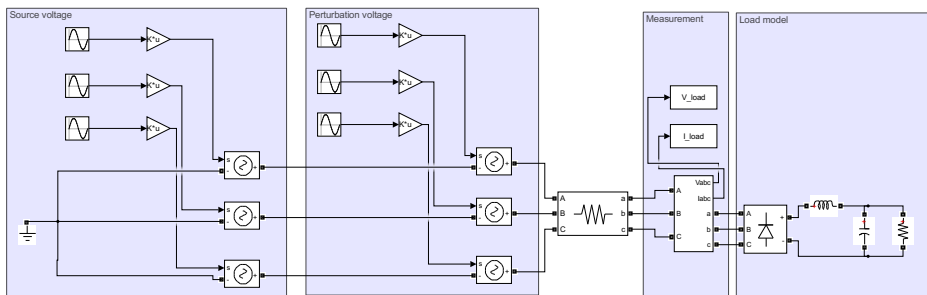


Figure C.7: Model in order to measure small-signal impedance of a three phase rectifier load

## C.8 DC Side Impedance Parameter Estimator Simulink Model

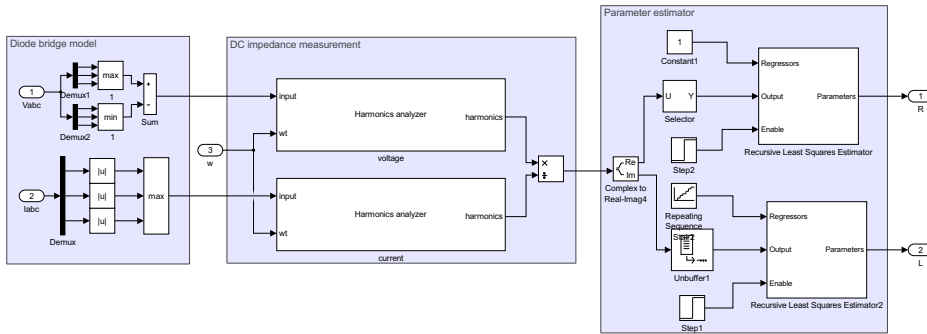


Figure C.8: Proposed method in order to extract DC side parameters

## C.9 AC side to DC side voltage and current Simulink model

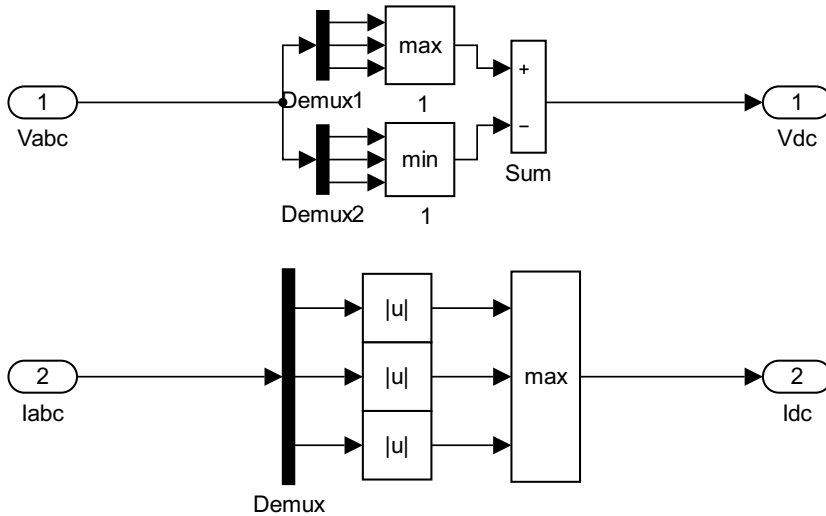


Figure C.9: DC side current and voltage estimate from AC side

## C.10 Harmonic Content and Parameter Estimator Simulink Model

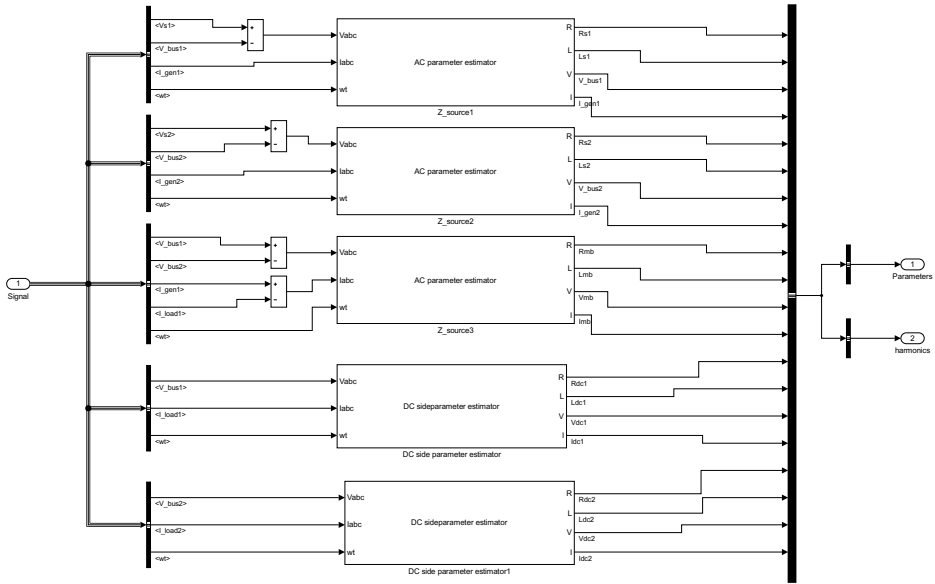


Figure C.10: Implemented block model for estimating all the harmonics and parameters of the grid



# Appendix D

## Matlab Code

In this appendix, some of the Matlab code used in this master's thesis is attached.

### D.1 Matlab Adaptive Kalman Filter Matlab Function Implementation

```
function [x_hat, P, Q] = adaptive_kalman...
(y, eps_adaptive, N_iterations, R, C, x_hat_last, P_last, Q_last)
%#codegen
coder.extrinsic('warning');

%%Constants
persistent A
if isempty(A)
    A = eye(size(Q_last));
end

%% Adaptive algorithm
q_last = Q_last(1,1);
Q = Q_last;
K = zeros(size(Q_last));
P_adaptive_ = P_last;
x_hat = x_hat_last;
iter = 0;
while iter < N_iterations
    P_adaptive_ = A*P_last*A + Q;
    K = P_adaptive_*C'*(C*P_adaptive_*C' + R)^(-1);
    x_hat =x_hat_last+K*(y-C*x_hat_last);
    w_adaptive = K*(y-C*x_hat);

    q = 1/length(w_adaptive)*sum(w_adaptive.^2);
    Q = q*A;
```

```
    if(abs(q-q_last)<eps_adaptive)
        break
    end
    q_last = q;

    iter = iter+1;
end
P = (A - K*C)*P_adaptive_;
```

## D.2 Matlab Function Single-Phase Measurement Matrix Calculation

```
function C = C_matrix(wt,h, N , ang_bias)
%#codegen
% allocate memory for the matrix
C = zeros(1, 2*length(h));
% fill C matrix
for i=1:length(h)
    M = [cos(h(i)*wt+ang_bias) -sin(h(i)*wt+ang_bias)];
    C(:,i*2-1:i*2) = M;
end
```

## D.3 Matlab Function Three-Phase Measurement Matrix Calculation

```
function C = C_matrix(wt,h_p, h_n, Np , Nn , ang_bias)
%#codegen
% allocate memory for the matrix
N = length(h_p) +length(h_n);
C = zeros(2, N*2);
% fill positive sequence harmonics
for i=1:Np
    M = [cos(h_p(i)*wt+ang_bias) -sin(h_p(i)*wt+ang_bias);
        sin(h_p(i)*wt+ang_bias) cos(h_p(i)*wt+ang_bias)];
    C(:,i*2-1:i*2) = M;
end
% fill negative sequence harmonics
for i=1:Nn
    M = [cos(h_n(i)*wt+ang_bias) -sin(h_n(i)*wt+ang_bias);
        -sin(h_n(i)*wt+ang_bias) -cos(h_n(i)*wt+ang_bias)];
    C(:,(2*Np+i*2-1):(2*Np+i*2)) = M;
end
```

## D.4 Matlab Function for Calculating Harmonic Phasor

```
function harm_complex = magPhase(x)
%#codegen
x1 = x(1:2:end);
x2 = x(2:2:end);

mag= sqrt(x1.^2+x2.^2);
phase = pi/180*atan2d(x2,x1);
harm_complex = mag.*exp(1j*phase);
```

## D.5 Matlab Function for Initializing the Adaptive Kalman Filter for Single-Phase Signal

```
function [ init_kalman ] = single_adaptive_kalman_struct( h, Q0, R, P, x0 )
%ADAPTIV_KALMAN_STRUCT Creates a struct necessary for the adaptive kalman
%simulink block for single phase signals

    init_kalman = struct;

    %% Constants, should not be necessary to change these
    init_kalman.eps_adaptive = 1e-5;
    init_kalman.N_iterations= 10;
    init_kalman.ang_bias = -pi/2;

    %% From input
    init_kalman.h = h;
    init_kalman.N = 2*length(h);
    init_kalman.Q = Q0;
    init_kalman.R = R;
    init_kalman.P0 = P;
    init_kalman.x0 = x0;
    init_kalman.eye = eye(init_kalman.N);
end
```

## D.6 Matlab Function for Initializing the Adaptive Kalman Filter for Three-Phase Signal

```
function [ init_kalman ] = three_adaptive_kalman_struct( hp, hn, Q0, R, P, x0 )
%ADAPTIV_KALMAN_STRUCT Creates a struct necessary for the adaptive kalman
%simulink block for three phase signals

    init_kalman = struct;
```

```
%% Constants, should not be necessary to change these
init_kalman.eps_adaptive = 0.00001;
init_kalman.N_iterations= 10;
init_kalman.ang_bias = -pi/2;

%% From input
init_kalman.hp = hp;
init_kalman.hn = hn;
init_kalman.Np = length(hp);
init_kalman.Nn = length(hn);
init_kalman.N = init_kalman.Np + init_kalman.Nn;
init_kalman.Q = Q0;
init_kalman.R = R;
init_kalman.P0 = P;
init_kalman.x0 = x0;
init_kalman.eye2N = eye(2*init_kalman.N);
```

```
end
```

# Linear KF Implementation for Three-Phase Harmonics Tracking

A linear Kalman filter based on the original KF from Kalman (1960) is used in this section. This type of implementation was not good enough for tracking harmonics when there is a fluctuation in the signals such as sudden drops.

## E.1 Implementation

The model using linear Kalman filter is implemented similarly as the one for the AKF with the same block for calculating the measurement matrix  $C$ . For the discrete-time KF, the Kalman filter block from the Simulink Control System Toolbox is used.

This model needs some parameters with a brief description in Table E.1. Where most of the parameters are equal to the ones in the adaptive Kalman filter except that the  $Q$  matrix is set to be a static matrix not varying with time.

Some experiments were done, where the same experiment conditions as in Section 4.3 is followed here.

Parameter	Brief description
$P_0$	Initial error covariance matrix
R	Measurement covariance matrix
Q	Input covariance matrix
$x_0$	Initial state
$H_p$	Set of positive sequence harmonics to measure
$H_n$	Set of negative sequence harmonics to measure
N	Number of positive and negative sequence harmonics

**Figure E.1:** Description of Kalman parameters

Parameter	Adaptive Kalman	Kalman
$\mathbf{H}_p$	[1, 3, 5]	[1, 3, 5]
$\mathbf{H}_n$	[7, 3, 10]	[7, 3, 10]
$N$	6	6
$\mathbf{P}_0$	$1 \times 10^3 \mathbf{I}_{2N}$	$1 \times 10^3 \mathbf{I}_{2N}$
$\mathbf{R}$	$1 \times 10^{-4} \mathbf{I}_2$	$1 \times 10^{-4} \mathbf{I}_2$
$\mathbf{Q}_0$	zeros(2N)	N/A
$\mathbf{Q}$	N/A	$\mathbf{I}_{2N}$
$\mathbf{x}_0$	zeros(2N,1)	zeros(2N,1)
$\epsilon_A$	$1 \times 10^{-5}$	N/A
$N_{max}$	10	N/A

Figure E.2: initialization of parameters for experiment 1

## E.2 Experiment 1

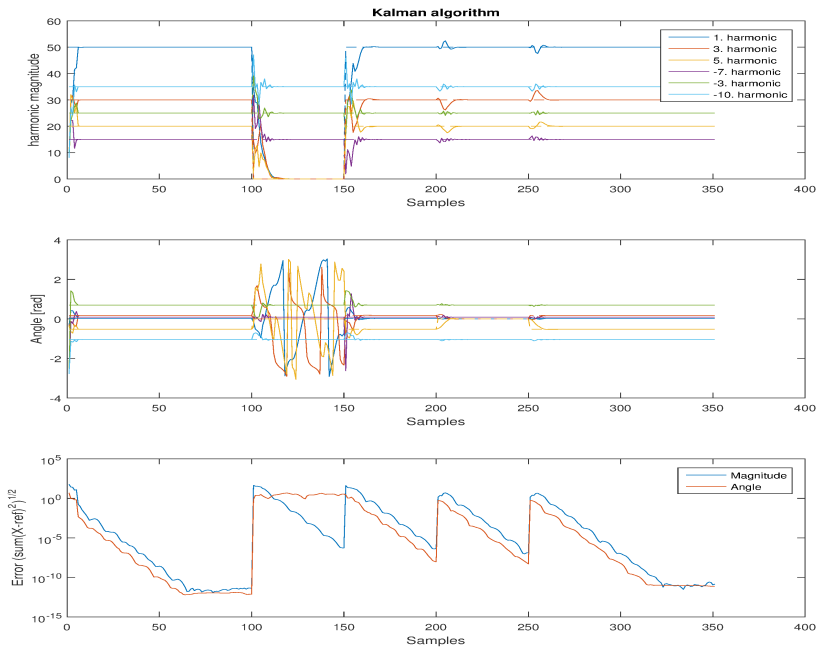


Figure E.3: Experiment 1 using linear KF

### E.3 Experiment 2

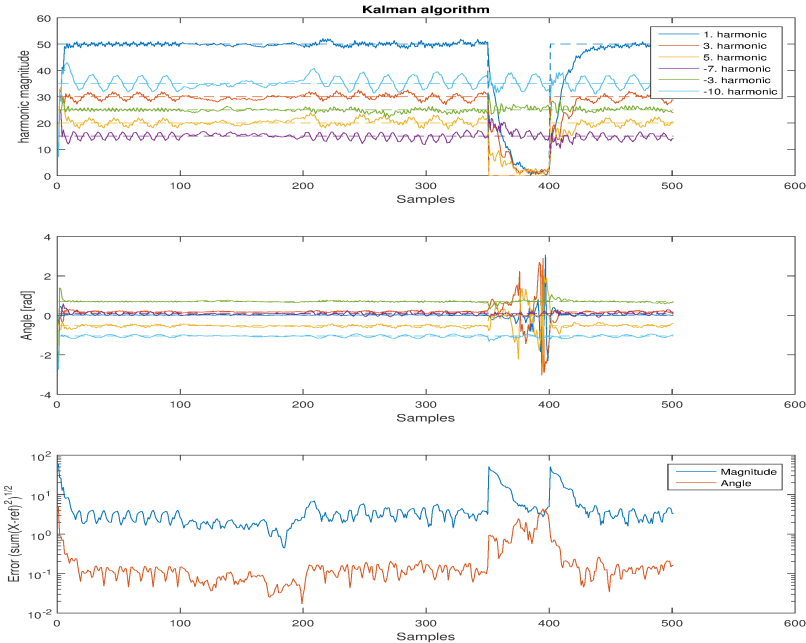


Figure E.4: Experiment 2 using linear KF with  $Q = I$

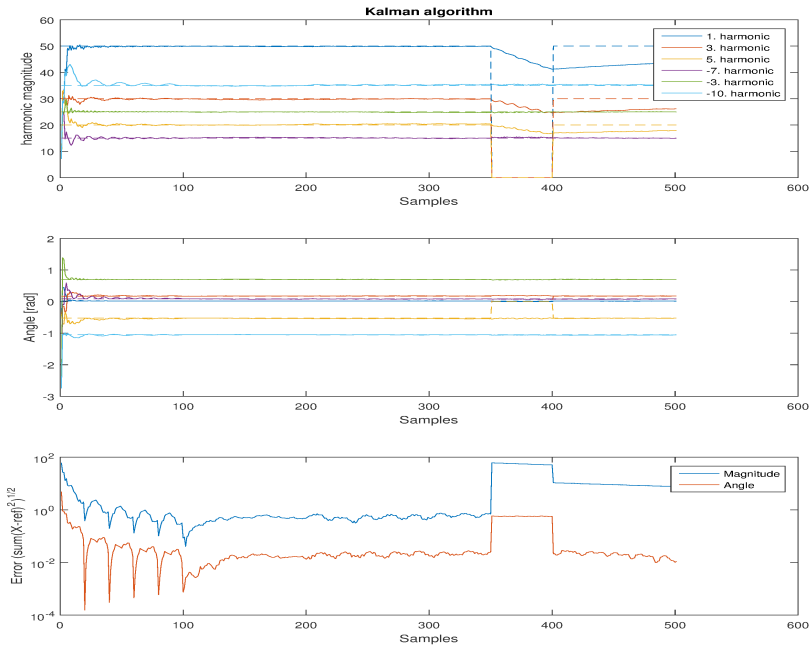


Figure E.5: Experiment 2 using linear KF with  $Q = 1 \times 10^{-3}I$

## E.4 Experiment 3

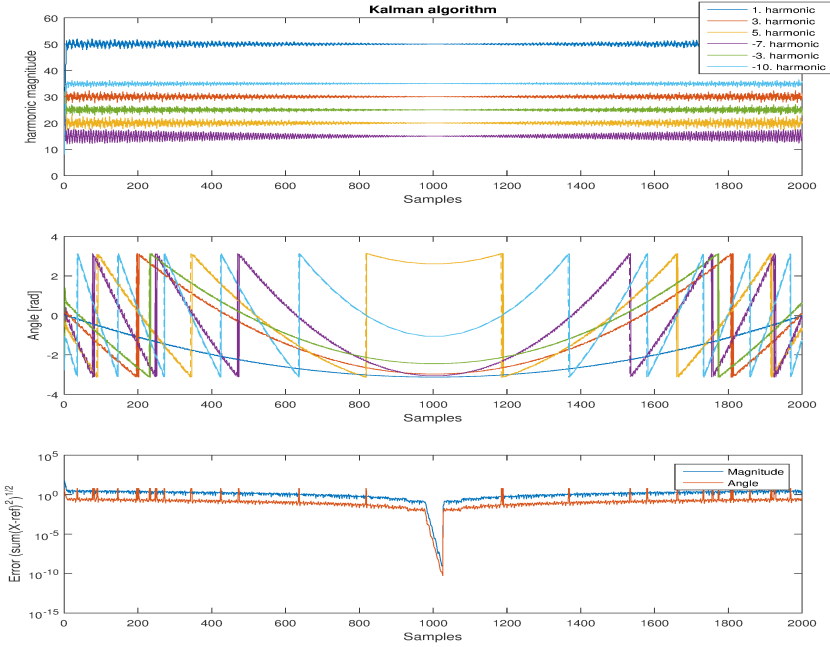


Figure E.6: Experiment 2 using linear KF with; magnitude, phase and deviation from the reference



# Algorithms

## F.1 Adaptive Kalman Filter

The algorithm from (Macias and Gomez Exposito, 2006, eq. 11-15) is given in (F.1).

Given a state transition matrix  $\Phi$ , measurement matrix  $H$  and a measurement covariance matrix  $R$  the algorithm construct the state vector  $x$  from measurements  $z$  by adapting the model covariance matrix  $Q(n)$  at time step  $n$ .

At each time step the following loop is repeated until the stopping criterion is when  $\sqrt{\hat{q}^j(n)} - \sqrt{\hat{q}^{j-1}(n)}$  is less than a defined  $\epsilon$ . The loop is started by setting the model covariance estimate to the last estimated value in previous time step  $\hat{Q}^0(n) = \hat{Q}(n-1)$ .

$$P^{j-} = \Phi(n-1)P(n-1)\Phi^T(n-1) + Q^j(n) \quad (\text{F.1a})$$

$$\hat{K}^j(n) = P^{j-}H^T(n)[H(n)P^{j-}(n)H^T(n) + R(n)]^{-1} \quad (\text{F.1b})$$

$$\hat{x}^j(n) = \hat{x}^-(n) + \hat{K}^j(n)[z(n) - H(n)\hat{x}^j(n)] \quad (\text{F.1c})$$

$$\hat{w}^{j+1}(n) = \hat{K}^j(n)[z(n) - H(n)\hat{x}^j(n)] \quad (\text{F.1d})$$

$$\hat{Q}^{j+1} = 0.5(w_1^{\hat{j}+1}(n)^2 + w_2^{\hat{j}+1}(n)^2) \quad (\text{F.1e})$$



# Appendix G

## Additional Plots

In this appendix some additional plots are attached.

### G.1 Harmonic Loads

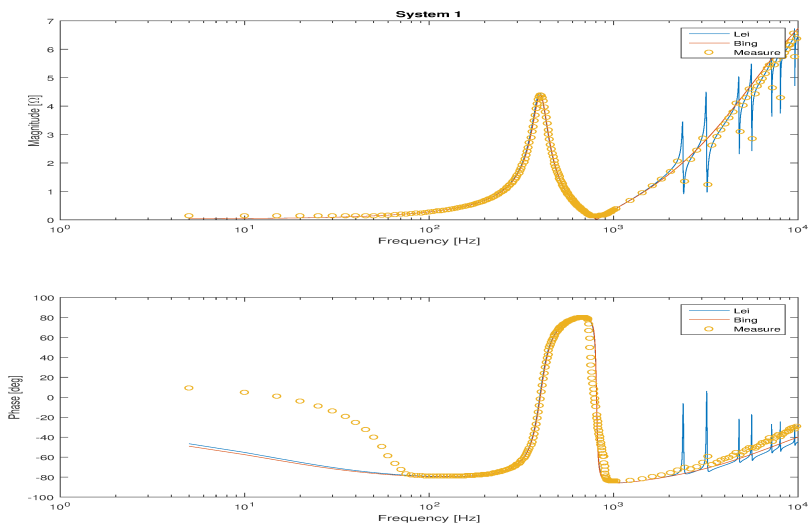


**Figure G.1:** Measured impedance using Figure C.7 and compared to the model Bing in Bing et al. (2007) and Lei in Lei et al. (2013) for system 1

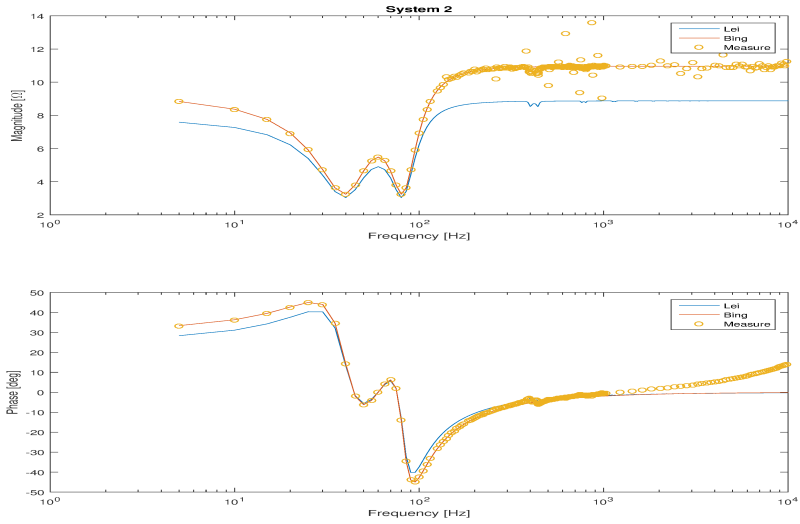


**Figure G.2:** Measured impedance using Figure C.7 and compared to the model Bing in Bing et al. (2007) and Lei in Lei et al. (2013) for system 2

## G.2 Low-pass Filter

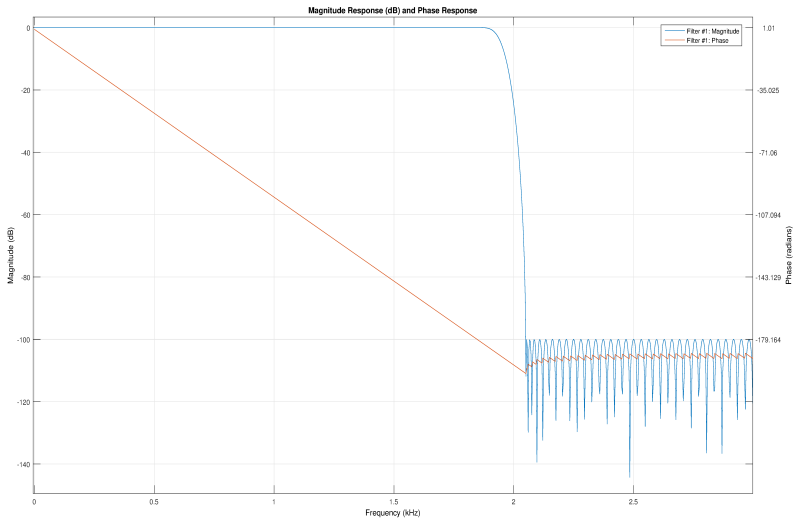
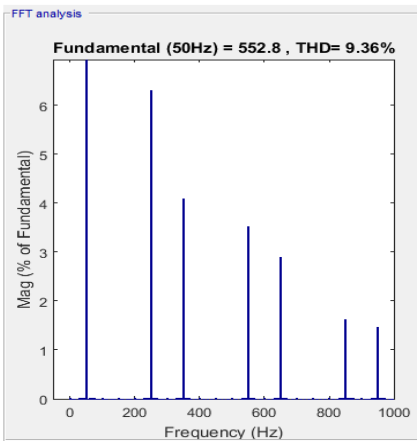
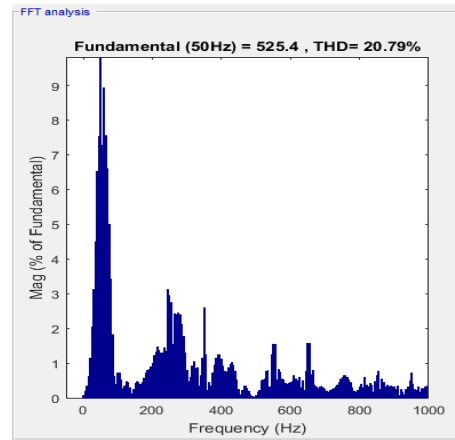


**Figure G.3:** Low-pass filter magnitude and phase response with configuration in Table 7.4

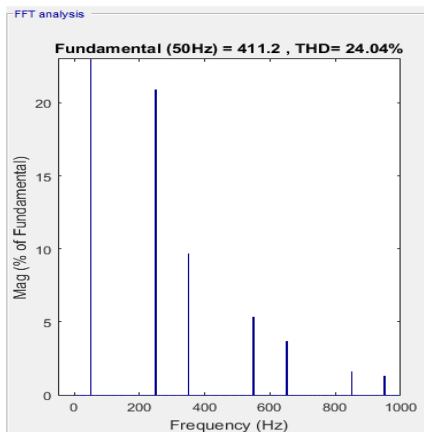
## G.3 FFT Analysis



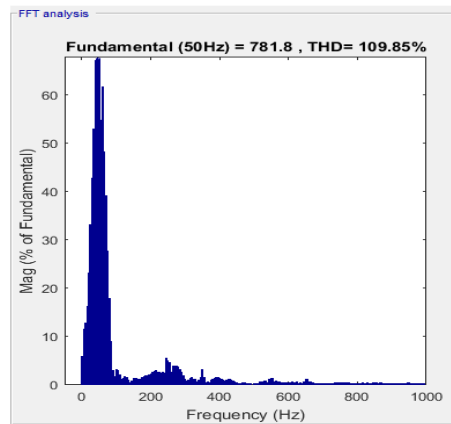
(a) Frequency content for  $V_{bus1}$  in steady state



(b) Frequency content for  $V_{bus1}$  transient response



(c) Frequency content for  $i_{s1}$  in steady state



(d) Frequency content for  $i_{s1}$  transient response

**Figure G.4:** FFT analysis of  $V_{bus1}$  and  $i_{s1}$  using FFT analysis tool

## G.4 Transient Analysis

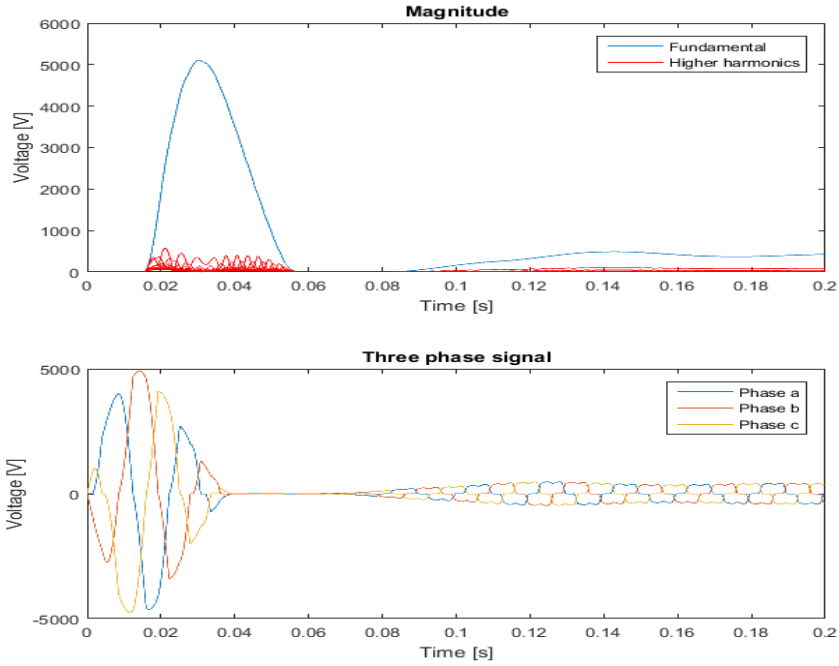


**Figure G.5:** The three-phase harmonics tracking used on  $i_{s1}$  dynamic system's transient response and the three-phase signal in  $abc$  frame